Drosophila melanogaster as a model to study ciliogenesis



Metta Bernou Pratt

Sir William Dunn School of Pathology and Brasenose College, Oxford

Trinity 2016

A thesis submitted in partial fulfilment of the requirements for the degree of Doctor of Philosophy at the University of Oxford

Part of the results presented in this thesis were published in:

Pratt, M.B., Titlow, J.S., Davis, I., Barker, A.R., Dawe, H.R., Raff, J.W., and Roque, H. 2016. *Drosophila* sensory cilia lacking MKS-proteins exhibit striking defects in development, but only subtle defects in adults. *Journal of Cell Science*. 129(20):3732-3743.

A copy of thesis has been deposited in the Bodleian Library, Oxford.

The *viva voce* examination was held on Thursday 1 December 2016. The examiners were Dr Eva Gluenz (Sir William Dunn School of Pathology, University of Oxford) and Professor Andrew Jarman (School of Biomedical Sciences, University of Edinburgh).

Abstract

Cilia are microtubule-based extensions of the cell membrane that extend from a mature centriole. Primary (non-motile) cilia are present on most human cells and have important roles in signalling pathways. At the base of the cilium is a selective barrier known as the transition zone (TZ). Defects in the TZ are associated with human congenital diseases such as Meckel-Gruber syndrome (MKS) and Nephronophthisis (NPHP). The TZ is formed by three protein complexes, the MKS, NPHP and Cep290 modules, although the fruit fly *Drosophila melanogaster* appears to lack the core components of the NPHP module. Results presented in this thesis shows that MKS proteins are spatially separated from Cep290 at the TZ in *Drosophila* spermatocyte cilia. The TZ of the spermatocyte cilia is perturbed in flies mutant for MKS1 ($MKS1^{\Delta 1}$) and fails to recruit key TZ proteins, although Cep290 and Chibby are recruited normally. Male fertility, however, is unaffected. Similarly, while there are substantial abnormalities in microtubule and membrane organisation in developing $MKS1^{\Delta 1}$mutant cilia, defects in mature $MKS1^{\Delta 1}$mutant cilia are limited to subtle changes in IFT and a membrane surrounded volume within the cilium. The function of sensory neurons is not negatively affected by the $MKS1^{\Delta 1}$mutation. Evidently, given enough developmental time, ciliary defects can be largely rescued in flies and the localisation of MKS module proteins to the cilia or flagella is not essential for viability or fertility in *Drosophila*.

Acknowledgements

There are many people who contributed to this thesis in one way or another. First and foremost, I would like to thank my supervisor, Jordan Raff, for his enduring support and encouragement over the years, tirelessly reading my drafts and also for letting me work on cilia! Special thanks also go to Hélio Roque, without whom, it is safe to say, this thesis would never have existed. If we were Team Cilia together, Hélio deserves to be Mr. Cilia, for really driving this project as well as teaching me valuable life skills such as electron tomography and custard tart appreciation. Many thanks to Alan Wainman for being the font of all fly wisdom, but particularly for helping me to generate the MKS1 mutant allele that is so central in my thesis. Days (Weeks? Months? It is all a bit a blur) of virgin collections and fly crosses would not have been the same without you and the motivational Maltesers. Thanks to Paul for supervising me when I first came to the lab and teaching me all about flies and live imaging. Please do not take it personally that I have not touched embryos or the Perkin Elmer since! Many other people have worked in the Raff Lab during the nearly five years I have been there and they have all fed my flies, helped me out with experiments, shared their reagents or simply made the lab a better place. Jenny, Nadine, Kasia and Janina, you may have defected to the Other Place, but thank you for being such good friends and genuinely caring people, you are endlessly supportive. Young Violet and Matt, thank you for being such good company in the young girls corner of the lab (sorry Matt, as you did not have your desk there, you could only ever be a guest in our corner..). Thanks to Cat

for starting the Raff Lab twitter account and bequeathing it to me when you left the lab, to Anna (Dr. Franz) for beautiful microscopy and true determination, to Zsófi and Lisa for enthusiastic cake baking and occasional exercise, to Sam for all the positive energy and for showing true bravery in following your dreams, to Saroj for endless lab managing and zest for life, to "my students" Leah and Zhai for allowing me to boss you around and being excellent students who will go on to graduate from Harvard with flying colours/become prime minister of Malaysia, to Adam, James, Jo, Rachel, Wonsang and other students who spent time in the lab for being such an important part of the lab in he short time you were there, and to Anna C, Inés and Mustafa for perpetuating the Raff Lab in true spirit.

When I first arrived in Oxford, I had the unbelievable luck to move into 23 Essex Street with the best housemates I could have asked for, Jaco, Geoff, Pirelli and Katue. Jaco, thanks to you Oxford was truly my home and you are an amazingly loyal friend. After living together for so long spending two Christmases together, I think of you as an honorary family member. Geoff, I probably owe you a substantial part of my sanity, but what better person to entrust it to? You and Sarah are both wonderful people and I am fortunate to call you my friends. Even though the both of you really reserve all the credit, I still see your marriage as my greatest achievement. Living in 23 Essex introduced me to, in no particular order, Giuliana, Kerry (and Léonie!), Emily and Tom, Phil and Maaike, Keith and a host of others. You have all made my life richer. Thanks also to "the friendly Germans" Falk, Corinna and Hazel for the delicious "dog food" you have fed me.

Dutch people are everywhere, and I have been lucky to have met some excellent ones in Oxford. Celine, thank you for your unabating enthusiasm, being the other half of Double Dutch and also the most passionate doctor I know. You and Dennis (The Agency) are extremely generous and welcoming people and I so glad we are still friends four years after only spending 5 months in the same city! Marloes and Anne, I can always count on you for theatre trips, book swaps and Dutch directness, "gezelligheid" and "lekker klagen" over

lunch, wine, tea, wine, coffee, wine or maybe wine. Finally, Laurien, for some reason your sixth sense means you always call me when I happen to be thinking of you!

In coming to Oxford, I also moved away from many great friends. I am sorry that I still have no answer to your persistent question of "wanneer kom je terug?", but I am glad that despite the distance, we always pick up where we left off last time. My friends from school, Carlijn, Irene and Jolien (058), exemplify this more than anyone else. We have shared so much and even though we have grown into four different women since we first met at 12, I know you will always be there to pick up the pieces, celebrate or whatever it is I need you to do. Farmachicks, Milou, Wendy, Sanneke, Anja and Dorien, I cannot quite believe it's 9 years ago we started university together. Only half of us actually became pharmacists, probably around the same number makes it to our well intentioned reunions each time, as we are all busy and in different places. I am looking forward to being able to attend more of those reunions and maybe even see everyone together. Dana, probably the most frequent visitor to Oxford after my mum. I really appreciate you taking the time to actually come and see me and I have really enjoyed all our adventures in and around Oxford. Friends I made in another lab, another life, Lianne and Nicolette, who knew that we would end up friends!? I think it is fair to say that we were all slightly sceptical, but I am glad that we fully moved past that. We may mostly communicate through selfies on whatsapp (some adorable, some gorgeous, some downright hideous), but you are always there for me. In this context also Marta, who supervised me for 6 months in Experimental Hematology. Marta was the best supervisor I could have hoped for and if we are a bit lax in sending our UFSoWs (Update Former Supervisor/Student on Whereabouts), it is due to lack of time, not interest. Also from the University of Groningen, I would like to thank everyone else at the "hemato", especially JJ Schuringa and everyone involved in the Topmaster MPDI, especially Ody Sibon. Without the support and inspiration all of you provided, I probably would not have come to Oxford in the first place, let alone return for a DPhil.

I am very glad that I learned to dive during my time in Oxford and that I again met some wonderful people along the way. Most importantly, I met Jean[1], which is without a doubt the best thing that happened to me in Oxford. Thank you for putting up with my sloth-like behaviour, my requests for having coffee delivered to me while I stay under my blanket and my inability to screw caps back onto anything, ever. I'm looking forward to finally bringing the tally of theses between us to 0 and getting to go on actual proper holidays.

Last, but definitely not least, I would like to thank my family. My mum, for being the strongest woman (and a scientist!) I know and for always encouraging me to do what I want, even it means I will be far away. My brother, Mark, a gentle giant of few words, for cramming surprisingly clever and witty observations into those few words. My dad, I so wish he could have seen me become a scientist. He would probably have been this manuscript's harshest (and most just) critic, but I like to think he would secretly have been quite proud to have another Dr. Pratt around. My grandparents, although sadly none of them is with us anymore either, for providing me with knowledge of the English language and culture that would later prove useful (oma Engeland) and for making my childhood so secure by looking after Mark and me every day (opa en oma Terpstra). Also, a very honorable mention for Jean's family (Max and Christiane, Claire and Christian, le papy de Biarritz et les grandparents de Castres) for putting up with the fact that I am not French and never make it to any family events on the account of "la thèse", merci à tous!

As a group of wise men once sang "Home is only a feeling you get in your mind, from the people you love and you travel beside". I am extremely fortunate to have many such homes, all over the world. Thank you.

[1] Je t'aime tant que je te dédie la seule note de bas de page de ma thèse

Contents

Contents **ix**

List of Figures **xv**

List of Tables **xvii**

List of Abbreviations **xx**

1 Introduction **1**

1.1 Centrioles, centrosomes and cilia 1

1.1.1 Centrioles 1

1.1.2 Centrosomes 5

1.1.3 Cilia 6

1.2 Cilia biology 7

1.2.1 Ciliogenesis 7

1.2.2 Transition zone 10

1.2.3 Intraflagellar transport 13

1.2.4 Types of cilia 14

1.3 Ciliated cells in *Drosophila melanogaster* 16

1.3.1 Spermatocytes 16

1.3.2 Sensory neurons 19

1.4 The role of cilia in development and signalling . . . 24
1.4.1 Left-right asymmetry . . . 24
1.4.2 Hedgehog signalling . . . 25
1.4.3 Other signalling pathways . . . 26
1.5 Ciliopathies . . . 30
1.5.1 Congenital ciliopathies . . . 30
1.5.2 Acquired ciliary disease . . . 32
1.5.3 Cilia disease mechanism . . . 34
1.6 Thesis outline . . . 35

2 Materials and methods **37**
2.1 Fly husbandry . . . 37
2.1.1 Fly handling . . . 37
2.1.2 *Drosophila melanogaster* stocks . . . 37
2.1.3 Generation of transgenic lines . . . 38
2.1.4 Generation of the $MKS1^{\Delta 1}$ allele . . . 40
2.1.5 Generation of the $B9D1^{\Delta 1}$, $CC2D2A^{\Delta 1}$ and $Cep104^{\Delta 1}$ alleles . . . 40
2.2 Behavioural assays . . . 41
2.2.1 Larval hearing assay . . . 41
2.2.2 Larval crawling assay . . . 41
2.2.3 Climbing assay . . . 42
2.2.4 Fertility . . . 42
2.2.5 Grooming assay . . . 42
2.2.6 Electrophysiology . . . 43
2.3 Bioinformatics . . . 43
2.3.1 BLAST . . . 43
2.3.2 Domain predictions . . . 43

2.3.3 gRNA design 44
2.4 Molecular biology 44
2.4.1 Genomic DNA preparation 44
2.4.2 PCR 44
2.4.3 HRMA 48
2.4.4 Construction of plasmids 49
2.4.5 Site-directed mutagenesis 50
2.4.6 DNA Sequencing 51
2.4.7 *In vitro* RNA transcription 51
2.5 Cell biology 51
2.5.1 Microinjection of RNA into living embryos 51
2.5.2 Fixation and immunostaining of pupal testes 52
2.5.3 Fixation and immunostaining of the pupal notum 52
2.5.4 Preparation of pupal notum for live cell imaging 53
2.5.5 Preparation of pupal testes for electron microscopy 53
2.5.6 Preparation of pupal notum for electron microscopy 53
2.5.7 Preparation of pupal notum for SBF-SEM 54
2.6 Microscopy and image analysis 55
2.6.1 Electron tomography 55
2.6.2 SBF-SEM 55
2.6.3 3D Structured Illumination Microscopy 55
2.6.4 Live cell imaging of bristle sensory neurons 56
2.6.5 Live cell imaging of RNA injections 56
2.7 Quantification and statistics 57
2.7.1 Electrophysiology 57
2.7.2 Grooming assay 57

2.7.3 Fluorescence intensity measurements . . . 57
2.7.4 NompB length measurements . . . 57
2.7.5 NompAGFP live imaging . . . 58
2.7.6 Cep104 localisation . . . 58

3 Generation and characterisation of MKS module mutations 59

3.1 Introduction . . . 59
3.2 Results . . . 61
3.2.1 Identification of *Drosophila* ciliopathy genes . . . 61
3.2.2 Generation of an MKS1 mutant allele, $MKS1^{\Delta 1}$ . . . 62
3.2.3 Generation of $B9D1^{\Delta 1}$ and $CC2D2A^{\Delta 1}$ . . . 64
3.2.4 Viability and fertility of MKS module mutations . . . 65
3.2.5 Behavioural studies of TZ mutations . . . 66
3.2.6 Electrophysiology of MKS module mutations . . . 69
3.3 Discussion . . . 71

4 Ultrastructural and localisation studies of spermatocyte cilia 73

4.1 Introduction . . . 73
4.2 Results . . . 75
4.2.1 Ciliopathy proteins localise to distinct regions within the TZ . . . 75
4.2.2 Key ciliopathy proteins fail to localise in $MKS1^{\Delta 1}$ cilia . . . 78
4.2.3 Localisation defects in $B9D1^{\Delta 1}$ mutant cilia . . . 78
4.2.4 Ultrastructural abnormalities in $MKS1^{\Delta 1}$, $B9D1^{\Delta 1}$ and $CC2D2A^{\Delta 1}$ mutant spermatocyte cilia . . . 79
4.3 Discussion . . . 83

5 Ultrastructural and localisation studies of sensory cilia 87

5.1 Introduction . . . 87

5.2 Results . . . 89
5.2.1 Ultrastructure of sensory cilia . . . 89
5.2.2 Ultrastructural abnormalities in *MKS1*$^{\Delta 1}$ mutant sensory cilia . . . 92
5.2.3 Larval behaviour assays . . . 96
5.2.4 NompA and NompC localise normally in *MKS1*$^{\Delta 1}$ . . . 97
5.2.5 Changes in IFT in *MKS1*$^{\Delta 1}$ mutant sensory cilia . . . 98
5.2.6 Live-cell imaging of ciliogenesis . . . 102
5.3 Discussion . . . 104

6 Cep104 **113**
6.1 Introduction . . . 113
6.2 Results . . . 115
6.2.1 Identification of key domains in *Cep104* . . . 115
6.2.2 Localisation of Cep104 in spermatocytes . . . 115
6.2.3 Microinjections of Cep104 mRNA constructs into living embryos . 116
6.2.4 Generation of an Cep104 mutant allele, Cep104$^{\Delta 1}$ . . . 119
6.2.5 *Cep104*$^{\Delta 1}$mutant flies are male and female sterile . . . 119
6.3 Discussion . . . 122

7 General discussion **127**
7.1 General discussion . . . 127
7.1.1 Establishing the TZ in *Drosophila* . . . 127
7.1.2 IFT and cilia function . . . 129
7.2 Future perspectives . . . 131

Bibliography **135**

List of Figures

1.1 Schematic of vertebrate and *Drosophila* centrioles. 2

1.2 Centriole duplication cycle. 4

1.3 Schematic of cilium. 9

1.4 Schematic summary of TZ super-resolution data. 12

1.5 *Drosophila* spermatogenesis. 18

1.6 *Drosophila* ciliated neurons. 21

1.7 Schematic of Hh signalling in mammals and *Drosophila*. 27

3.1 Schematic overview of MKS1, B9D1 and CC2D2A. 63

3.2 Fertility and sperm axonemes in $MKS1^{\Delta 1}$ mutant males. 65

3.3 Climbing assays in WT and $MKS1^{\Delta 1}$ mutant flies. 67

3.4 Grooming assays in WT and $MKS1^{\Delta 1}$ mutant flies. 68

3.5 Electrophysiology of sensory bristles in WT and TZ mutants. 70

4.1 Localisation of TZ proteins in wild type and $MKS1^{\Delta 1}$ mutant spermatocyte cilia. 76

4.2 Compound electron tomography and 3D-SIM images. 77

4.3 Localisation of MKS1 and B9D2 in WT and 9mut mutant spermatocyte cilia. 79

4.4 Electron microscopy of WT, $MKS1^{\Delta 1}$ mutant, and $MKS1^{\Delta 1}$, GFP-MKS1 spermatocyte cilia. 80

4.5 Electron microscopy of WT and *B9D1*$^{\Delta 1}$, *CC2D2A*$^{\Delta 1}$and *Cep290*^{MecH} mutant spermatocyte cilia. 82

5.1 SBF-SEM of WT sensory bristle cilia. 90
5.2 SBF-SEM and electron tomography of WT sensory bristly cilia. 91
5.3 Electron tomography of sensory bristle cilia at 48 hours APF. 93
5.4 Electron tomography of sensory bristle cilia at 72 hours APF. 94
5.5 Electron tomography of sensory bristle cilia membrane surrounded inner volume. 95
5.6 Quantification of behaviour in WT and *MKS1*$^{\Delta 1}$ mutant larvae. 97
5.7 Localisation of NompA and NompC in WT and *MKS1*$^{\Delta 1}$mutant cilia. . . . 99
5.8 IFT in sensory bristle cilia. 101
5.9 Live cell imaging of NompA-GFP in bristle cilia. 103

6.1 Schematic overview of Cep104. 115
6.2 Localisation of Cep104-GFP in testes. 116
6.3 Localisation of Cep104-GFP in embryos. 118
6.4 Electron micrograph of *Cep104*$^{\Delta 1}$ mutant sperm axonemes. 120
6.5 Relative positions of *Cep104* and *CG10165*. 121

List of Tables

2.1 *Drosophila* stocks used in this thesis 38
2.2 Transgenic *Drosophila* lines used in this thesis 39
2.3 gRNAs used in this thesis 41
2.4 Primers used in this thesis 45
2.5 Plasmids used in this thesis 49

3.1 *Drosophila* orthologues of human ciliopathy genes 62

List of Abbreviations

Asl	Asterless
BBS	Bardet-Biedl syndrome
Cep	Centriolar protein
Ch organ	Chordotonal organ
DNA	Deoxyribonucleic acid
ES organ	External sensory organ
GFP	Green fluorescent protein
Hh	Hedgehog
IFT	Intraflagellar transport
JBTS	Joubert syndrome
LB	Luria-Bertani broth
MBP	Maltose binding protein
MKS	Meckel-Gruber syndrom
NPHP	Nephronophtisis
PAGE	Polyacrylamide gel electrophoresis
PBS	Phosphate buffered saline
PCM	Pericentriolar material
PCR	Polymerase chain reaction
RNA	Ribonucleic acid

List of Abbreviations

mRNA	Messenger RNA
sgRNA	Short guide RNA
ROI	Region of interest
RPE-1 cells	(Human) retinal pigment epithelial cells
SBF	Serial block-face
SDS	Sodium dodecyl suphate
SEM	Scanning electron microscopy
Shh	Sonic Hedgehog
SOP	Sensory organ precurser
TEM	Transmission electron microscopy
TMEM	Transmembrane protein
TZ	Transition zone
Ubq	Ubiquitin
Wnt	Wingless
WT	Wild type
ZNF	Zinc finger
3D-SIM	Three-dimensional structured illumination microscopy

Chapter 1

Introduction

1.1 Centrioles, centrosomes and cilia

1.1.1 Centrioles

Centrioles are barrel shaped organelles consisting of microtubules that form two important cell organisers: centrosomes and cilia (Carvalho-Santos et al., 2010; Marshall, 2009). Centrosomes are the main microtubule organising centres in many animal cells, while cilia have important roles in cellular sensation, signalling and motility (Chavali et al., 2014; Nigg and Raff, 2009). To form a centriole, 9 microtubule blades are arranged radially around a central cartwheel structure (Figure 1.1). The cartwheel is formed of a central tube and 9 radial spokes to which the mictrotubules attach (Cottee et al., 2011). This structure depends on the oligomerisation of Sas6 and Ana2 and is widely thought to be responsible for the 9-fold symmetery of the centriole. Centriolar microtubule blades may be singlets, doublets or triplets, depending on the organism or cell type (Delattre and Gönczy, 2004). The inner most microtubule, the A tubule, consists of 13 protofilaments. The B tubule, which is the second microtubule in doublets or triplets, and the C tubule, which is the outermost mi-

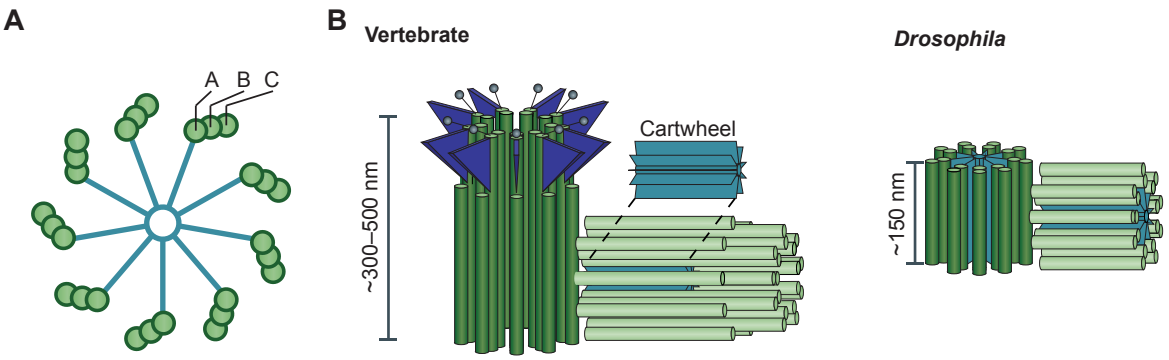

Figure 1.1 Schematic of vertebrate and *Drosophila* centrioles. A) End on view of the centriole with A, B and C tubules (*green*) arranged around the cartwheel (*aquamarine*) B) Schematic of the vertebrate centriole pair (*left panel*) and the *Drosophila* centriole pair (*right panel*). The mother centriole (*dark green*) can be distinguished from the daughter centriole (*light green*) by the distal (*grey*) and subdistal (*dark blue*) appendages in the vertebrate system. *Drosophila* mother centrioles lack (sub)distal appendages. Figure B is adapted from (Conduit et al., 2015b).

crotubule in triplets are incomplete rings and consist of 10 protofilaments each (Linck and Stephens, 2007).

Unlike most cellular microtubules, which are dynamic, the centriolar microtubules are very stable, probably due to several post-translational modifications including polyglutamation, detyrosination and acetylation (Bobinnec et al., 1998; Eddé et al., 1990; Gundersen and Bulinski, 1986; Piperno and Fuller, 1985). When a cell is born it usually contains two duplication competent centrioles that are often held together by a fibrous matrix (Fu et al., 2015; Nigg and Raff, 2009). The centriole pair comprises an older, mother centriole and her younger daughter that was generated during S-phase of the previous cell cycle (Fu et al., 2015; Nigg and Raff, 2009). In most organisms, the mother centriole can be distinguished from the daughter by distal and subdistal appendages, although these are absent in *C. elegans* and *Drosophila melanogaster* (Figure 1.1) (Reina and Gonzalez, 2014; Vorobjev and Chentsov, 1982).

Centrioles duplicate once per cell cycle (Figure 1.2) (Chavali et al., 2014; Fu et al., 2015; Nigg and Raff, 2009). In G_1-phase, each cell has a pair of centrioles consisting of a mother and a daughter. These centrioles are connected by a fibrous matrix at their bases. In

S-phase, one daughter centriole grows from each pre-existing centriole, that are both now referred to as mother centrioles. The mother centrioles and their growing daughters are arranged in a tight orthogonal fashion, with the base of the daughter connected ("engaged") at the side of the mother centriole towards the proximal end. During G_2-phase, the fibrous connection between the two pairs of centrioles are severed and the two centriole pairs separate. Concomitantly, the two mother centrioles recruit pericentriolar material (PCM) thus forming two centrosomes that will form the two poles of the mitotic spindle. The centrioles then disengage and the cell divides.

Recently great progress has been made in identifying the key proteins that are required for the assembly of the daughter centriole. Pioneering genome-wide RNAi studies in *C. elegans* showed that only five genes are essential for centriole assembly, and a similar set of proteins seem to be required in flies and humans (Dobbelaere et al., 2008; Kleylein-Sohn et al., 2007; Pelletier et al., 2006). The protein kinase Sak/Plk4 is recruited to the side of the mother centriole by either Asl (in flies), Spd-2 (in worms), or a combination of the two (Cep152 and Cep192, respectively in humans). This kinase then recruits and phosphorylates SAS-5/Ana2/STIL (worms/flies/humans, respectively) which in turn recruits SAS-6/Sas-6 to form the central cartwheel structure. This structure then recruits SAS-4/CPAP, which in turn helps recruit the centriolar microtubules.

In mammalian multiciliated cells, such as the ones present in the human trachea, hundreds of centrioles are required to form the motile cilia on these cells (Brooks and Wallingford, 2014; Yan et al., 2016). The majority of these centrioles are derived from electron dense structures called deuterosomes, around which new centrioles form all around in a flower like arrangement (Klos Dehring et al., 2013; Yan et al., 2016). The deuterosome consists of only two identified proteins, Deup1 and Ccd278, which recruit Cep152 and Plk4 in order to drive centriole amplification. Recently, it was shown that these deuterosomes are formed on the daughter centriole and that procentrioles simultaneously form around the

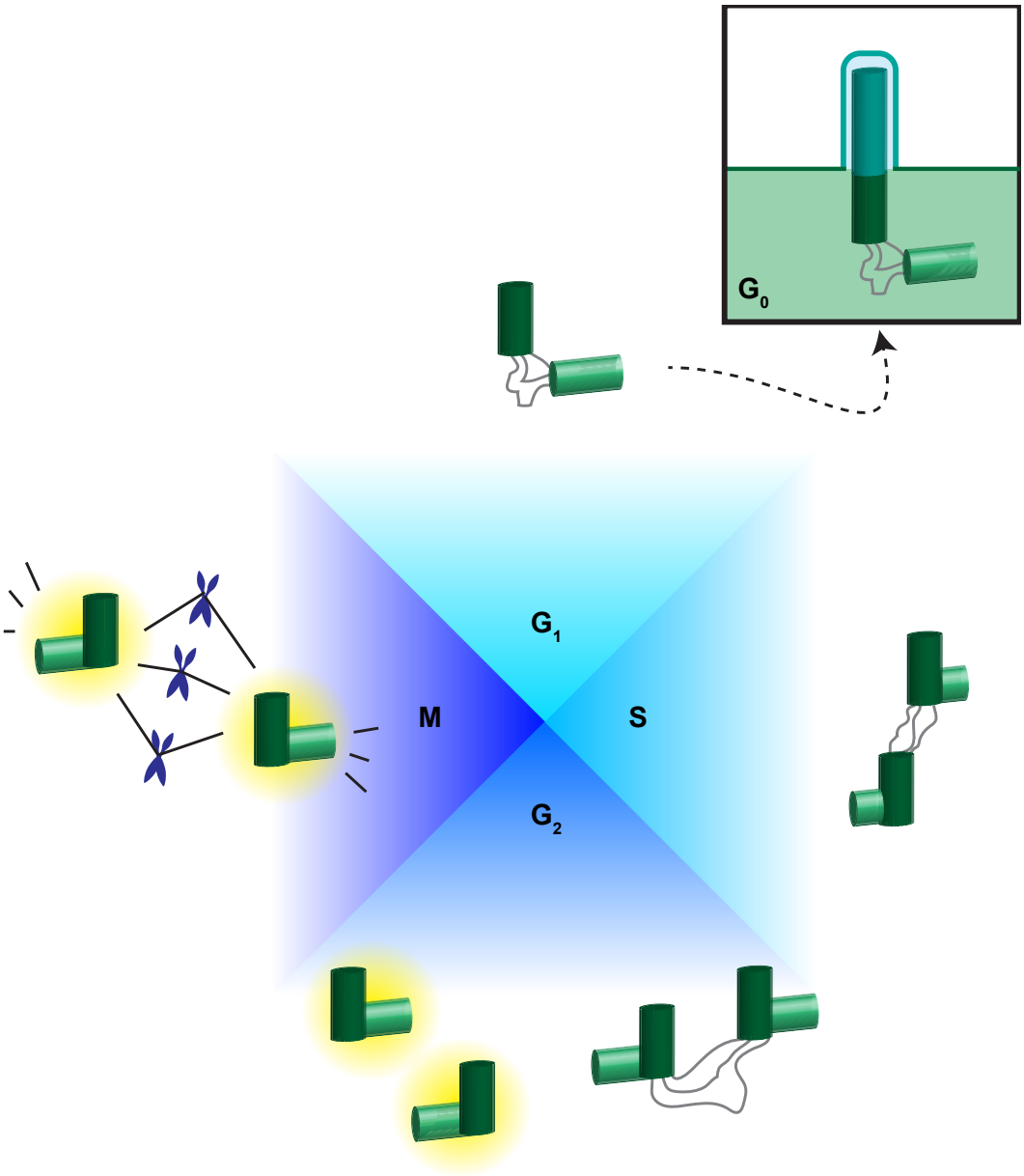

Figure 1.2 Centriole duplication cycle. Schematic of the centriole duplication cycle showing the arrangement of the centrioles throughout the cell cycle. In G_1-phase, each cell has a pair of centrioles consisting of a mother (*dark green*) and a daughter (*light green*), that are loosely connected by a fibrous matrix (*grey*). The centrioles duplicate in S-phase, when a daughter centriole forms from the side of the mother centriole. The mother and daughter centrioles are tightly connected (engaged). Daughter centrioles reach their final length in G_2-phase, when the two pairs of centrioles separate and acquire PCM (*yellow*) in late G_2-phase, thus maturing into centrosomes. In M-phase, the centrosome nucleates microtubules that form the mitotic spindle prior to cytokinesis and centriole disengagement. After division, the cell may enter the cell cycle again or go into quiescence (G_0-phase). In G_0-phase, the centrioles migrates to the plasma membrane, where the mother centriole docks and extends its microtubules to form a cilium (*aquamarine*). Figure adapted from (Nigg and Raff, 2009).

deuterosomes and the mother centriole (Al Jord et al., 2014).

1.1.2 Centrosomes

In dividing cells, centrioles recruit an amorphous mass of proteins known as the pericentriolar material (PCM) to form a centrosome (Figure 1.2, G_1-phase). The centrosome is the main microtubule organising center of most animal cells. While lacking in higher plants, the role of the centrosome is otherwise extremely conserved throughout evolution (Carvalho-Santos et al., 2010; Marshall, 2009). Centrosomes organise the microtubules along which organelles may migrate through the cell. Their most important role, however, is the organisation of the spindle during cell division. Interestingly, only mother centrioles are able to recruit PCM (Conduit et al., 2015a; Wang et al., 2011). During their first round of mitosis, phosphorylation of Sas4 primes daughter centrioles for the recruitment of Asl, thus converting them to mature mother centrioles capable of recruiting PCM (Novak et al., 2014; Novak et al., 2016). Asl is required not only for centriole duplication (see Section 1.1.1), but also for the recruitment of Cnn and Spd2 (Conduit et al., 2010; Conduit et al., 2014). These two proteins form a scaffold around the centriole, which allows other PCM proteins to localise to the centrosome (Conduit et al., 2014). The PCM nucleates microtubules by recruiting γ-tubulin ring complexes (γ-TuRCs) (Moritz et al., 1995). Centrosomes are not strictly required for cell division in many systems, since there are alternative mechanisms for nucleating the mitotic spindle. These include stabilisation of microtubules originating from the chromosomes at the kinetochores and the recruitment of γ-TuRCs to existing microtubules by the Augmin complex (Hayward et al., 2014; Meunier and Vernos, 2012; O'Connell and Khodjakov, 2007). *Drosophila*, for example, develop relatively normally without centrosomes, relying on other pathways of spindle assembly (Basto et al., 2006). Flies without centrioles eclose at nearly the same rate as WT flies and are morphologically normal, although they are unable to form cilia and are therefore uncoordinated. However,

the centrosomal pathway of generating the mitotic spindle is more efficient than acentrosomal pathways, which is important in rapidly dividing cells. Furthermore, centrosomes appear to play a particularly important part in asymmetric divisions, where cells divide asymmetrically to form two daughters of different fates (Basto et al., 2006).

1.1.3 Cilia

Cilia are microtubule based extensions of the plasma membrane that have important motility, sensory and signalling roles (Berbari et al., 2009; Singla and Reiter, 2006). In non-dividing cells, the centrioles migrate to the plasma membrane, where the older, mother centriole docks and forms the basis of the cilium (Figure 1.2, insert) (Garcia-Gonzalo and Reiter, 2012; Ishikawa et al., 2005; Seeley and Nachury, 2010). In the context of cilia, centrioles are more commonly called basal bodies. Cilia may be either motile or immotile. Motile cilia or flagella beat in a coordinated fashion, which serves to either displace fluid over the surface of the cell or propel the cell itself. Typically, the term motile cilia is used when the organelle is present in large numbers on the cell, while flagella is used when one or a few are present on the cell. However, cilia and flagella are often used interchangeably. Immotile cilia, on the other hand, do not beat. They are, however, present on most human cells. Their presence has long been thought to be a vestige of evolution (Wheatley, 1995). Over the past decade, it has become apparent that immotile primary cilia are key signalling centres (Reiter et al., 2012). The crucial developmental Hedgehog pathway relies on cilia and cilia have also been implied in Wingless (Wnt), Ca^{2+} and G-protein coupled receptor (GPCR) signalling (Basten and Giles, 2013; Hilgendorf et al., 2016; Singla and Reiter, 2006). Defects in cilia are associated with human disease. These diseases include congenital ciliopathies that result in developmental abnormalities, but also more common diseases such as retinopathies and cancer (Basten and Giles, 2013; Gerdes et al., 2009; Oh and Katsanis, 2012).

1.2 Cilia biology

1.2.1 Ciliogenesis

In most multicellular organisms, cilia are assembled only in quiescent cells (G_0-phase) or in cycling cells that are in G_1-phase of the cell cycle, and they are usually disassembled prior to mitosis or, in the case of quiescent cells, upon re-entry into the cell cycle (Bornens, 2012; Seeley and Nachury, 2010). Since the centriole at the base of the cilium is not only the ciliary basal body, but also part of the centrosome, it is thought that the cilium disassembles in dividing cells in order to allow the centriole to recruit PCM and form the mitotic spindle (Basten and Giles, 2013; Ishikawa and Marshall, 2011; Seeley and Nachury, 2010).

At the transcriptional level, ciliogenesis is under the control of a highly conserved master regulator, regulatory factor X (RFX). In many systems, including *C. elegans*, *Xenopus*, zebrafish and mice, knock-down or knock-out or RFX genes results in gross defects in ciliogenesis (Choksi et al., 2014). Another family of key transcriptional regulators, the forkhead box transcriptions factors, also appears to be important for the biogenesis of cilia, particularly motile cilia. Mammalian FOXJ1 and its functional *Drosophila* orthologue FBF3 are expressed in motile cilia and are required for motile cilia biogenesis (Brody et al., 2000; Chen et al., 1998; Newton et al., 2012). While it is clear that RFX and FOXJ1/FBF3 are critically important for all cilia to form, there is a wide variety of cilia morphology and function between and even within organisms. It seems likely that, analogous to homeotic transcription factors, the levels of RFX and FOXJ1/FBF3 and the presence of cell type specific transcription factors cooperate to generate the appropriate cilium for each cell type. Indeed, studies in *Drosophila* show that low and high levels of RFX drive the expression of different genes (Cachero et al., 2011; Newton et al., 2012). Furthermore, there is some evidence that suggests that cell type specific transcription factors contribute to ciliary diversity (Gresh et al., 2004; Kiselak et al., 2010).

To form a cilium, the centrioles, which lose most of their PCM in interphase, migrate to the plasma membrane (Ishikawa et al., 2005; Palazzo et al., 2000). In mammalian cells, the distal appendages of the mother centriole dock at the plasma membrane (Ishikawa et al., 2005; Sorokin, 1968). The daughter centriole remains in close contact with the mother, but does not participate in ciliogenesis. *Drosophila* centrioles lack distal appendages and the exact mechanism of docking is not fully understood (Reina and Gonzalez, 2014). After docking, the A and B microtubules of the basal body extend to form the axoneme (Anderson, 1972; Czarnecki and Shah, 2012). The migrating basal body becomes associated with vesicles that subsequently fuse with the plasma membrane, causing the membrane to expand in order to accommodate the growing axoneme (Sorokin, 1968). Concomitantly, the transition zone (TZ) forms at the distal end of the basal body. Here, the C tubule terminates and transition fibres and Y-links connect the microtubules to the ciliary membrane at the base of the axoneme (Figure 1.3) (Czarnecki and Shah, 2012; Hu and Nelson, 2011; Ishikawa and Marshall, 2011). The TZ is a selective barrier at the base of the cilium that helps to establish and maintain the cilium as a compartment separate from the rest of the cytoplasm and the plasma membrane. Since no protein synthesis occurs within the cilium, ciliogenesis is dependent on the delivery of ciliary building blocks to the ciliary tip. Motor proteins and intraflagellar transport (IFT) protein complexes are therefore essential for ciliogenesis. Evidence in *Chlamydomonas* suggests that tubulin in the flagellum turns over and that IFT remains important once the flagellum reaches its final length (Marshall and Rosenbaum, 2001). Furthermore, Hedgehog signalling in the mouse cilium requires IFT proteins (Huangfu et al., 2003). The role of IFT in growing and steady state cilia and flagella will be discussed in more detail in Section 1.2.3. The length of the cilium appears to be highly regulated. The length of cilia on specific cell types fall within a narrow range and even small increases or decreases may have pathological consequences (Avasthi and Marshall, 2012). However, at present the exact mechanisms of ciliary length regulation are unclear.

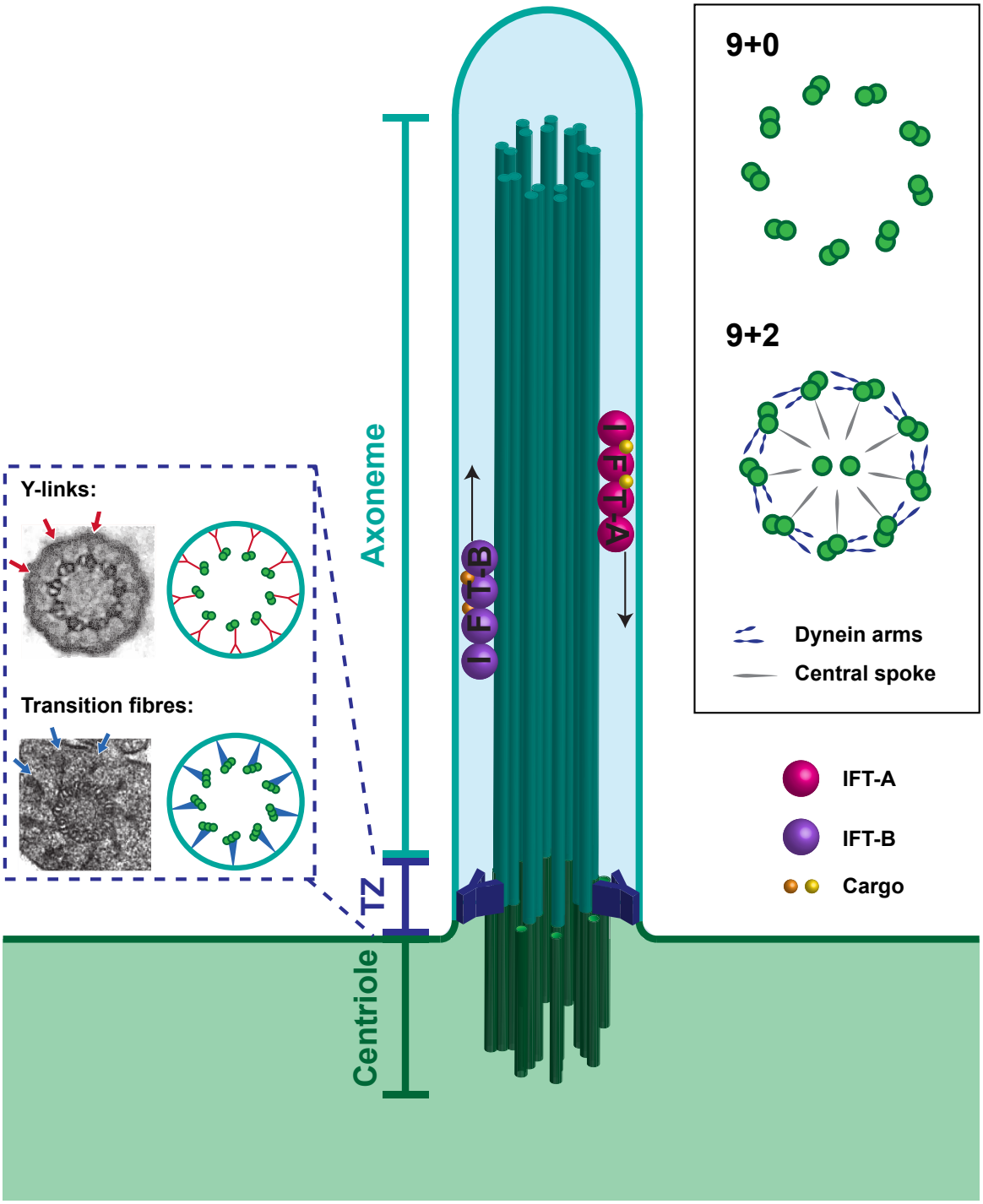

Figure 1.3 Schematic of cilium. Schematic of a canonical cilium showing the centriole/basal body (*dark green*), TZ (*dark blue*), including the transition fibres (*light blue arrows and triangles* in zoom of the TZ) and Y-links (*red arrows and Y-shapes* in zoom of the TZ) and axoneme (*aquamarine*). IFT-B (*violet*) is shown transporting cargo (*orange*) in the anterograde direction and IFT-A (*pink*) is shown transporting cargo (*yellow*) in the retrograde direction. In the insert, cross sections of 9+0 and 9+2 cilia are shown. Dynein arms (*dark blue lines*) and central spokes (*grey lines*) are depicted in the 9+2 cilium. Images in the zoom of the TZ are reproduced and adapted from (Reiter et al., 2012).

1.2.2 Transition zone

The TZ is a morphologically distinct region at the base of the cilium (Czarnecki and Shah, 2012; Reiter et al., 2012; Takao and Verhey, 2015). By transmission electron microscopy (TEM), the TZ appears in longitudinal sections as an area of increased electron density at the ciliary membrane immediately distal to the basal body. In transverse sections, connections between the microtubules and the membrane may be observed (Gilula and Satir, 1972). Transition fibres connect the microtubules to the ciliary membrane at the distal end of the basal bodies (Anderson, 1972). Distal to the transition fibres, a row of Y-links forms further connections between the proximal axoneme and the membrane (Gilula and Satir, 1972).

Genetic and interaction studies suggest that the formation of the TZ depends on three distinct protein complexes or modules, known as the Cep290, Meckel-Gruber syndrome (MKS) and Nephronophtisis (NPHP) modules (Sang et al., 2012; Schouteden et al., 2015; Williams et al., 2008; Williams et al., 2011; Yee et al., 2015). In *C. elegans*, a hierarchy of TZ assembly is emerging. RGRIP1L (also known as MKS5 or NPHP8) is at the top of this hierarchy, with the Cep290, MKS and NPHP modules below. Cep290 requires RGRIP1L to localises to the center of the TZ (Li et al., 2016; Yang et al., 2015). Here, Cep290 builds a scaffolding structure (Li et al., 2016; Schouteden et al., 2015). This central cylinder scaffold is required for the rest of the TZ to form. In worms, Cep290 is also required for the attachment of the tip of the dendrite to the extracellular material (Schouteden et al., 2015). Since dendrites form by backward migration of the cell body in *C. elegans*, loss of this adhesion of the dendritic tip results in defects in retrograde extension and consequently dendrite formation (Heiman and Shaham, 2009). RGRIP1L also interacts genetically and functionally with both the MKS and the NPHP modules and is required for the ciliary localisation of both these modules (Jensen et al., 2015; Williams et al., 2011). In *C. elegans*, mutating a gene from either the MKS or NPHP results does not result in gross defects in cilia. When a gene from both modules is mutated, on the other hand, dendrites are shortened and cilia are

found at random points between the cell body and the cuticle. Furthermore, these mutants did not take up a fluorescent dye as effectively as wild type worms in a dye-filling assay (Williams et al., 2008). Since the cilia are in contact with the external environment, the sensory neurons fill with dye when the animal is placed in a dye. A reduction in dye filling is therefore suggestive of defective cilia. Thus, the MKS and NPHP modules appear to act in a redundant fashion in worms to form the transition fibres and Y-links (Williams et al., 2011). Recently, a similar redundancy was also observed in mice when Tectonic, which is part of the MKS complex, was mutated simultaneously with either NPHP1 or NPHP4 (Yee et al., 2015). When a gene of all three modules is mutated, TZ features are completely absent and axonemes are perturbed in *C.elegans* (Schouteden et al., 2015).

Recent advances in super-resolution microscopy allow for more detailed studies of the TZ (Figure 1.4). In retinal pigment epithelial (RPE-1) cells, the protein most proximal to the basal body appears to be Cep164, which is part of the distal appendages (Graser et al., 2007; Yang et al., 2015). Both Cep290 and RGRIP1L localise to the center of the axoneme, with RGRIP1L localising distal to Cep290 (Lambacher et al., 2015; Yang et al., 2015). MKS1 partially overlaps with RGRIP1L, but also extends further away from the axoneme. This localisation is consistent with the proposed role of the MKS module in forming the Y-links. Other MKS associated proteins, including TCTN2 (one of the mammalian Tectonic isoforms) and MKS3 (also known as Transmembrane protein 67, TMEM67) link MKS1 and the ciliary membrane (Lambacher et al., 2015; Yang et al., 2015). NPHP1, TMEM107, TMEM216 and TMEM231 all localise in a similar pattern to MKS1 and MKS3 (Lambacher et al., 2015). These findings are consistent with reports that the NPHP module cooperates with the MKS module to form the Y-links (Jensen et al., 2015; Williams et al., 2011). MKS module proteins often have membrane interacting domains such as B9 or C2 domains, suggesting that they help to connect the Y-links to the membrane (Garcia-Gonzalo et al., 2011). Transmembrane proteins likely anchor the TZ in the ciliary membrane through their trans-

membrane domains (Basten and Giles, 2013). Two other TZ proteins, Ahi1 and Chibby both form slightly larger rings than TMEM237 (Lee et al., 2014). At present, a limited number of combinations of TZ proteins has been studied in a limited number of cell types and model systems. Some caution is therefore required in interpreting the relative localisations, however, the field is evolving rapidly and it is to be expected that more data will emerge soon.

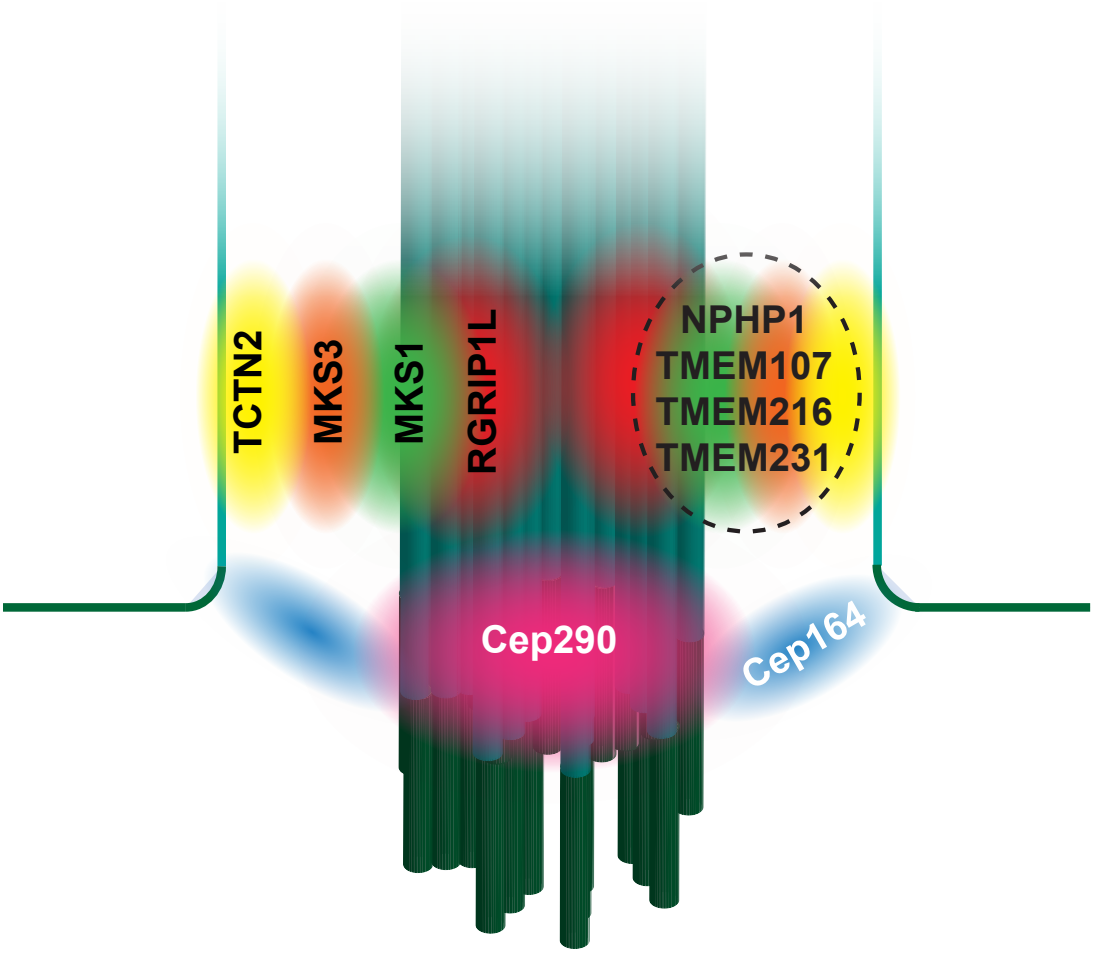

Figure 1.4 Schematic summary of TZ super-resolution data. Schematic overview of the localisation of Cep164 (*blue*), Cep290 (*pink*), RGRIP1L (*red*), MKS1 (*green*), MKS3 (*orange*), TCTN2 (*yellow*), and NPHP1, TMEM107, TMEM216 and TMEM231 (*dashed line*). Note that although super-resolution data is available for Ahi1, Chibby and TMEM237, these proteins have not been studied in relation to the microtubules or any of the proteins depicted. Therefore their relative localisations could not be accurately shown here. This figure represents data from studies in *C. elegans* and RPE-1 cells (Lambacher et al., 2015; Yang et al., 2015)

1.2.3 Intraflagellar transport

Protein translation does not take place in the cilium and the TZ forms a barrier at the base of the cilium. While small molecules will be able to diffuse through the TZ, molecules larger than 60 nm need to be actively transported across the TZ by IFT (Anderson, 1972). IFT proteins and their cargo, known as IFT trains, assemble at the TZ and are transported along the microtubules by motor proteins (Figure 1.3) (Hsiao et al., 2012; Ishikawa and Marshall, 2011). IFT is bidirectional, although there are some characteristics that distinguish anterograde (base to tip) and retrograde (tip to base) transport. In *Clamydomonas*, anterograde IFT trains are generally longer ($\sim$ 700 nm) and less electron dense than retrograde IFT trains ($\sim$ 400 nm) (Pigino et al., 2009). Furthermore, while anterograde movement is driven by the kinesin-2 family of motor proteins, retrograde transport is driven by dynein-2 (Pedersen and Rosenbaum, 2008; Rosenbaum and Witman, 2002). Recently, it was shown in *Chlamydomonas* that anterograde IFT trains are transported along four specific protofiliaments on the B-tubules, while retrograde IFT trains are transported along a specific pair of protofilaments in the A-tubule (Stepanek and Pigino, 2016). This result explains why antrograde and retrograde IFT trains have never been observed to collide, while faster and slower moving trains of each type have been shown to catch up with one another and continue their journey as one. It is worth noting that these studies were performed on the motile cilia of *Chlamydomonas*, where the presence of the ciliary dynein motors means that there is only limited space on the axonemal microtubules available for IFT cargoes to bind. It will be important to test whether IFT also only occurs on specific protofiliaments of the A- and B-tubules in non-motile cilia. IFT proteins form different complexes depending on the direction of transport. IFT-B proteins are predominantly associated with anterograde transport, while IFT-A proteins are mostly required for retrograde transport (Figure 1.3) (Cole et al., 1998; Pazour et al., 1998; Pazour et al., 1999). In the assembling cilium, IFT is required for the transport of axonemal components, including tubulin, to the growing cilia and flagella tips

(Engel et al., 2009; Hao et al., 2011). Consequently, loss of IFT-B proteins often results in short or even absent cilia. Conversely, IFT-A does not seem to be essential for the assembly of cilia, although mutations in IFT-A components do result in ciliary abnormalities, such as the mislocalisation of ciliary proteins or defects in ciliary signalling (Goetz and Anderson, 2010; Lee et al., 2008).

Several lines of evidence suggest that once the cilium has reached its final length, IFT continues to be required. First, inhibiting anterograde transport leads to shortening of flagella over time, suggesting that even in steady-state, tubulin at the ciliary tip is turning over (Marshall and Rosenbaum, 2001). Second, different types of cilia require other, non-axonemal, proteins. Primary cilia, for example, rely on IFT to import Hedgehog receptors and signalling molecules (Huangfu et al., 2003). Although the exact mechanism of IFT train assembly and regulation is not know, the IFT-B complex and axonemal proteins generally appear to accumulate at the base of the cilium (Follit et al., 2009; Qin et al., 2004), implicating a role for the TZ in the assembly and loading of IFT trains.

1.2.4 Types of cilia

While cilia have many shared characteristics, such as originating from a basal body docked at the apical membrane and an axoneme that forms a microtubule based extension of the plasma membrane, there are many different types of cilia. The most obvious distinction between cilia is between motile and immotile cilia, although distinctions can be made between subtypes in these two groups. Most motile cilia have a 9+2 microtubule configuration, with a central pair of microtubules in the middle of the axoneme that connects to the axonemal microtubules via radial spokes (Figure 1.3) (Choksi et al., 2014; Ishikawa and Marshall, 2011; Oh and Katsanis, 2012). These cilia contain a specialized form of dynein (termed ciliary dynein) that uses the energy released upon ATP hydrolysis to generate either a wave-like or a rotational movement of the cilia. Importantly, however, it is now known that some

motile cilia can have a 9+0 microtubule configuration. The mouse node, for example, appears to have a random distribution of both 9+0 and 9+2 motile cilia that generate liquid flows in the extracellular space that are important for establishing left-right asymmetry (discussed in more detail in Section 1.4.1) (Caspary et al., 2007; Odate et al., 2016). It is also important to note that some specialized cells contain more than one motile cilium. Such multi-ciliated cells are present in the human airway and fallopian tubes and seem to specialise in the movement of viscous liquids (Brooks and Wallingford, 2014; Garcia-Gonzalo and Reiter, 2012; Ishikawa and Marshall, 2011).

Immotile cilia (often termed primary cilia) have important sensory and signalling roles. The canonical primary cilium is a single cylindrical structure with a 9+0 microtubule configuration and is involved in signalling, most notably through the Hedgehog pathway (discussed in more detail in Sections 1.4.2 and 1.4.3) (Goetz and Anderson, 2010). However, many immotile cilia appear to be sensory in nature. The structure of the canonical primary cilium is similar to the sensory cilia in the kidney that sense fluid flow. In the retinal sensory neurons, a 9+0 cilium connects the dendrite to the outer segment, a specialised protrusion packed with photoreceptors. Although primary or sensory cilia do not require a central pair of microtubules for motility, some of these cilia nevertheless do have a 9+2 microtubule configuration. Olfactory cilia, for example, have a central pair of microtubules, although they do not possess the dynein arms that are required for motility (Jenkins et al., 2009). Olfactory cilia are arranged in groups of 10-30 cilia extending from olfactory knobs into the nasal mucosa and covered in olfactory receptors. Similar to olfactory cilia, the transient kinocilium in the inner ear also possess a central pair of microtubules (Schwander et al., 2010).

Cilia and flagella are present across eukaryotes and are can be traced to the last eukaryotic common ancestor (LECA) (Mitchell, 2016; Satir et al., 2008; Sung and Leroux, 2013). The widespread presence of cilia suggests a selective advantage (Silverman and Ler-

oux, 2009). Studies of different and distantly related branches of evolution suggests that the LECA had a 9+2 microtubule arrangement and most likely had both motile and sensory functions (Satir et al., 2008). It is thought that many ciliary proteins, including cilia trafficking complexes such as the IFT proteins and the BBSome, were also present in this common ancestor (Mitchell, 2016). Ultrastructural studies suggest variations in the number and arrangement of ciliary microtubules, the length and morphology of cilia as well as the presence of structures such as ciliary caps and the transition zone (Barker et al., 2014; Silverman and Leroux, 2009). An elegant study in *C. elegans* used electron tomography to reconstruct 50 out of 60 sensory cilia in the worm at high resolution and in 3D (Doroquez et al., 2014). This work highlights the variations on the canonical cylindrical mono-cilium that exist within one organism. Although all cilia share many shared characteristics, it is important to remember the different features that the organelle may present within and between species. The data presented in this thesis was obtained in *Drosophila*, which also has different types of cilia (discussed in more detail in Section 1.3).

1.3 Ciliated cells in *Drosophila melanogaster*

1.3.1 Spermatocytes

Unlike humans and other mammals, which have cilia on most cells, *Drosophila* have cilia only on two cell types; cells of the sperm lineage and a subset of sensory neurons (Kernan, 2007). *Drosophila* sperm are derived from male germ line stem cells (Figure 1.5). These cells divide asymmetrically (Yamashita et al., 2003) to regenerate the stem cell and produce a spermatogonial cell. Each spermatogonium proceeds through four rounds of mitotic division, to produce a cyst of 16 spermatocytes (Tates, 1971). The spermatocytes grow extensively over several days and then undergo two rounds of meiotic division to give rise to 64 haploid spermatids. In the 16 spermatocytes, both centrioles dock at the plasma

membrane to form a short cilium. Although this cilium is well documented, its function is unknown (Gottardo et al., 2013; Riparbelli et al., 2012; Tates, 1971). During the subsequent meiotic divisions these cilia remain intact, but are internalised in a deep membrane pocket that translocates to the nucleus; although the centrioles are still organizing a short cilium, they nevertheless recruit PCM and participate in the formation of the meiotic spindles (Riparbelli et al., 2012; Tates, 1971). After meiosis II, the mitochondria fuse and form a major and minor mitochondrial derivative that wrap around each other to form a structure known as the nebenkern (Stanley et al., 1972; Tokuyasu, 1975). In the newly formed spermatids the nebenkern forms an interleaved structure that resembles the layers of an onion, and this stage is often referred to as the "onion" stage. At this stage in spermatogenesis, the basal body is embedded in the nuclear envelope (Stanley et al., 1972). Next, both the mitochondrial derivative and the nucleus elongate (Phillips, 1970; Tokuyasu, 1974). Finally, the mature sperm are individualised (Fabrizio et al., 1998; Tokuyasu et al., 1972b; Tokuyasu et al., 1972a). This process is initiated by the individualisation complex that assembles at the mature elongated nucleus and strips away organelles, membrane and cytoplasm as it moves along the spermatids (Fabrizio et al., 1998). The mature and individualised sperm are then stored in the seminal vesicle until mating. Mature sperm have a flagellum that is approximately 1.8 mm long (Tates, 1971). Despite this great length, the assembly of the flagellum is independent of IFT in *Drosophila* (Han et al., 2003). Presumably, this is due to the fact that *Drosophila* sperm flagella are assembled in the cytoplasm, with only the last 1µm encased in a membrane (Tates, 1971; Tokuyasu, 1975). Thus, tubulin subunits could reach the growing flagellar tip by diffusion.

The flagellum axoneme is made up of 9 sets of outer doublet microtubules with a central pair of microtubules with associated dynein arms for motility. Conversely, the spermatocyte cilium is made up of triplet microtubules, like the basal body. The spermatocyte cilium lacks a central pair of microtubules, although a single tubular structure can be observed in

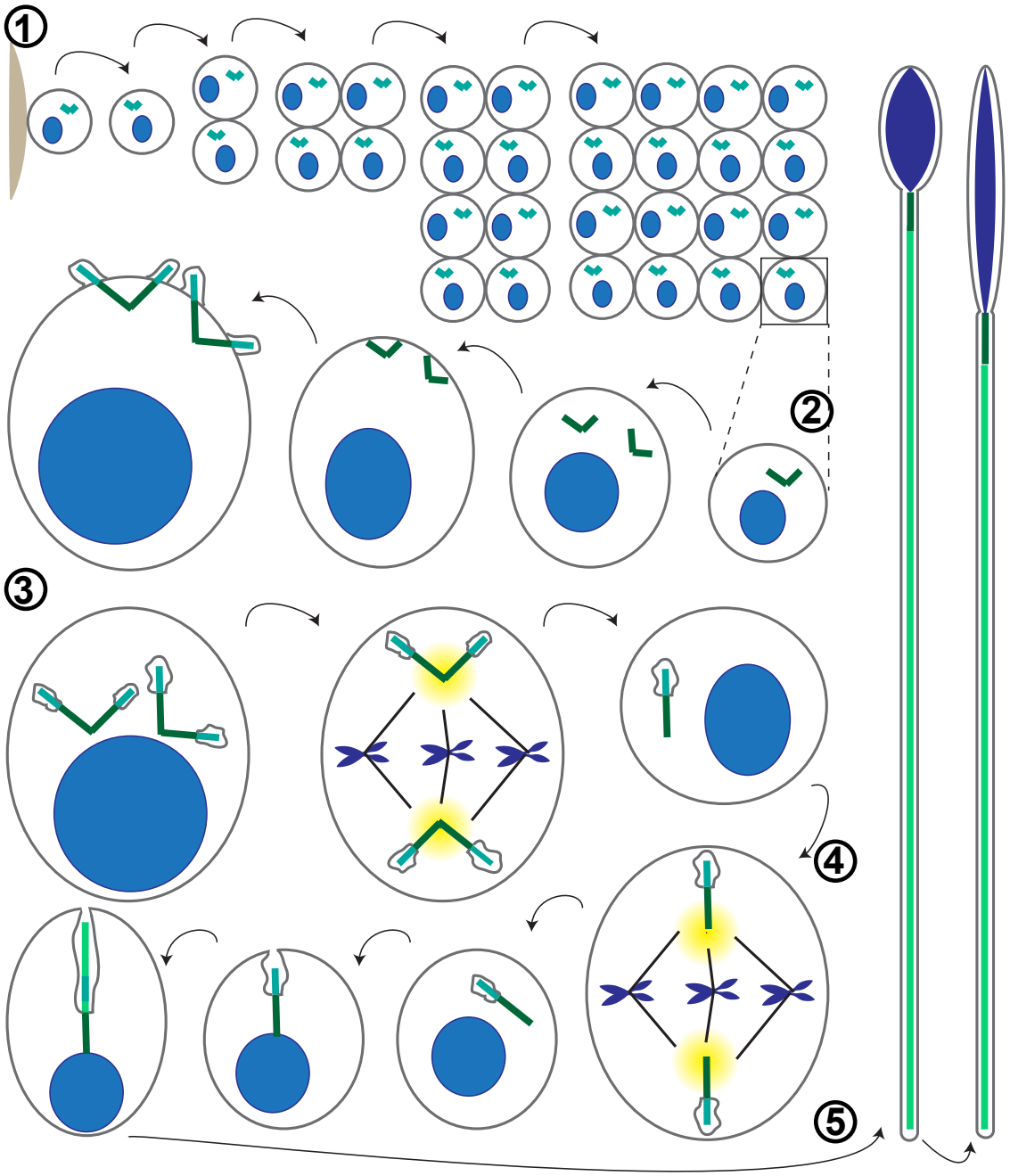

Figure 1.5 *Drosophila* spermatogenesis. Schematic overview of spermatogenesis in *Drosophila melanogaster*. 1) The GSC divides to give rise to one new GSC attached to the hub (*beige*) and one spermatogonium. Through four mitotic divisions, the spermatogonium produces 16 spermatocytes, arranged in a cyst. 2) As the spermatocytes grow and mature, the centrioles (*dark green*) duplicate, migrate to the plasma membrane and form four cilia (*aquamarine*). 3) When the spermatocytes enter mitosis, the cilia remain intact, but are internalised. The centrioles/cilia recruit PCM (*yellow*) and build the meiotic spindle. 4) The second round of meiosis gives rise to haploid spermatids with only one centriole/cilium. The cilium is remodelled and extends to form the flagellar axoneme (*light green*) The TZ migrates along the axoneme in elongating spermatids. 5) Spermatids elongate, mature and are individualised before coiling and storage in the seminal vesicle. Figure adapted from (Basiri et al., 2014; Riparbelli et al., 2012; Riparbelli et al., 2013).

the center of the basal body in spermatocyte, extending into the cilium (Fabian and Brill, 2012; Tates, 1971). The formation of this central tubular structure requires Cep135/Bld10, a protein that is also required for the formation of the central pair of microtubules in the flagellum of mature sperm (Carvalho-Santos et al., 2012; Mottier-Pavie and Megraw, 2009; Roque et al., 2012). Although it has been suggested this tubular structure is a microtubule, the conserved cartwheel proteins Sas6 and Ana2 localise to this structure, raising the possibility that it is related to the central tube of the cartwheel (Roque et al., 2012). Despite these clear differences in organisation between the spermatocyte cilium and the mature sperm flagellum, TEM analysis of different stages of spermatogenesis and microtubule regrowth assays suggest that the spermatocyte cilium persists throughout spermatogenesis and is extensively remodelled to form the sperm flagellum (Tates, 1971; Gottardo et al., 2014). It is interesting that all four centrioles form a short cilium in the spermatocyte, as in most cell types only the mother centriole can form a cilium (Vorobjev and Chentsov, 1982). This may help ensure that each of the daughter cells inherits an already established cilium after the two rounds of meiosis, perhaps indicating that the cilium serves as an important template for flagellum assembly. It remains unclear why the cilium forms two cell divisions before the flagellum, and whether this short cilium has any function that is independent of a role in guiding flagellum assembly.

1.3.2 Sensory neurons

The peripheral nervous system (PNS) of *Drosophila* comprises ciliated type I and non-ciliated type II neurons (Brewster and Bodmer, 1995; Kernan, 2007). Type I neurons each have a single dendrite with a cilium at the distal end. They are surrounded by three to four support cells, that each have a specialised role (Figure 1.6). The neuron and its support cells are all derived from a single ectodermal sensory organ precursor (SOP) cell (Brewster and Bodmer, 1995; Ghysen and Dambly-Chaudiere, 1989). In contrast, type II neurons all have

multiple dendrites and no support cells. Type I neurons may have either external sensory (ES) structures in the cuticle or internally located stretch receptors, known as chordotonal (Ch) organs (Jarman, 2002; Kernan, 2007).

Clusters of five Ch organs are involved in larval proprioception, which is required for normal locomotion (Caldwell et al., 2003a; Cachero et al., 2011; Jarman et al., 1995). In the adult, Ch organs are present in the joints of the legs and the Johnston's organ, the fly auditory apparatus (Gillespie and Walker, 2001; Göpfert and Robert, 2003; Kernan, 2007). Ch organs are made up of functional units called scolopodia. Although there may be tissue specific variations, generally, each scolopidium contains a sensory neuron, a scolopale cell that encloses the cilium in a fluid filled cavity and secretes the dendritic cap to which the tip of the cilium is attached, and a cap cell (also known as attachment cell) that connects the dendritic cap and the cuticle (Bodmer et al., 1989; Brewster and Bodmer, 1995; Brewster and Bodmer, 1996; Styczynska-Soczka and Jarman, 2015; Uga and Kuwabara, 1965). These cells are all derived from a single SOP, which also produces a ligament cell and an ectodermal cell through a series of orchestrated asymmetric cell divisions (Figure 1.6 A). Each scolopale may enclose up to three cilia (Kernan, 2007). The tip of the cilia is attached to the dendritic cap by the protein No Mechanoreceptor Potential A (NompA), while the base of the cilium is anchored by the ciliary rootlet (Chung et al., 2001; Styczynska-Soczka and Jarman, 2015). Upon mechanical stimulation, the dendritic cap pulls on the cilia and stretches them, resulting in the opening of Transient Receptor Potential ion channels (TRPs) in the ciliary membrane to generate an action potential. These TRPs are built from subunits including NompC, Nanchung (Nan) and Inactive (Iav) (Gong, 2004; Kim et al., 2003; Lee et al., 2010; Liang et al., 2011; Walker et al., 2000; Zhang et al., 2013). NompC is thought to attach to microtubules through the Ankyrin repeats at its N-terminus (Liang et al., 2013a; Zhang et al., 2015a). This mechanical tether may act as a "gating spring", transferring the macroscopic stimuli acting on the cells into microscopic stimuli that open the ion channel.

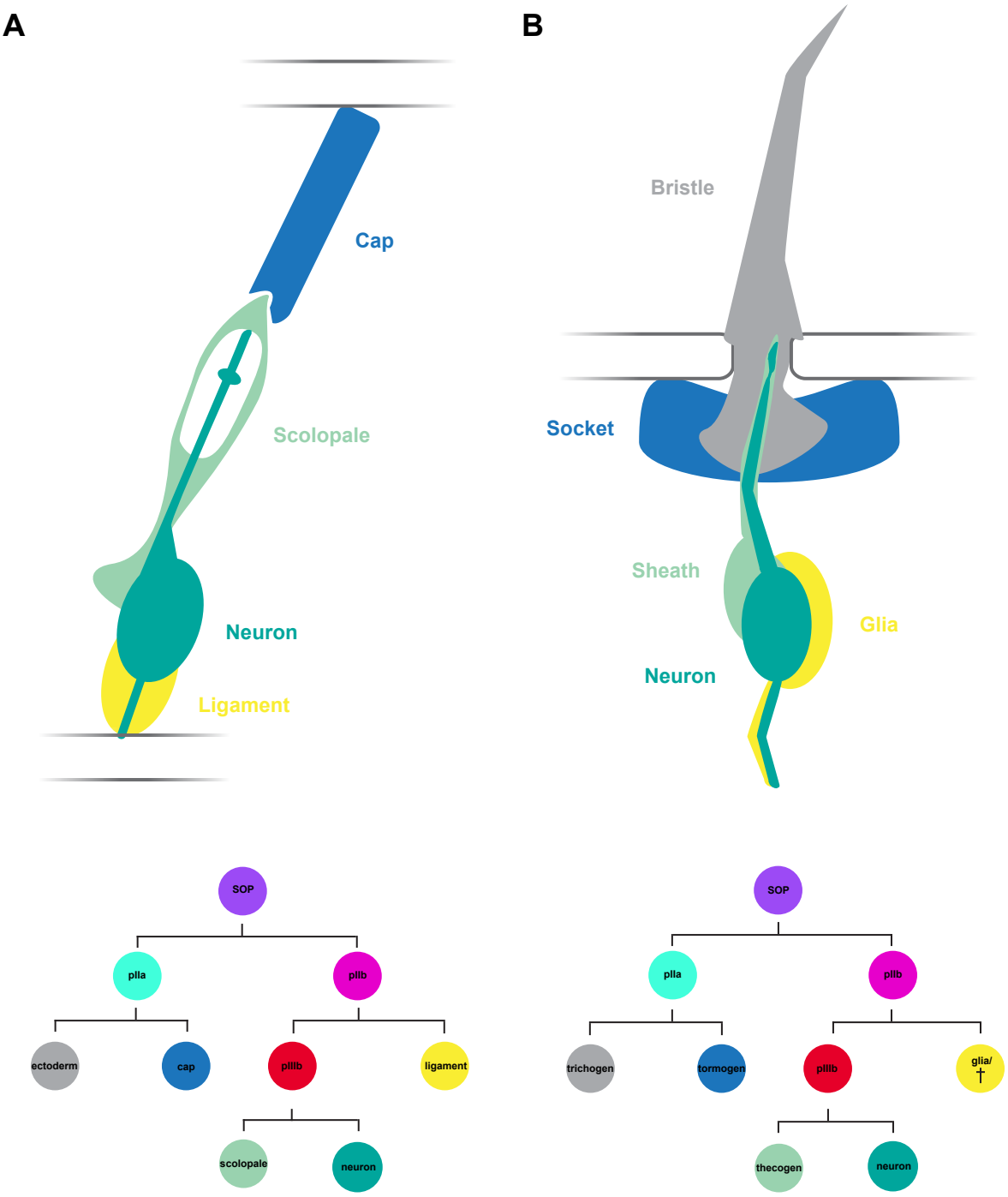

Figure 1.6 *Drosophila* ciliated neurons. Schematic overview of ciliated neurons *Drosophila melanogaster*. A) Chordotonal organ with the ciliated neuron (*aquamarine*) and the scolopale (*light green*), cap (*blue*) and ligament (*yellow*) cells (top panel) and the cell lineage of the Ch organs (bottom panel). B) External sensory organ with the ciliated neuron (*aquamarine*), the bristle and shaft (*grey*), sheath (*light green*), socket (*blue*) and glial (*yellow*) cells (top panel) and the cell lineage of the ES organs (bottom panel). Figure adapted from (Cachero et al., 2011; Kernan, 2007).

ES organs may be either mechanosensory or chemosensory. The chaete, or sensory bristles are the most abundant and best characterised ES organs. Other ES organs include the campaniform sensilla that are present on the legs, wings and haltere of the fly and that sense deformation of the cuticle (Keil, 1997). Like Ch organs, all cells of the ES organ are derived from a single SOP. In addition to the neuron, the SOP produces three other cells, the thecogen, tormogen and trichogen (Hartenstein, 1988; Hartenstein and Posakony, 1989). The thecogen is the support cell most closely associated with the neuron, while the trichogen secretes the bristle shaft and the tormogen forms the socket (Figure 1.6 B). The bristle shaft is physically connected to the tip of the cilium by NompA (Chung et al., 2001). Like in Ch organs, NompC ion channels open in response to a mechanical stimulus to generate an action potential (Kernan, 2007; Lee et al., 2010; Liang et al., 2011). The ion channel formed by the Iav and Nan subunits, however, appears to be specific to Ch organs (Gong, 2004). In addition to NompA and TRP subunits, genetic screens have revealed a number of genes required for sensory cilia function in *Drosophila* (Kernan et al., 1994; Willingham and Keil, 2004). These include two genes that are required for IFT, reduced mechanoreceptor potential A (RempA) and NompB. RempA is a member of the IFT-A complex, which is primarily associated with retrograde transport, while NompB is part of the predominantly anterograde IFT-B complex. Furthermore, NompH encodes a cytochrome P450 that is only expressed in sensory bristles, while the function of NompD is unknown (Kernan et al., 1994; Willingham and Keil, 2004).

Arguably, a third class of cilated neurons can be distinguished (Andrew Jarman, personal communication). Olfactory sensilla in the antenna are hollow sensory hairs (Benton, 2007; Joseph and Carlson, 2015; Pellegrino and Nakagawa, 2009). At first glance they appear similar to ES organs, with a cilium extending into a sensory hair. However, while ES organs extend to the base of the bristle and form a mechanical connection to the hair, the olfactory cilia are not attached to the hair at the ciliary tip. Instead, the cilia extend further

into the hair and are surrounded by a lymph that is in contact with the external environment (Benton, 2007). The olfactory sense odorants in this lymph via GPCRs embedded in the ciliary membrane. Like ES and Ch organs, olfactory ciliated neurons are surrounded by supporting cells that originate from the same SOP as the neuron (Barish and Volkan, 2015). In summary, although Ch, ES and olfactory sensilla function in different tissues, sense different stimuli and are morphologically different, there are parallels in their biogenesis and function.

Both Ch and ES organ development begins with the expression of proneural genes in specific groups of ectodermal cells called proneural clusters (Furman and Bukharina, 2012; Ghysen et al., 1993). The expression of proneural genes in these proneural clusters is most likely the result of developmental patterning (Ghysen and Dambly-Chaudiere, 1989; Ghysen et al., 1993). The proneural gene most associated with Ch organs is *atonal* (*ato*) (Jarman et al., 1993). ES organs, on the other hand, depend primarily on the *achaete-scute* complex (*AS-C*) (Campuzano and Modolell, 1992). Although initially all cells in these proneural clusters express proneural genes, only one cell goes on to become the SOP. This selection of the SOP is mediated by Notch signalling (Lai and Orgogozo, 2004). Both *ato* and *AS-C* are expressed transiently, suggesting that they initiate a signalling cascade that ultimately results in the differentiation of the sensory organs (Cachero et al., 2011). The ciliogenesis master regulator Rfx is required by both Ch and ES organs, but interestingly, Rfx is expressed at different levels in the Ch and ES lineages (Cachero et al., 2011). Furthermore, the ciliary transcription factor Fdf3 is expressed only in Ch organs and regulates the genes required for aspects of Ch ciliary specialisation (Newton et al., 2012). Therefore, it seems that by regulating the levels of expression of transcription factors and expressing a different combination of transcription factors, the proneural clusters can generate ciliated neurons with similar, yet distinct lineages and characteristics.

1.4 The role of cilia in development and signalling

1.4.1 Left-right asymmetry

A first breakthrough in understanding primary cilia function in metazoans came with the realization that primary cilia are crucial for establishing the left-right (L-R) asymmetry early in murine development. Although the cilia in the mammalian node exhibit both a 9+0 and 9+2 organisation in apparently random distribution, they are motile and rotate clockwise to displace fluid over the embryonic node (Caspary et al., 2007; Odate et al., 2016). Elegant experiments with fluorescent beads showed that the resulting fluid-flow is uni-directional, and always towards the left (Nonaka et al., 1998; Takeda et al., 1999). This displacement of fluid is therefore known as leftward flow. Following the discovery of leftward flow as the regulator of L-R asymmetry, theories proposing a molecular mechanism fell broadly in two models. The first model proposes that leftward flow could generate a gradient signalling molecules that specify the fate of the cells along the gradient, known as morphogens. The second model relies on mechanosensation of the flow by cilia and downstream signalling to pattern the embryo. Although the question has not been completely resolved, no morphogens have been identified and under experimental conditions, as few as two cilia are enough to break symmetry (Yoshiba et al., 2012). Immotile cilia surrounding the node sense this flow and rely on the Ca^{2+} ion channel PKD2 (Yoshiba et al., 2012). Defects in the rotational movement of the nodal cilia or in the ciliary localisation of PKD2 result in a failure to break symmetry or randomised asymmetry (Hirokawa et al., 2006; Yoshiba et al., 2012). It remains unclear, however, how Ca^{2+} signalling establishes L-R asymmetry (Babu and Roy, 2013). In humans, a reversed asymmetry, known as situs inversus, or non-reversed asymmetry defects, known as situs ambiguus, is a hallmark of some ciliopathies (Bisgrove and Yost, 2006; Czarnecki and Shah, 2012; Ong and Gubler, 2011; Shapiro et al., 2014; Praveen et al., 2015). The normal asymmetric arrangement of abdominal organs is known

as situs solitus. While the data described above was gathered in mammalian systems, other vertebrates including *Xenopus* and *Danio rerio*, orchestrate L-R asymmetry in similar ways (Matsui and Bessho, 2012; Schweickert et al., 2007).

1.4.2 Hedgehog signalling

The second breakthrough that established the functional importance of metazoan primary cilia came with the realization that the Sonic Hedgehog (Shh) signalling pathway relies on cilia. The Shh (Hedgehog, or Hh in *Drosophila*) signalling pathway is one of the best studied pathways and is required for developmental pattern formation, proliferation and tissue homeostasis (Huangfu and Anderson, 2005; Liu et al., 2005). In mammals, extracellular Sonic Hedgehog (Shh) binds to Patched (Ptc), a transmembrane receptor enriched in the cilium (Figure 1.7) (Rohatgi et al., 2007). Upon Shh binding, repressive mechanisms that act on the transmembrane protein Smoothened (Smo) are removed, allowing Smo to accumulate in the cilium. In the presence of Smo, Suppressor of Fu (SUFU), disassociates from Gli. This allows Gli to translocate to the nucleus where it activates the transcription of target genes (Briscoe and Thérond, 2013; Hui and Angers, 2011). In the absence of Shh ligand, Gli is phosphorylated and proteolytically processed into a repressor form (GliR). The conformational change in Smo upon Shh binding results in the release of uncleaved, active Gli (GliA). In *Drosophila*, where Hh signalling was first discovered, the pathway is very similar to mammalian Shh signalling (Nüsslein-Volhard and Wieschaus, 1980). The *Drosophila* orthologue of Gli is known as Cubitus interruptus (Ci) and relies on the activation of Fu and phosphorylated Costal2 (Cos2) for activaiton. Interestingly, *Drosohila* Ptc and Smo localise to the plasma membrane, rather than the primary cilium (Corbit et al., 2005; Rohatgi et al., 2007). Indeed, unlike in vertebrates, most cells in *Drosophila* do not have a primary cilium. It is unclear why mammalian Shh signalling requires a cilium, and there is much debate in the field about how the complex relationship between cilia assembly and Hh signalling

evolved (Goetz and Anderson, 2010; Roy, 2012). Note that it is also possible that cilia and Hh signalling evolved together and that the link between Hh and cilia has become lost in *Drosophila*. Perhaps the most likely explanation is that the gated nature of the cilium allows for enrichment of Hh signalling molecules, both in the ciliary membrane and in the ciliary cytoplasm. Such enrichment would make the pathway more efficient, which may be critically important in mammals, but not in lower eukaryotes such as the fly (Nachury, 2014).

1.4.3 Other signalling pathways

Although Hh signalling is one of the most important metazoan ciliary signalling pathways, the number of signalling pathways associated with the primary cilium is ever increasing (Nachury, 2014). It is important to note, however, that the evidence linking the function of these other pathways to cilia is usually not clear cut: whereas cilia are essential for Shh signalling in vertebrates, it seems that cilia can modulate several other pathways, often in complex ways, but that cilia are not essential for the activity of these pathways.

Although the role of the cilium in the Wnt signalling pathway has been the subject of much research and discussion, it is still not very well understood and the data is sometimes contradictory. Briefly, in canonical Wnt signalling, the binding of Wnt to the receptors Frizzled (Fz) and lipoprotein receptor-related protein 5/6 (LRP5/6) results in the disassembly of a destruction complex that sequesters β-catenin in the absence of the ligand. Accumulation of β-catenin in the nucleus switches on target genes via the activation of transcription factors (Gao and Chen, 2010). Downregulation and mutation of ciliary genes such as Kif3a, IFT88, OFD1 and Chibby has been reported to lead to an increase in nuclear β-catenin and therefore increased activation of Wnt target genes (Corbit et al., 2008; Voronina et al., 2009). However, other studies involving the downregulation or mutation of the same genes did not show any effect on Wnt signalling (Huang and Schier, 2009; Ocbina et al., 2009). These

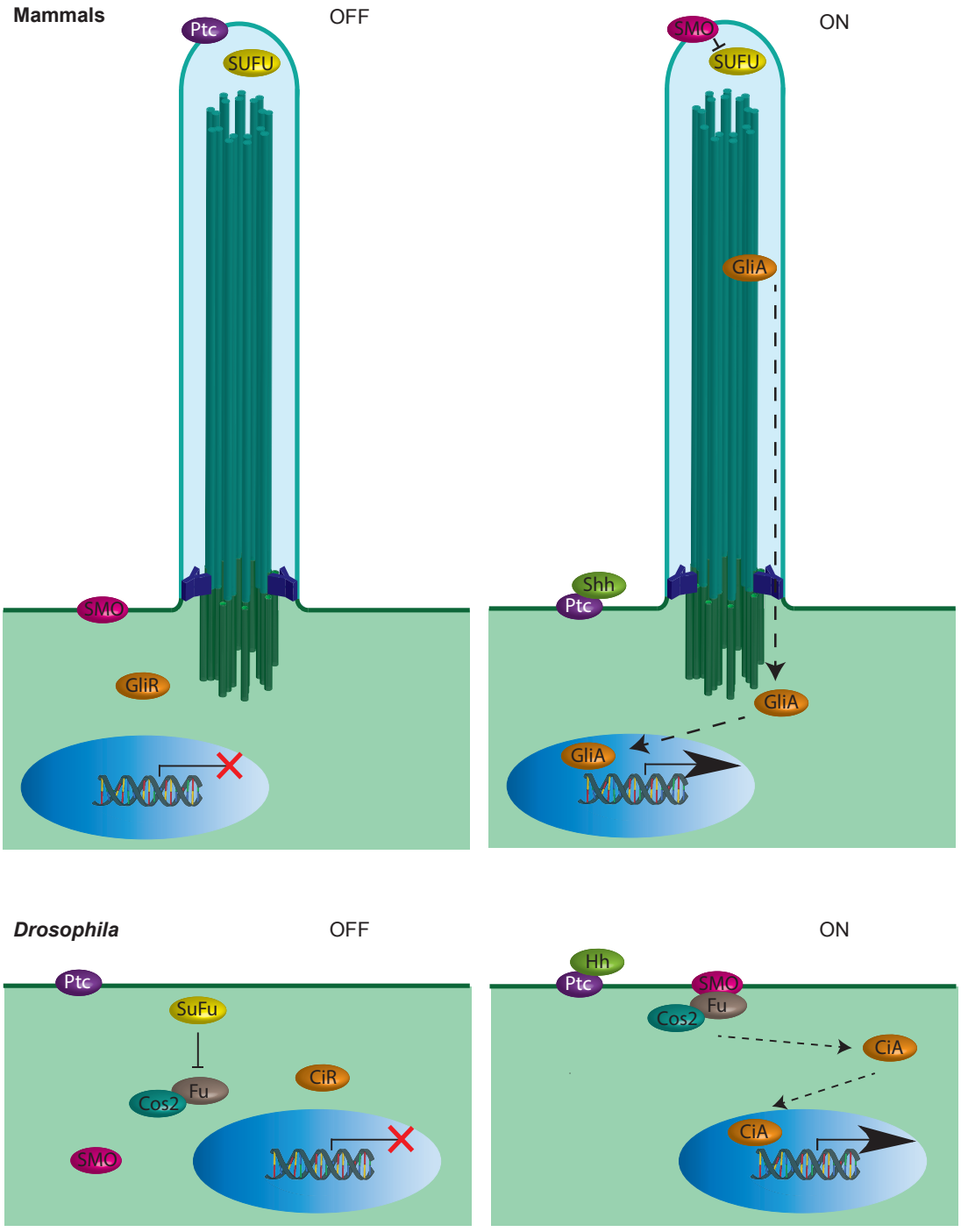

Figure 1.7 Schematic of Hh signalling in mammals and *Drosophila*. Schematic overview of Hh receptors and signalling molecules in the absence (left panel) and presence (right panel) of the Hh ligand. In mammals (top panel), binding of Hh to Ptc allows Smo to accumulate in the cilium. Smo accumulation inhibits SuFu, thus relieving the brake on Gli. GliA translocates to the nucleus where it activates the transcription of target genes. In *Drosophila* (bottom panel), Hh binding to Ptc allows Smo to translocate to the plasma membrane, which results in the activation of Fu and Cos2 and thereby the release of CiA and the transcription of target genes in the nucleus. Image adapted from (Briscoe and Thérond, 2013)

apparently contradictory results may be due to species differences, or differences between tissues and/or developmental stages. In addition to canonical signalling through β-catenin, Wnt binding to Fz, but not LRP5/6 may also mediate planar cell polarity (PCP) signalling (Wallingford and Mitchell, 2011). This non-canonical Wnt signalling is less well understood than canonical Wnt signalling, but appears to modulate intracellular Ca^{2+} levels and PCP factors (Katoh, 2005). Similar to canonical Wnt signalling, the role of cilia in PCP is not very well understood. Although PCP defects are associated with ciliopathies, there is a developing view that these defects are not due to defects in the cilium (Basten and Giles, 2013). Rather, it is thought that PCP positions the centrosomes and that defects in this positioning may explain PCP defects such as problems with convergent extension (body axis elongation) during gastrulation and subsequent defects in formation and closure of the neural tube (Carvajal-Gonzalez et al., 2016; Keller et al., 2008; Wallingford and Mitchell, 2011). Indeed, the IFT-B protein IFT88 is required for the correct positioning of the mitotic spindle (Delaval et al., 2011). Mutations in *IFT88* or related genes may then result in a failure to position the centrosome correctly downstream of PCP signalling and result in PCP defects without necessarily involving the cilium. Finally, it has been postulated that cilia may play a role in shifting the balance between canonical and non-canonical Wnt signalling (Corbit et al., 2008; Simons et al., 2005). Given the lack of understanding of Wnt signalling in general and the role of the cilium in Wnt and PCP signalling in particular, this hypothesis will require further study.

The ubiquitous second messenger Ca^{2+}, is often associated with cilia. In the human kidney, for example, the sensation of flow results in the opening of the polycystin complex (encoded by ciliopathy genes *PKD1* and *PKD2*) and the import of extracellular Ca^{2+}. Elevated Ca^{2+} mediates the conversion of cAMP to AMP by phosphodiesterase (Abdul-Majeed and Nauli, 2011). Understanding the role of Ca^{2+} signalling in the cilium is complicated not only by the variety of potential targets, but also by crosstalk between the Ca^{2+} signalling

pathway, the Wnt pathway (described above) and the mTOR pathway (Abdul-Majeed and Nauli, 2011). Furthermore, Ca^{2+} levels are not only affected by ion channels importing it from the extracellular environment, but also by release from the endoplasmatic reticulum as a downstream effect of ligand binding to GPCRs or receptor tyrosine kinases (RTKs).

RTKs were first linked to primary cilia when the ciliary localisation of platelet-derived growth factor receptor-α (PDGFRα) was found to be required for downstream activation of downstream Mek1/2-Erk1/2 signalling (Schneider et al., 2005). Following the discovery of a role for the primary cilium in PDGF signalling, the cilium has also been implicated in other RTK pathways including epidermal growth factor (EGF), insulin-like growth factor (IGF1), fibroblast growth factor (FGF) and angiopoietin (Tie2) mediated signalling (Basten and Giles, 2013; Christensen et al., 2012). Generally, the binding of a ligand to an RTK induces dimerisation and a conformational change that activates the intracellular tyrosine kinase domain. This facilitates phosphorylation of nearby RTKs and the subsequent assembly and activation of downstream signalling molecules (Lemmon and Schlessinger, 2010). RTKs form a broad family of proteins that are required for normal embryonic development and tissue homeostasis (Blume-Jensen and Hunter, 2001). As such, misregulation of these pathways may contribute to tumourigenesis. While some RTKs localise to the primary cilium, such as PDGFRα, others, including PDGFRβ localise to the plasma membrane (Schneider et al., 2005; Christensen et al., 2012). While it is not yet clear why some RTKs, but not others, localise to the primary cilium, it is possible that the primary cilium is a site for crosstalk with other signalling pathways (Christensen et al., 2012).

The Hippo pathway helps regulate tissue growth and homeostasis and has been linked to the primary cilium since NPHP4 was recently shown to negatively regulate the Hippo pathway through inhibition of the Lats1 kinase (Habbig et al., 2011). The Hippo pathway was discovered in *Drosophila melanogaster*, where it regulates tissue growth control and members of this pathway act as tumour suppressors and oncogenes in mammals (Harvey

and Tapon, 2007). Several other effector molecules of the Hippo pathway also localise to the primary cilium, although the exact role of the cilium in the Hippo pathway remains unclear (Basten and Giles, 2013).

In addition to these main signalling pathways, an ever increasing list of receptors and signalling molecules are being identified as potential components of the cilium. Recent discoveries include GPCRs somatostatin receptor 3 (Sstr3) and serotonin subtype 6 receptor (5-HT_6) as well as TGF-β and Notch (Basten and Giles, 2013; Oh and Katsanis, 2012). It seems likely that the list of signalling pathways modulated by the cilium will continue to grow over the coming years.

1.5 Ciliopathies

1.5.1 Congenital ciliopathies

While most human cells have a cilium, only a few of these cilia are motile. Motile cilia are present in the trachea, where they clear the airways of mucus and debris, in the fallopian tubes, where they propel the ovum from the ovaries to the uterus, while sperm rely on motile flagella for their movement (Brooks and Wallingford, 2014; Ishikawa and Marshall, 2011). Defects in these motile cilia have long been associated with human disease. Primary cilia dyskinesia (PCD), also known as Kartagener syndrome, is caused by impaired motility of cilia and associated with infertility in both males and females, situs defects and respiratory problems (Praveen et al., 2015). Confusingly, despite its name, PCD does not involve the dysfunction of primary cilia, but rather reflects that the disease is congenital, as opposed to secondary cilia dyskinesia, which is acquired (Praveen et al., 2015). PCD is often caused by mutations in genes required for the correct formation of dynein arms and the central pair of microtubules that are essential for motility(Bisgrove and Yost, 2006; Praveen et al., 2015).

Unlike motile cilia, primary cilia have long been regarded as a remnant of evolution.

However, genetic studies of patients suffering from diseases such as Meckel Gruber and Joubert syndrome, now known as ciliopathies, identified mutations in cilia associated genes as the cause of these diseases. This discovery sparked a renewed interest in the organelle. Many proteins encoded by ciliopathy genes localise to the base of the cilium, suggesting that defects in the TZ can cause disease (Reiter et al., 2012).

Ciliopathies tend to have overlapping phenotypes that range in severity. Renal cysts are among the most prevalent symptoms of ciliopathies. In polycystic kidney disease (PKD), cysts arise throughout the kidneys and the kidneys are massively enlarged (Boucher and Sandford, 2004). In contrast to other ciliopathies described below, PKD is caused by dominant mutations. Mutations in PKD1 and PKD2 account for >95% of the disease. Nephronophthisis (NPHP) is also characterised by kidney cysts. In contrast to PKD, the cysts are restricted to the cortico-medullar junction in the kidney and although the kidneys progressively become more cystic, they are not typically enlarged (Bergmann et al., 2008). NPHP is the mildest form of a continuum of ciliopathies. When associated with degeneration of the photoreceptors and loss of vision as a result of retinis pigmentosa, the disease is known as Senior-Løken syndrome (SLSN). Joubert syndrome (JBTS) includes both retinal degeneration and cortico-medullar renal cysts, but is also associated with CNS defects. In Magnetic Resonance Imaging (MRI), a "molar tooth sign" can be observed in JBTS. This is a malformation of the hindbrain that resembles a molar tooth and is associated with hypotonia, ataxia and intellectual disability. More severe central nervous system (CNS) defects, including encephaloce, as well as polydactyly and hepatic fibrosis are associated with MKS. Given the severity of the disease, MKS usually results in fetal or perinatal death (Czarnecki and Shah, 2012; Ong and Gubler, 2011). A genetically and clinically distinct ciliopathy is Bardet-Biedl syndrome (BBS). In addition to the ciliopathy symptoms described above, BBS is also commonly associated with obesity, diabetes, hypertension and congenital heart disease (Bisgrove and Yost, 2006; Forsythe and Beales, 1993). Unlike the NPHP-SLSN-

JBTS-MKS continuum of ciliopathies, BBS is typically not associated with mutations of TZ genes. Instead, the disease is caused by mutations in the BBSome (named after the disease), which forms a cilia specific transport complex (Jin et al., 2010).

Interestingly, mutations in the same gene can underlie different ciliopathies. For example, mutations in *MKS1* and *Tectonic* are associated with both MKS and JBTS. Recent research suggests that truncating mutations are associated with the more severe MKS syndrome, while non-truncating mutations underlie the milder JBTS (Huppke et al., 2014; Slaats et al., 2015; Szymanska et al., 2014). However, in many cases the genotype-phenotype correlation is still poorly understood. A better understanding of protein function and interaction as well as the identification of key residues and domains will help to achieve a better understanding of the mechanism by which mutations in the same gene are associated with milder or more severe manifestations of disease along the spectrum of ciliopathies.

1.5.2 Acquired ciliary disease

Since cilia are present on most human cells and are involved in a multitude of signalling pathways, they have the potential to cause or modulate many different human diseases. Indeed, in addition to congenital ciliopathies, cilia dysfunction has now been linked with more common diseases such as cancer and obesity. Many different cilia-associated genes, including *Gli1*, *RGRIP1L*, *NPHP9*, have been found to be mutated in a wide range of cancers (Hassounah et al., 2012). A wide range of cancers including glioblastoma, melanoma, medullablastoma and basal cell carcinoma as well as breast, pancreatic, prostate and ovarian cancer require upregulated Hh signalling in order to survive and progress (Basten and Giles, 2013; Hassounah et al., 2012; Teglund and Toftgard, 2010). Interestingly, cilia can both promote and repress an increase in Hh signalling (Barakat et al., 2010; Han et al., 2009; Hassounah et al., 2012; Pasca di Magliano and Hebrok, 2003; Seeley and Nachury, 2010). While mutations in upstream Hh genes, such as Ptc, Smo and Shh, require cilia for the pro-

cessing of the signal and the activation of target genes, mutations in downstream genes such as GliA, bypass the requirement for cilia (Han et al., 2009; Wong et al., 2009). In tumours driven by downstream Hh mutations, the presence of cilia can dampen Hh signalling by the presence of GliR and these cancers often lose cilia (Hassounah et al., 2012). The dual role of cilia in Hh signalling as well as the distinction between upstream and downstream mutations has implications for the potential success of Hh inhibitors in cancer therapy. While Hh inhibitors are effective in trials in cell lines and some mouse models, the efficacy in clinical trials has been mixed (Hassounah et al., 2012; Ng and Curran, 2011). This is partially due to the fact that most Hh inhibitors target upstream Hh signalling, which is not effective in tumours with downstream mutations and is susceptible to resistance by tumours acquiring downstream Hh mutations (Ng and Curran, 2011; Gonnissen et al., 2015). Some success has been reported for clinical trials using Gli inhibitors such as GANT61, although further studies of the efficacy and toxicity in different types of cancer will be required (Gonnissen et al., 2015).

Cilia have long been associated with metabolic defect in the context of ciliopathies such as BBS. This has led to speculation that cilia may play a role in acquired hypertension, obesity and diabetes (Davenport and Yoder, 2005). Recently, advances have been made in understanding how the cilium and ciliopathy genes influence blood pressure, appetite and glucose levels. Normal Shh signalling is required for the correct development of the pancreas, with defects in cilia associated with loss of endocrine tissue (Lodh et al., 2014). Furthermore, cilia are required for the regulation of adipogenesis, uptake of insulin in muscle and modulation of the satiety hormone leptin (Andersen and Sandholt, 2015; Oh et al., 2015). Primary cilia appear to required for an adequate response to shear stress in the vascular endothelial cells, while kidney cysts result in renal ischaemia. Cilia defects, therefore, misregulate the angiotensin-aldosterone system, which results in hypertension (Ando and Yamamoto, 2013; Chapman et al., 2010). However, at present there is little evidence of

a major causal role for cilia in hypertension or metabolic disorders outside of congenital ciliopathies (Andersen and Sandholt, 2015; Davenport and Yoder, 2005).

1.5.3 Cilia disease mechanism

In the motile ciliopathy PCD, the respiratory and fertility symptoms observed are a direct result of the reduced or abnormal beating patterns of cilia in the airways and reproductive system (Bisgrove and Yost, 2006; Basten and Giles, 2013; Praveen et al., 2015). Situs defects, which include both situs inversus, or a mirrored organ system and situs ambiguus, non-mirrored organ laterality defects, are present in ~ 50 % of patients, suggesting situs organisation is random in PCD patients (Shapiro et al., 2014). Since cilia are required for L-R asymmetry (see Section 1.4.1), situs defects can be traced to defects in the beating of the motile cilia in the node (Praveen et al., 2015).

For immotile ciliopathies, the disease mechanism is less straightforward and less well understood. As discussed above (Section 1.5.1), immotile ciliopathies have an overlapping range of symptoms that may include kidney cysts, situs inversus, polydactyly and neural tube defects (Bisgrove and Yost, 2006; Ong and Gubler, 2011; Powles-Glover, 2014). Kidney cysts are caused by a defect in Ca^{2+} signalling, which leads to overproliferation of the kidney epithelium via changes in Wnt, Ras/Raf/ERK and mTOR pathways (Abdul-Majeed and Nauli, 2011). Similar to PCD, situs defects are due to defects either in the generation of leftward flow by the motile cilia of the node, or a failure to sense this flow by the sensory cilia that surround the node, or both (Basten and Giles, 2013; Bisgrove and Yost, 2006; Czarnecki and Shah, 2012; Ong and Gubler, 2011; Powles-Glover, 2014). Since Shh signalling is required for limb patterning and many polydactyly mouse mutants have defects in Shh signalling, polydactyly is most likely a Hh defect, rather than a defect in the cilium itself (Haycraft et al., 2005; Laufer et al., 1994; Ocbina and Anderson, 2008; Wang et al., 2000). Similarly, the patterning of the neural tube is dependent on Shh (Pal and Mukhopadhyay,

2015; Sasai and Briscoe, 2012; Vogel et al., 2012). The Wnt and PCP signalling pathways have also been implicated in neural tube defects (see Section 1.4.3), suggesting that the proper patterning of the neural tube depends on several signalling pathways that can be influenced by cilia (Sasai and Briscoe, 2012; Vogel et al., 2012). Defects in the neural tube lead to clinical defects including encephalocele, hydrocephalus and intellectual disability (Czarnecki and Shah, 2012; Davis and Katsanis, 2012; Powles-Glover, 2014; Vogel et al., 2012). As these examples illustrate, the dependency of Hh and other signalling pathways on cilia makes it hard to distinguish Hh defects from pure cilia defects in mammals. For this reason, *Drosophila* could be a useful system to study cilia biogenesis and to separate Hh defects in particular from cilia defects. This information will be a valuable addition to studies of animal models of ciliopathies.

1.6 Thesis outline

In this thesis, the suitability of *Drosophila* as a model organism to study ciliogenesis *in vivo* is addressed, with a particular focus on genes involved in the assembly of the TZ that have been implicated in human disease. In Chapter 3, the generation and characterisation of novel mutant alleles for three *Drosophila* ciliopathy genes are described. Further characterisation of the *MKS1* mutant allele, $MKS1^{\Delta 1}$, is described in Chapter 4 for spermatocyte cilia and in Chapter 5 for the sensory cilia that innervate the bristles. Finally, preliminary *in vivo* studies of Cep104, which may be involved in ciliogenesis, are described in Chapter 6. The data presented on the MKS module was part of a collaborative project with a post-doc in the lab, Dr. Hélio Roque, who acquired some of the data presented in this thesis. Some of the data presented in Chapter 6 was acquired by a part II student, Zai Gen Tan, who I supervised. Wherever there is any data acquired by or in collaboration with others, this is indicated in the text.

Chapter 2

Materials and methods

2.1 Fly husbandry

2.1.1 Fly handling

Flies were reared on *Drosophila* culture medium (5.5% glucose, 5% yeast extract, 3.5% wheat flour, 1% penicillin/streptomycin, 0.4% propionic acid, 0.25% nipagen) in 8x2.5 cm plastic vials or 0.25 pint plastic bottles. These were kept at 18°C or 25°C. Embryos were collected at 25 °C on fruit juice agar plates (25% fruit juice, 2.5% sucrose, 2.1% agar), supplemented with fresh yeast. Standard fly handling techniques were used (Roberts, 1986).

2.1.2 *Drosophila melanogaster* stocks

w^{67} was used as the wild type stock in all experiments. Phenotypic markers and balancer chromosomes used in this study have been described previously (Lindsley and Zimm, 1992). *Drosophila* stocks used in this thesis are listed in Table 2.1.

Table 2.1 *Drosophila* stocks used in this thesis

Stock name	Description	Origin
p{EPgy2}CG2556^{EY2042}	Used to create *MKS1*$^{\Delta 1}$	Bloomington Stock Center
Sb[Sco]/CyPTb	p-element transposase	Bloomington Stock Center
MKS1$^{\Delta 1}$	MKS1 mutant	This thesis
NosG4VP16 UAS-cas9	Used to generate *B9D1*$^{\Delta 1}$	Simon Bullock, MRC LMB
B9D1$^{\Delta 1}$	B9D1 mutant	This thesis
CC2D2A$^{\Delta 1}$	CC2D2A mutant	Hélio Roque, Raff Group
Cep290^{MecH}	Cep290 mutant	Tomer Avidor-Reiss, University of Toledo
Plp^{5}	Plp mutant	Maruxa Martinez-Campos, Raff Group
DfPlp	Plp deficiency	Bloomington Stock Center

2.1.3 Generation of transgenic lines

Transgenic fly lines were generated through microinjection of the transgene in a p-element transformation vector marked with the red eye colour w^+ gene (see Section 2.4.4) into w^{1118} embryos. Microinjection, selection of transgenic flies and mating of individual transgenic flies to establish a line were carried out by either BestGene Inc or the Department of Genetics, University of Cambridge. Upon arrival in the laboratory, the transgenes were mapped and balanced using standard protocols (Greenspan, 2004). Stocks were kept as either homozygous or balanced stocks. All transgenic lines used in this thesis are listed in Table 2.2.

Table 2.2 Transgenic *Drosophila* lines used in this thesis

Stock name	**Description**	**Origin**
pUbq-GFP-MKS1	N-terminal GFP fusion to MKS1	This thesis
pUbq-MKS1-GFP	C-terminal GFP fusion to MKS1	This thesis
pUbq-B9D1-GFP	C-terminal GFP fusion to B9D1	This thesis
pUbq-B9D2-GFP	C-terminal GFP fusion to B9D2	This thesis
eMKS1-mCherry	C-terminal mCherry fusion to MKS1	This thesis
eCC2D2A-GFP	C-terminal GFP fusion to CC2D2A	Hélio Roque, Raff Group
pUbq-TMEM216-GFP	C-terminal fusion to TMEM216	Alan Wainman, Raff Group
pUbq-Tectonic-GFP	C-terminal fusion to Tectonic	Alan Wainman, Raff Group
eCby-GFP	C-terminal GFP fusion to Chibby	Bénédicte Durand, Claude Bernard University
pGFP-P6YM2 GFP-NompA	NompA GFP trap	Maurice Kernan
pUAS-NompC-GFP	C-terminal GFP fusion to NompC	Yuh Nung Jan, HHMI
NompC-Gal4	Gal4 driver under NompC control	Yuh Nung Jan, HHMI
eGFP-NompB(32-2)	N-terminal GFP fusion to NompB	Maurice Kernan, Stony Brook University
eRempA-YFP	C-terminal YFP fusion to RempA	Maurice Kernan, Stony Brook University
Jupiter-mCherry	C-terminal GFP fusion to Jupiter	Renata Basto, Institute Curie

2.1.4 Generation of the *MKS1*$^{\Delta 1}$ allele

The *MKS1*$^{\Delta 1}$ allele was generated through imprecise p-element excision. A p-element 581 bp upstream of *MKS1*, P{EPgy2}CG2556^{EY02042}, was mobilised by the transposase Δ2-3Sb through crossing. The p-element is marked with a w^+ and progeny where the p-element has been excised can therefore be selected by screening for the absence of the red eye colour. When p-element excision is imprecise, some of the flanking genomic DNA is deleted. This was screened for by single fly diagnostic PCR and confirmed by Sanger sequencing (see Section 2.4.2 and Section 2.4.6, respectively).

2.1.5 Generation of the *B9D1*$^{\Delta 1}$, *CC2D2A*$^{\Delta 1}$ and *Cep104*$^{\Delta 1}$ alleles

The *B9D1*$^{\Delta 1}$, *CC2D2A*$^{\Delta 1}$ and *Cep104*$^{\Delta 1}$ mutant alleles were all generated by CRISPR genome engineering (Jinek et al., 2012). Synthetic guide RNAs (sgRNAs) were designed to target the 5' end of *B9D1*, *CC2D2A* and *Cep104* for cleavage by the Cas9 endonuclease (see Table 2.3). Repair of the double-strand breaks induced by the Cas9 endonuclease through non-homlogous end joining (NHEJ) can result in small insertions or deletions (indels), which may cause a frameshift. The sgRNA sequences were cloned into the pCDF3-dU6:3gRNA plasmid (Port et al., 2014), Addgene plasmid #49410) and microinjected into *Drosophila* embryos expressing the Cas9 gene under the control of the Nanos promoter (Port et al., 2014). Injected embryos were left to develop into adults and screened for indels by single wing PCR and high-resolution melt analysis (HRMA) (see Section 2.4.3). Indels were then precisely determined by Sanger sequencing.

Table 2.3 gRNAs used in this thesis

Gene	Construct name	Target sequence
B9D1	JR_CG14870_1	GAAAGGTGGCCGAGACTATTTGG
	JR_CG14870_2	CATCGTGGGCCAAATAGTCTCGG
	JR_CG14870_3	CATCAGTCTCCCGGGCAACGAGG
CC2D2A	CG43370_exon1_3	GCAAAAGTTGATAAGGGCAACGGAAGGCAG
Cep104	Cep104_exon1_1	CCTGAGGCGAACACCACGTTAAA
	Cep104_exon3_1	TGTGTCCACGTAGGGGCACA

2.2 Behavioural assays

2.2.1 Larval hearing assay

10 third instar larvae per experiment were selected and transferred to a fruit juice agar plate. This was placed on top of a speaker through which 10 pure 500 Hz tone of 1 second duration were played at 10 second intervals. The responses of the larvae were filmed and movies were blinded before scoring the behaviour. Pauses and changes of direction were scored as 1, retractions as 2 and freezing over between two time points as 3. Each of the 3 technical replicates is presented as an average of the behaviour of 10 larvae over 10 time points.

2.2.2 Larval crawling assay

10 third instar larvae per condition were selected and transferred to a fruit juice agar plate. The larvae were filmed for 2 minutes while crawling around without stimuli. The movies were then blindly analysed in Fiji (Schindelin et al., 2012), using the NeuronJ plugin. The movements of the larvae were traced manually and the length and number of vertices mea-

sured. Each larvae is presented as a separate data point.

2.2.3 Climbing assay

For the standard climbing assay, 15 1-3 day old adult flies were collected in a plastic 25 ml measuring cylinder and knocked to the bottom of the cylinder by tapping. The flies were then allowed to crawl up the sides of the measuring cylinder and the number of flies above 12 cm was counted. Data is presented as the averages of 3 technical replicates. To measure the distance climbed by individual flies, 10 1-3 day old adult flies were collected in a glass 10 ml measuring cylinder. The flies were filmed being knocked to the bottom and crawling up the sides of the measuring cylinder. To allow the flies being filmed, a glass measuring cylinder had to be used. As this was shorter than the 25 ml measuring cylinder used above, the experimental time was reduced to 7 seconds to prevent flies reaching the top of the measuring cylinder within the experimental time frame. The distance climbed by each fly was measured in Fiji (Schindelin et al., 2012). Data is represented as the average of 5 technical replicates.

2.2.4 Fertility

To asses whether flies were sterile, 25 single mutant or WT flies were crossed to 3 WT flies of the opposite sex. Progeny was counted and flies were classed as sterile if no progeny was obtained. To quantify male fertility, single mutant or WT flies were crossed to 3 WT females. Hatched embryos were counted every morning and evening for 6 days. Each of the 25 biological replicates is presented as the average number of hatched embryos per day.

2.2.5 Grooming assay

10 flies for each time point were covered in Reactive Yellow 86 dust (Organic Dyestuffs Corporation) by shaking them in a vial. Excess dust was removed by gently tapping the

flies against the mesh of a cage (Seeds et al., 2014). The flies were then left to groom themselves for 0, 30, 60 or 90 minutes before being anaesthetised and decapitated. Pictures of the head and the notum were then taken on a dissecting microscope equipped with a Digital Sight camera (Nikon). Images were analysed using Fiji (Schindelin et al., 2012).

2.2.6 Electrophysiology

Individual 2-4 day old males were collected and immobilised on a dissection plate. A tungsten wire reference electrode was placed in the thorax. Bristles were cut at the midpoint before placing a measuring electrode filled with 121 mM K^+, 9mM Na^+, 0.5 mM Ca^{2+}, 4 mM Mg^{2+}, 35 mM glucose and 5 mM HEPES (pH 7.1) over them (Kernan et al., 1994). The bristles were then moved 30µm towards the body to evoke a mechanical response potential (MRP) using a piezo electric stage. MRPs were calculated using Clampfit 10.5 (Molecular Devices).

2.3 Bioinformatics

2.3.1 BLAST

Uniprot BLAST (n->n) was used to find candidate orthologues of human ciliopathy proteins in the *Drosophila* database and assess the conservation from humans to *Drosophila*.

2.3.2 Domain predictions

The COILs server (Lupas et al., 1991) and PSIPRED Protein Sequence Analysis Workbench (Jones, 1999) were used to predict protein structure and domains from the nucleotide sequence.

2.3.3 gRNA design

The CRISPR target finder (Gratz et al., 2013) was used to find 18-21 nt 5'-NGG-3' protospacer adjacent motif (PAM) sites, required for Cas9 cleavage. Candidate gRNAs with low off-target potential as assessed by the CRISPR target finder and close to the 5' end of the coding sequence were selected. Since a 5' guanine is required for transcription from U6 promoters, gRNAs that lacked a 5' guanine were extended with a guanine at the 5' end.

2.4 Molecular biology

2.4.1 Genomic DNA preparation

Individual flies or severed wings were squashed in squishing buffer (10 mM Tris HCl pH 8, 1 mM EDTA, 25 mM NaCl), supplemented with 200 µg/ml proteinase K just before use. 50 µl of buffer was used for whole flies, 10 µl for wings. DNA was extracted from the samples by incubating at 55°C for 30 minutes and the proteinase was inactivated by incubating at 95°C for 10 minutes.

2.4.2 PCR

PCRs for cloning purposes were performed using Phusion High-Fidelity PCR 2x Master Mix (NEB), using the following protocol:

98°C	30 seconds	
98°C	10 seconds	} repeat 30 times
45-72°C	30 seconds	
72°C	30 seconds/kb	
72°C	10 minutes	

Diagnostic PCRs were performed using One*Taq* Quick-Load 2x Master Mix (NEB) using the following protocol:

94°C	30 seconds	
94°C	30 seconds	} repeat 30 times
45-68°C	1 minute	
68°C	1 minute/kb	
68°C	5 minutes	

PCR products were analysed using 1% agarose gel and prestained markers (NEB) to assess their size. All primers used in this thesis are listed in Table 2.4.

Table 2.4 Primers used in this thesis

Primer name	**Direction**	**Sequence**	**Use**
Pratt_Oligo5	Forward	GGGGACAAGTTTGTACAAAAA AGCAGGCTCCCAAAAAAGCA GAGACATAAAGC	Clone pUbq-GFP-MKS1
Pratt_Oligo6	Reverse	GGGGACCACTTTGTACAAGAA AGCTGGGTCTTAAAACTCAGC CTGGTAGT	Clone pUbq-GFP-MKS1
Pratt_Oligo7	Forward	GGGGACAAGTTTGTACAAAAA AGCAGGCTCCATGCAAAAAA GCAGAGACAT	Clone pUbq-MKS1-GFP
Pratt_Oligo8	Reverse	GGGGACCACTTTGTACAAGAA AGCTGGGTCAAACTCAGCCT GGTAGTATG	Clone pUbq-MKS1-GFP
Pratt_Oligo73	Reverse	AAACTCAGCCTGGTAGTATGC	Clone eMKS1-mCherry

Pratt_Oligo73a	Forward	AGGCCTAAATTCTCCATCGTC	Clone eMKS1-mCherry
Pratt_Oligo75	Reverse	GGGGACCACTTTGTACAAGAA AGCTGGGTCAAACTCAGCCT GGTAGTATGC	Clone eMKS1-mCherry
Pratt_Oligo75a	Forward	GGGGACAAGTTTGTACAAAAA AGCAGGCTCCAGGCCTAAATT CTCCATCGTC	Clone eMKS1-mCherry
Pratt_Oligo39	Forward	CACCGTCTCTGCATCTTCCA	Screen for MKS1 deletions
Pratt_Oligo40	Reverse	CTGTTTATCGGCGGTTGCG	Screen for MKS1 deletions
Pratt_Oligo53	Forward	GTACATACATATGCTTCTCAC GTTT	Screen for MKS1 deletions
Pratt_Oligo68	Reverse	GGGGACCACTTTGTACAAGAA AGCTGGGTCTTAATCCGG ATAGACATAGAG	Clone MKS1 NT antibody fragment
Pratt_Oligo69	Forward	GGGGACAAGTTTGTACAAAAA AGCAGGCTCCGACGATGAT GGTTTCTCT	Clone MKS1 CT antibody fragment
Pratt_Oligo70	Reverse	ATCCGGATAGACATAGAG	Clone MKS1 NT antibody fragment
Pratt_Oligo71	Forward	GACGATGATGGTTTCTCT	Clone MKS1 CT antibody fragment

Pratt_Oligo85	check	ATGAGCGCCAGCGAAGGCAT	Clone pUbq-B9D1-GFP
Pratt_Oligo86	Reverse	GGAGTGCCAATGGTAGCCCA	Clone pUbq-B9D1-GFP
Pratt_Oligo87	Forward	ATGGCGGAGGTGCACATAATC	Clone pUbq-B9D2-GFP
Pratt_Oligo88	Reverse	CTTGAACTCCACGCCGTATTC	Clone pUbq-B9D2-GFP
Pratt_Oligo89	Forward	GGGGACAAGTTTGTACAAAA AAGCAGGCTCCATGAGCG CCAGCGAAGGCAT	Clone pUbq-B9D2-GFP
Pratt_Oligo90	Reverse	GGGGACCACTTTGTACAAGAA AGCTGGGTCGGAGTGCC AATGGTAGCCCA	Clone pUbq-B9D2-GFP
Pratt_Oligo91	Forward	GGGGACAAGTTTGTACAAAA AAGCAGGCTCCATGGCGG AGGTGCACATAATC	Clone pUbq-B9D2-GFP
Pratt_Oligo92	Reverse	GGGGACCACTTTGTACAAGAA AGCTGGGTCCTTGAACTC CACGCCGTATTC	Clone pUbq-B9D2-GFP
Pratt_Oligo157	Forward	TTCGCGTCAGGCTCAGGACC GC	Cep104 F482A mutagenesis
Pratt_Oligo158	Reverse	TAGAACTGCTCCACCAGC	Cep104 F482A mutagenesis

Pratt_Oligo159	Forward	AGAGATGCCGATTACTCCGT GTTTAG	Cep104 V532D mutagenesis
Pratt_Oligo160	Reverse	TACAGCGCGATGCAGCAG	Cep104 V532D mutagenesis
Pratt_Oligo161	Forward	AGAGATGCCGCTTACTCCGTG	Cep104 V532A mutagenesis
Pratt_Oligo162	Reverse	TACAGCGCGATGCAGCAG	Cep104 V532A mutagenesis
Pratt_Oligo163	Forward	GGAGCCTGTGGCAAAGGTG GCC	Cep104 R667A mutagenesis
Pratt_Oligo164	Reverse	GCTGGATGATGGATGCCG	Cep104 R667A mutagenesis

2.4.3 HRMA

Primers were designed to give 100-200 nucleotide PCR products spanning the region to which the sgRNAs were targeted. Indels result in a shift in the melting temperature of the heteroduplex, which can be detected by labelling the DNA with a dye that fluoresces only when bound to double stranded DNA and following the fluorescence signal during a 70°C-90°C temperature gradient. PCR reactions were assembled with 5 µl 2x Hotshot Diamond PCR MasterMix (Clent Lifescience), 1 µl genomic DNA, 200 nM of each primer and 1µl LC Green Plus dye (BioFire Diagnostics) and amplified and analysed in a RotorGeneQ real time cycler, using the RotorGeneQ software (Qiagen). Samples with non-WT melting curves were treated with ExoSAP (Affymetrix) to remove nucleotides and primers before Sanger sequencing to verify and map the indels.

2.4.4 Construction of plasmids

cDNAs for all genes were obtained from the Berkeley Drosophila Genome Project and prepared for use in the Gateway cloning system (Invitrogen) by adding attB sequences at both ends of the constructs by PCR as described in section 2.4.2. The PCR products were purified using the QIAquick PCR Purification kit (Qiagen) and recombined into the pDONR Zeo entry vector, before recombining into pUbq, pRNA, pMal-cx2 plasmids or a promotorless plasmid modified from the pUbq as listed in Table 2.5. Plasmids were transformed into competent cells according to manufacturer's instructions and purified using Miniprep or Midiprep kits (Qiagen). All plasmids were fully sequenced to verify the inserts (see Section2.4.6).

Table 2.5 Plasmids used in this thesis

Construct	**Type of plasmid (selection cassette)**
pUbq-GFPMks1	Gateway expression vector (KanR)
pUbq-Mks1GFP	Gateway expression vector (KanR)
pUbq-B9D1GFP	Gateway expression vector (KanR)
pUbq-B9D2GFP	Gateway expression vector (KanR)
eMks1mCherry	Gateway expression vector (KanR)
pMal-cx2-Mks1$^{1\text{-}905}$	MBP-fusion protein expression vector (AmpR)
pMal-cx2-Mks1$^{1218\text{-}2100}$	MBP-fusion protein expression vector (AmpR)
pRNA-Cep104GFP	T3 RNA polymerase promoter vector (AmpR)
pRNA-Cep104$^{\Delta APC}$GFP	T3 RNA polymerase promoter vector (AmpR)
pRNA-Cep104$^{\Delta APC\text{-}l1}$GFP	T3 RNA polymerase promoter vector (AmpR)
pRNA-Cep104$^{\Delta APC\text{-}CC}$GFP	T3 RNA polymerase promoter vector (AmpR)
pRNA-Cep104$^{\Delta APC\text{-}l2}$GFP	T3 RNA polymerase promoter vector (AmpR)
pRNA-Cep104$^{\Delta APC\text{-}TOG}$GFP	T3 RNA polymerase promoter vector (AmpR)

pRNA-Cep104$^{\Delta APC\text{-}l3}$GFP	T3 RNA polymerase promoter vector (AmpR)
pRNA-GFPCep104	T3 RNA polymerase promoter vector (AmpR)
pRNA-GFPCep104$^{\Delta ZNF}$	T3 RNA polymerase promoter vector (AmpR)
pRNA-GFPCep104$^{\Delta l3\text{-}ZNF}$	T3 RNA polymerase promoter vector (AmpR)
pRNA-GFPCep104$^{\Delta TOG\text{-}ZNF}$	T3 RNA polymerase promoter vector (AmpR)
pRNA-GFPCep104$^{\Delta l2\text{-}ZNF}$	T3 RNA polymerase promoter vector (AmpR)
pRNA-GFPCep104$^{\Delta CC\text{-}ZNF}$	T3 RNA polymerase promoter vector (AmpR)
pRNA-GFPCep104$^{\Delta l1\text{-}ZNF}$	T3 RNA polymerase promoter vector (AmpR)
pCDF3-dU63:gRNA-JR_CG14870_1	Nanos gRNA vector (AmpR)
pCDF3-dU6:3gRNA-JR_CG14870_2	Nanos gRNA vector (AmpR)
pCDF3-dU6:3gRNA-JR_CG14870_3	Nanos gRNA vector (AmpR)
pCDF3-dU63:gRNA-Cep104_exon1_1	Nanos gRNA vector (AmpR)
pCDF3-dU6:3gRNA-CG43370_exon1_3	Nanos gRNA vector (AmpR)

2.4.5 Site-directed mutagenesis

Site-directed mutagenesis was performed on pDONRCep104 using the Q5 Site-Directed Mutagenesis kit (NEB). Primers were designed using the NEBaseChanger tool and can be found in table 2.4. The PCRs were performed using the following protocol:

98°C	30 seconds	
98°C	10 seconds	} repeat 30 times
50-72°C	30 seconds	
72°C	30 seconds/kb	
72°C	5 minutes	

Mutated PCR products were then purified and transformed into competent cells according

to manufacturer's instructions. Plasmids were fully sequenced to verify the mutations, see section 2.4.6.

2.4.6 DNA Sequencing

Sanger sequencing was performed by SourceBioscience using standard sequencing protocols. Sequencing data was analysed using ApE - A plasmid editor (University of Utah).

2.4.7 *In vitro* RNA transcription

PCR amplified cDNA was cloned into a pRNA vector using the Gateway cloning system (Invitrogen) and linearised by AscI restriction digest and ethanol precipitated overnight at -20°C. *In vitro* transcription using the mMessage mMachine T3 Kit (Ambion) resulted in capped mRNAs that were purified using the RNeasy MinElute Clean Up kit (Qiagen). RNA was diluted to a concentration of 3 mg/ml in DPEC treated H_2O (Ambion) for full length constructs and stored at -20°C. RNA was injected at equimolar concentrations to allow for comparison across constructs.

2.5 Cell biology

2.5.1 Microinjection of RNA into living embryos

Flies were allowed to lay eggs on a fruit juice agar plate with fresh yeast for 30-45 minutes. Embryos were then collected, dechorionated manually and lined up on a glass bottom dish. Embryos were then dessicated for 3-5 minutes in a 25°C incubator before covering them in Voltalef oil (VWR). The RNA was injected into the posterior of syncytial embryos using finely drawn glass needles. Embryos were left for 1 hour to allow translation of the RNA

and maturation of the resulting fluorescent fusion protein before imaging on a Perkin Elmer ERS Spinning Disk confocal system.

2.5.2 Fixation and immunostaining of pupal testes

Testes were dissected from late male pupae in PBS and fixed in 4% paraformaldehyde for 30 minutes and then squashed between one high precision thickness 1.5 coverslip (Marienfeld) and one thickness 1 coverslip (VWR), the latter coated in silicone. The coverslips were immediately put in liquid nitrogen to facilitate the chipping away of the thinner coverslip using a razor blade. The high precision coverslips with the sample were then incubated in ice cold ethanol for 15 minutes at -20°C, followed by a 10 minute incubation in PBT and washes in PBS. The samples were stained in Asl antibody in a wet chamber overnight at 4°C. The Asl antibody was raised in either guinea pigs (Raff lab number 199) or rabbits (Raff lab number 11). The samples were then washed in PBS again before staining in secondary antibody for 2 hours in a wet chamber. Secondary antibodies conjugated to Alexa 405, -488 or - 594 (Molecular Probes) were used 1:1000 in PBS. For samples with GFP, GFP booster (Chromotek) was added 1:500 at this step as well. Finally, samples were washed in PBS several times, mounted in Vectashield (Vectorlabs) and sealed with nail varnish. The samples were imaged using a Deltavision OMX V3 microscope (GE Healthcare).

2.5.3 Fixation and immunostaining of the pupal notum

Newly formed male pupae were identified by their white cases and marked. The pupae were then left to develop for 48 hours as described before being removed from the pupal case and fixed in 4% paraformaldehyde and 2.5% in 0.2 M PIPES and heptane in an Eppendorf tube for 1 hour. After this initial fixation, the notum of the pupa was dissected and fixed overnight in 4% paraformaldehyde and 2.5% in 0.2 M PIPES at 4°C. Samples were then dehydrated in methanol for 1 hour, incubated in PBT for 2 hours and washed in PBS for 3

hours before overnight staining in primary antibody at 4°C. After extensive washing in PBS, samples were stained with fluorescently labelled secondary antibodies overnight at 4°C. The samples were mounted in Vectashield (Vectorlabs), sealed with nail varnish ab imaged using a Deltavision OMX V3 microscope (GE Healthcare).

2.5.4 Preparation of pupal notum for live cell imaging

Pupae were staged as described above and left to develop for 30 hours. Pupae were then immobilised on a microscope slide and the pupal case covering the head and thorax was removed. 4 coverslips were stacked on either side of the sample using nail varnish. These coverslips form a spacer to prevent squashing of the pupae before covering the pupae with a coverslip coated in Voltalef oil (VWR) and imaging using an Andor Revolution XD Spinning Disk confocal system.

2.5.5 Preparation of pupal testes for electron microscopy

Pupal testes were dissected in PBS and fixed in 2.5% glutaraldehyde in 0.1 M PIPES buffer (pH 7.2) for 1 hour at room temperature and then at 4°C overnight. Samples were washed in 0.1 M PIPES buffer and post-fixed in 1% OsO_4 for 2 hours. After rinsing in H_2O, samples were stained en-bloc in 1% uranyl acetate for 2 hours at 4°C, rinsed in H_2O and dehydrated in an ethanol series before gradual epoxy resin infiltration and embedding in Agar100 resin (Agar Scientific). Blocks were polymerised overnight at 60°C before trimming, sectioning and imaging on a TECNAI T12 transmission electron microscope (FEI).

2.5.6 Preparation of pupal notum for electron microscopy

Pupae were staged, dissected and fixed as described in section 2.5.3 up to overnight fixation in 4% paraformaldehyde and 2.5% in 0.2 M PIPES at 4°C. Samples were then washed in 0.2 M PIPES, before en-bloc staining in 1% OsO_4 in H_2O for 90 minutes at room temperature.

After staining, the samples rinsed in H_2O. Secondary fixation was performed in 1% uranyl acetate in H_2O overnight at 4°C. After rinsing in H_2O the samples were dehydrated in an ethanol series, followed by 100% acetate before gradual epoxy resin infiltration and embedding in Agar100 resin (Agar Scientific). Blocks were polymerised over 24 hours at 60°C before trimming, sectioning and imaging on a TECNAI T12 transmission electron microscope (FEI).

2.5.7 Preparation of pupal notum for SBF-SEM

Pupae were staged, dissected and fixed as described in section 2.5.3 up to overnight fixation in 4% paraformaldehyde and 2.5% in 0.2 M PIPES at 4°C. 0.1% tannic acid in PIPES was also added to the fixative. Samples were washed in 0.1 PIPES, followed by neutralisation of residual glutaraldehyde in 50 mM glycine in 0.1 M PIPES for 30 minutes. Samples were then embedded in 4% porcine gelatin and 4% low melting point agarose in H_2O and allowed to set for 15 minutes at 4°C. Initial en-bloc staining was performed by rotating samples in 3% $K_4[Fe(CN)_6]$ and 4% OsO_4 in H_2O for 1 hour at 4°C. Samples were rinsed in H_2O before incubating in freshly prepared 1% CH_6N_4S in H_2O for 20 minutes at room temperature. Further en-bloc staining in 2% OsO_4 for 30 minutes at 4°C was performed before rinsing and secondary fixation in 1% uranyl acetate in H_2O overnight at 4°C. After rinsing, the samples were stained en-bloc in 20 mM lead nitrate in aspartic acid (pH 5.5) for 30 minutes at room temperature. Samples were the rinsed in H_2O and dehydrated in an ice-cold ethanol series, followed by ice-cold acetone. The samples were gradually infiltrated and embedded in Durcupan resin over 3 days. The resin was polymerised for 48-72 house at 60°C. The quality of the sample preparation was assessed by preparing and imaging a few sections on a TECNAI T12 transmission electron microscope (FEI). The samples were then trimmed and mounted on an aluminium specimen pin using conductive epoxy glue, which was set at 60°overnight. A smooth block face was created using a Reichert-Jung Ultracut C

microtome (Leica Microsystems) and samples were coated in gold using a Q150R ES Dual Carbon/Sputter Coater (Quorum Technologies) for 2 minutes. Samples were imaged on a Merlin Compact Field Emission Gun SEM (FEG-SEM) with Variable Pressure (VP) mode (Zeiss) with a 3View System (Gatan).

2.6 Microscopy and image analysis

2.6.1 Electron tomography

150 nm ultrathin sections were obtained using a Reichert-Jung Ultracut C (Leica Microsystems) and collected on Cu slot grids. Samples were post-stained in lead citrate and 10 nm colloidal gold particles were applied to both sides of the grid to facilitate the reconstructions of tomograms. Dual-axis tilt series were acquired using Serial EM (Mastronarde, 2005) on a TECNAI T12 transmission electron microscope (FEI). Tomograms were reconstructed using the IMOD package (Kremer et al., 1996).

2.6.2 SBF-SEM

Samples were sectioned and imaged on a Merlin Compact Field Emission Gun SEM (FEG-SEM) with Variable Pressure (VP) mode (Zeiss) with a 3View System (Gatan). The accelerating voltage was 3.5 kV, the variable pressure 50 Pa and the aperture size was 20 µm. Images were reconstructed using the IMOD package (Kremer et al., 1996). The axial resolution of the images is 50 nm, the theoretical lateral resolution is 2.5 nm.

2.6.3 3D Structured Illumination Microscopy

Fixed samples were analysed on a Deltavision OMX V3 microscope (GE Healthcare), using a 60x/1.42 oil UPlanSApo objective (Olympus), 405 nm, 488 nm, 593 nm diode lasers and

Edge 5.5 sCMOS cameras (PCO). 3D Structured Illumination Microscopy (3D-SIM) image stacks were acquired with 5 phases, 3 angles per image plane and a 0.125 µm distance between the planes, using the OMX Deltavision software. Raw images were computationally reconstructed using softWoRx 6.1 (Applied Precision) using channel specific optical transfer functions. Reconstructed images were aligned using OMX Editor software with alignment parameters obtained from automatically aligning 0.2 µm TetraSpec beads (Life Technologies). Processing of images and measuring of distances was done using Fiji. Images shown are maximum intensity projections of several z planes.

2.6.4 Live cell imaging of bristle sensory neurons

Living pupae were imaged at 21°C on an Andor Revolution XD Spinning Disk confocal system mounted on an inverted TE-2000E microscope (Nikon), using a 488 nm diode laser and an EMCCD camera (iXon, Andor). Image stacks were acquired using IQ2 software (Andor) with a 500 nm distance between the planes. For NompA-GFP, a 40x air objective was used and stacks were acquired every 5 minutes for 20+ hours from 30 hours APF. For NompB-GFP, RempA-YFP and NompC-GFP, a 60x oil objective was used and a single stack was acquired at 72 hours APF. Movies and images were processed and analysed using Fiji.

2.6.5 Live cell imaging of RNA injections

Living embryos were imaged on a Perkin Elmer ERS Spinning Disk confocal system mounted on an inverted Axiovert 200M microscope (Carl Zeiss Ltd), using a 63x/1.4 oil objective, 488 nm and 568 nm diode lasers and a CCD camera (Orca ER, Hamamatsu). Image stacks were acquired using Ultraview ERS software (Perkin Elmer) with a 500 nm distance between the planes. The data was then blinded, analysed using Fiji and scored into different categories as described in section 2.7.6.

2.7 Quantification and statistics

2.7.1 Electrophysiology

MRPs were calculated using Clampfit 10.5. The means were then compared using a one-way ANOVA with Tukey's multiple comparisons test in Prism 6 (Graphpad).

2.7.2 Grooming assay

Images were analysed in Fiji. The head or notum was selected as an ROI using the polygon tool, and the area was measured. Next, the color threshold was set to the Reactive Yellow 86 dust to select the areas covered in the dust. The area of these parts within the original ROI was also measured and the ratio was determined. Data is represented as the average over 10 flies.

2.7.3 Fluorescence intensity measurements

Images were analysed in Fiji. A sum projection of the z stack was made and a circle was drawn around the signal at the ciliary base and the mean gray value was determined. The same circle was drawn to measure the background next to the signal, which was deducted from the signal. Data is represented as an average per pupa.

2.7.4 NompB length measurements

Images were analysed in IMOD. The signal was traced with open contours and the length of the trace was measured.

2.7.5 NompAGFP live imaging

Movies were processed using Fiji. Maximum intensity z projections were converted to 8 bit files. Subtraction of background, contrast enhancement and finding edges of the cilia were all done automatically. The length of 10 cilia was then measured and tracked through all time frames automatically using the JFilament 2D plugin (Smith et al., 2010). Background was set to the mean fluorescence intensity of the field of view and foreground was set to 3.5 standard deviations of the mean fluorescence intensity. Ciliary length was then plotted against time in Excel (Microsoft). The growth rate was determined by fitting a line to the curves in the linear growth phase. Data for the first 4 hours is presented as the average per pupae over 10 cilia. Where the whole growth curve is show, the mean growth rate with a 95% confidence interval was plotted.

2.7.6 Cep104 localisation

Stacks were analysed using a Fiji macro. Centrioles were detected as 10-50 pixel objects with intensities more than 2 standard deviations above the mean. GFP intensity at the centrioles was then measured and the background around each individual centriole was deducted. Intensities within 1 standard deviation of the mean were considered absent, 1-1.5 standard deviations above the mean intensity as moderate and >1.5 as strong. Data is represented as the averages of at least 15 embryos.

Chapter 3

Generation and characterisation of MKS module mutations

3.1 Introduction

Over the past decade, several genetic studies have linked cilia related genes to human disease, sparking a renewed interest in the organelle (Gerdes et al., 2009; Czarnecki and Shah, 2012; Davis and Katsanis, 2012). Most of the mutations that underlie ciliopathies, such as Meckel-Gruber (MKS) and Joubert syndrome (JBTS), are now identified. Interestingly, the proteins encoded by the disease genes all localise to the TZ at the base of the cilium (Czarnecki and Shah, 2012; Davis and Katsanis, 2012; Hu and Nelson, 2011; Reiter et al., 2012). The TZ is a complex structure at the basal body/axoneme interface (Garcia-Gonzalo and Reiter, 2012; Ishikawa and Marshall, 2011). Y-links and transition fibres form connections between the microtubules and the membrane, which are thought to contribute to a selective barrier that allows the cilium to form a separate compartment within the cell (Czarnecki and Shah, 2012; Hsiao et al., 2012; Hu and Nelson, 2011; Nachury et al., 2010; Reiter et al.,

2012).

Within the TZ, proteins can be grouped into three distinct complexes, or modules, MKS (containing proteins such as MKS1, B9D1 and B9D2), NPHP (containing proteins such as NPHP1 and NPH2) and Cep290 (containing proteins such as Cep290 and ATXN1) (Garcia-Gonzalo et al., 2011; Chih et al., 2012; Sang et al., 2012; Schouteden et al., 2015; Williams et al., 2008; Williams et al., 2011; Yee et al., 2015). Studies in *C. elegans* indicate that there is a redundancy between the MKS and NPHP modules (Williams et al., 2008; Williams et al., 2011). The MKS and NPHP modules required Cep290 to localise to the TZ, which in turn requires RGRIP1L (Li et al., 2016; Schouteden et al., 2015; Yang et al., 2015). Interestingly, *Drosophila* appear to lack an NPHP module (Barker et al., 2014). The Cep290 module has been shown to be essential for ciliogenesis in flies (Basiri et al., 2014), but the MKS module has not been studied. The lack of an NPHP module in *Drosophila* potentially simplifies the analysis of TZ assembly and function in this organism. Furthermore, the essential developmental Hedgehog pathway is independent of cilia in *Drosophila* (Varjosalo et al., 2006; Roy, 2012). This means flies offer an attractive opportunity to study the function of ciliopathy genes *in vivo* and to dissect cilia defects that are independent of Hedgehog signalling defects.

In this chapter I describe the identification and characterisation of the *Drosophila* orthologues of MKS module genes *MKS1*, *B9D1* and *CC2D2A*. MKS1 was first identified as a ciliopathy gene in 2006 (Kyttälä et al., 2006) when it was found to be mutated in MKS patients. Several genetic studies have since identified mutations in the gene that underlie either MKS or Joubert syndrome (Auber et al., 2007; Szymanska et al., 2012; Romani et al., 2014; Slaats et al., 2015). Mutations that truncate the gene are associated with MKS, while non-truncating mutations underlie the less severe Joubert syndrome. Mutations in both B9D1 and CC2D2A are also associated with MKS and Joubert syndrome and, as with MKS1, the mutations that underlie MKS are distinct from the mutations associated with

Joubert syndrome. (Tallila et al., 2008; Mougou-Zerelli et al., 2009; Doherty et al., 2010; Hopp et al., 2011; Szymanska et al., 2012; Romani et al., 2014). In *Drosophila*, mutants for *MKS1*, *B9D1* and *CC2D2A* ($MKS1^{\Delta 1}$, $B9D1^{\Delta 1}$ and $CC2D2A^{\Delta 1}$, respectively, are all viable and lack obvious developmental defects. Since flies have cilia only on cells of the sperm lineage and sensory neurons, these phenotypes were analysed in detail. No defects in fertility or coordination were observed in $MKS1^{\Delta 1}$, $B9D1^{\Delta 1}$or $CC2D2A^{\Delta 1}$mutants. If anything, the cilia of $MKS1^{\Delta 1}$and $B9D1^{\Delta 1}$mutants, but not $CC2D2A^{\Delta 1}$mutants appeared slightly more sensitive than WT.

3.2 Results

3.2.1 Identification of *Drosophila* ciliopathy genes

Drosophila orthologues of human ciliopathy genes were identified through Uniprot BLAST analysis. Hits with an e-value below 1e-0.5 were validated by reciprocal BLAST analysis, followed by comparison of key domains between human and fly proteins. These orthologues are in broad agreement with orthologues identified in *Drosophila* by Dr. Helen Dawe (University of Exeter, personal communication), whose findings have since been published (Barker et al., 2014). All orthologues identified in this thesis are listed in Table 3.1. The *Drosophila* orthologue of *MKS1*, *CG15730*, is a 2203 bp (699 amino acids) gene located on the X chromosome. It has a predicted B9-C2 domain at amino acids 437-613 that is conserved from flies to humans (Figure 3.1, top panel). This domain is conserved with 29% identity. *CG14870*, the *Drosophila* orthologue of *B9D1*, is 999 bp (421 amino acids) gene located on third chromosome. This protein also has a predicted B9-C2 domain at amino acid position 56-226 (Figure 3.1, middle panel), which is conserved with 39% identity from humans to flies. The *Drosophila* orthologue of *CC2D2A*, *CG43370*, is an 4788 bp (1337 amino acids) gene, located on the second chromosome. The protein does not contain a B9

Table 3.1 *Drosophila* orthologues of human ciliopathy genes

Human gene	***Drosophila* gene**	**Amino acid identity**	**Amino acid similarity**
MKS1	CG15730	24%	40%
B9D1	CG14870	34%	55%
B9D2	CG42730	44%	65%
MKS3	CG15923	25%	43%
TMEM216	CG8116	32%	52%
TMEM237	CG14186	11%	42%
CC2D2A	CG43370	27%	46%
Tectonic	CG42731	24%	36%
Cep290	CG13889	19%	31%

domain, but there are 2 predicted C2 domains at amino acids 421-560 and 772-914 (Figure 3.1, bottom panel). The region containing these C2 domains is conserved with 28% identity between humans and flies.

3.2.2 Generation of an MKS1 mutant allele, *MKS1*$^{\Delta 1}$

Since there are no published mutant alleles for *MKS1* in *Drosophila*, a new mutant allele was generated for this thesis by p-element excision. Mobilisation of the p-element by a transposase may occur imprecisely and remove some of the flanking genomic DNA, thus generating a deletion. A fly stock with a p-element inserted 581 bp upstream of *MKS1*, P{EPgy2}CG2556^{EY02042}, was obtained. The p-element was mobilised by crossing the stock to a stock expressing the p-element transposase Δ2-3 (Robertson et al., 1988). P{EPgy2}CG2556^{EY02042} is marked with w^+, allowing for screening for the loss of the p-

element from the genome by eye colour. 536 white eyed F1 females were obtained and individually crossed to generate a stock with the putative deletions balanced over FM7h. The F1 females were then screened for deletions in *MKS1* by single fly diagnostic PCR and Sanger sequencing. 15 deletions of varying sizes were obtained. The largest deletion spans 1.4 kb and removes 474 of the 699 amino acids of MKS1, including the ATG and part of the conserved B9 domain (Figure 3.1, top panel, *capped line*) and will be referred to as $MKS1^{\Delta 1}$.

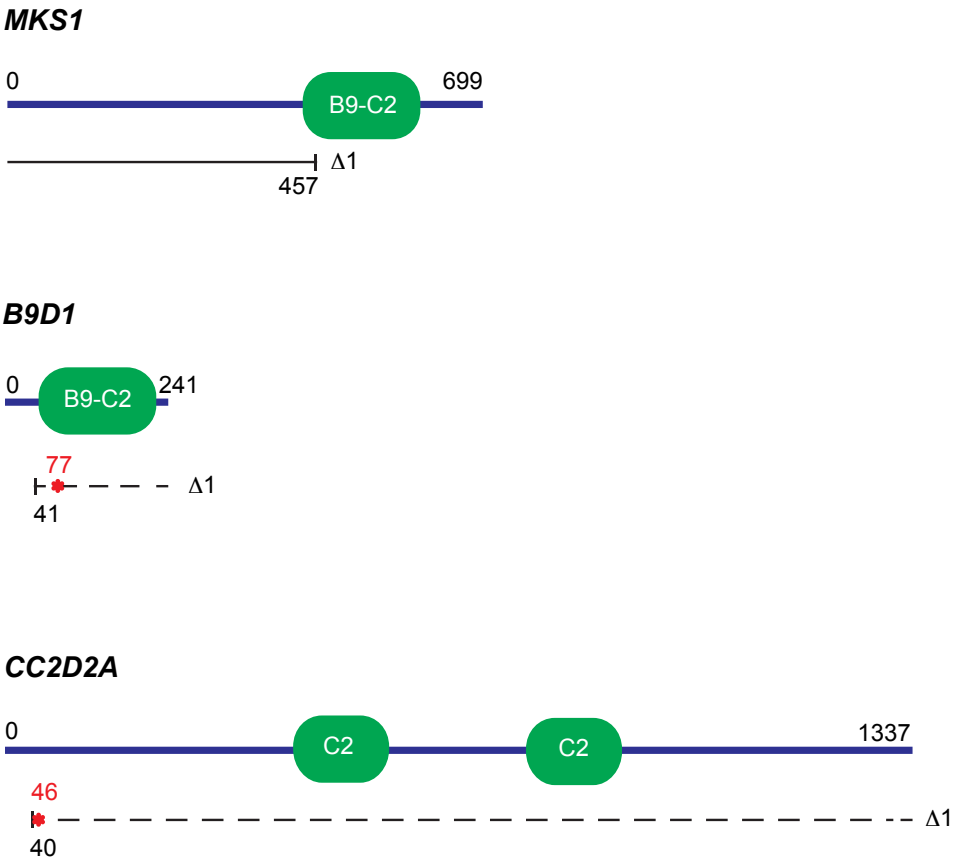

Figure 3.1 Schematic overview of MKS1, B9D1 and CC2D2A. Domains (*green*) and mutations (*capped lines and asterisks*) are marked on the schematic. The deletion in *MKS1* removes the ATG and the first 474 amino acids (*capped line*). The deletion in B9D1 induce a frameshift at amino acid 41, leading to miss sense codons (*dashed capped line*) and a premature stop codon (*red asterisk*) at amino acid 77. In CC2D2A, the deletion creates a frameshift at amino acid 40, creating miss sense codons (*dashed capped line*) and a premature stop codon at amino acid 46 (*red asterisk*).

3.2.3 Generation of *B9D1*$^{\Delta 1}$ and *CC2D2A*$^{\Delta 1}$

MKS1 is part of the MKS module of proteins. To gain more insight into the role of MKS1 within this module and into the complex as a whole, mutations were also generated in the genes encoding MKS module proteins B9D1 and CC2D2A. No published mutations were available for these genes and new mutant alleles were generated by CRISPR genome engineering. Synthetic guide RNAs (sgRNAs) were used to target the Cas9 endonuclease to the 5' end of *B9D1* and *CC2D2A* and generate double strand breaks. These double strand breaks may be repaired imprecisely by non-homologous end-joining, generating small insertions or deletions (indels). These indels are often small, but can create a frame shift, which will result in scrambled code and usually the introduction of a premature stop codon. sgRNAs (see Table 2.3) were designed for each gene, cloned into the pCDF3-dU6:3gRNA vector and microinjected into *Drosophila* embryos expressing the Cas9 gene under the Nanos promoter, which drives expression of the Cas9 gene in the *Drosophila* germline. 38 surviving "founder" adults for *B9D1* and 8 for *CC2D2A* were individually crossed to generate a stock with putative mutations balanced over TM6C or SM5, respectively, before screening for indels by high resolution melt analysis (HRMA) and Sanger sequencing. A 127 bp deletion at position 185 was selected from 10 indels in *B9D1*. This deletion induces a frameshift at amino acid 41, leading to scrambled code and a premature stop codon at amino acid 77 (Figure 3.1, middle panel, *capped line and red asterisk*, respectively). A 14 bp deletion at position 117 was selected from 3 indels in *CC2D2A*. This deletion results in a frameshift at amino acid 40 and a premature stop codon at amino acid 46 (Figure 3.1, bottom panel, *capped line and red asterisk*, respectively). These alleles will be referred to as *B9D1*$^{\Delta 1}$ and *CC2D2A*$^{\Delta 1}$, respectively.

3.2.4 Viability and fertility of MKS module mutations

Homozygous or hemizygous *MKS1*$^{\Delta 1}$, *B9D1*$^{\Delta 1}$ and *CC2D2A*$^{\Delta 1}$ mutant adult flies are viable and fertile; no obvious developmental abnormalities were observed and all three stocks have now been maintained in the laboratory for several years. Male *Drosophila* without functional cilia are sterile as they can not produce motile sperm, so the fertility of the *MKS1*$^{\Delta 1}$, *B9D1*$^{\Delta 1}$ and *CC2D2A*$^{\Delta 1}$ mutants indicates that their sperm flagella are at least partly functional. In *MKS1*$^{\Delta 1}$mutants, male fertility was quantified by counting the number of F1 larvae per day for individual WT, *MKS1*$^{\Delta 1}$mutants and *MKS1*$^{\Delta 1}$mutants rescued by GFP-MKS1 males (Figure 3.2 A).

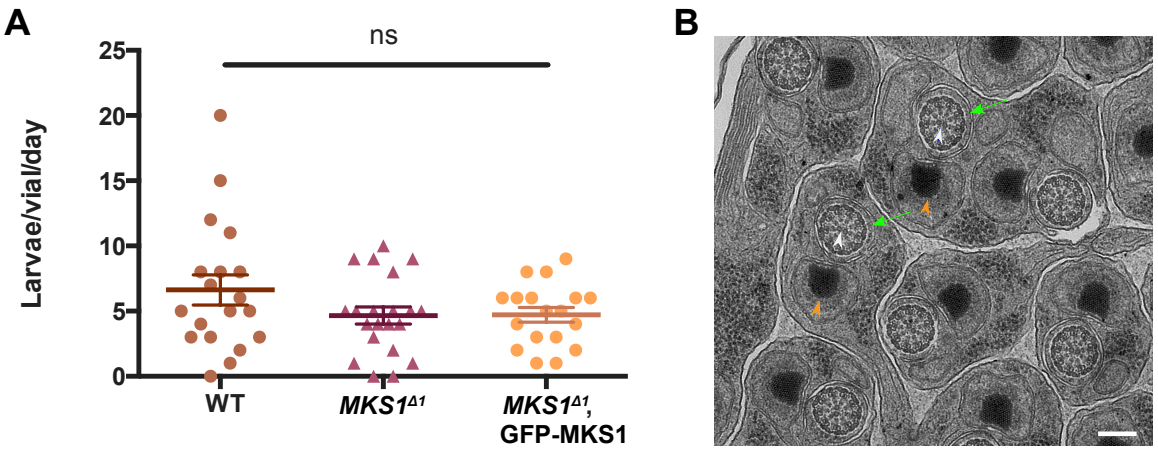

Figure 3.2 Fertility and sperm axonemes in *MKS1*$^{\Delta 1}$mutant males. A) Quantification of the number of eclosed embryos per vial per day when individual *MKS1*$^{\Delta 1}$ mutant and *MKS1*$^{\Delta 1}$, GFP-MKS1 rescue males were mated with 3 WT females. B) Electron micrograph of mature sperm in cross-section in *MKS1*$^{\Delta 1}$, the flagella (*green arrows*) have a normal 9-fold symmetry with intact microtubules, in which the central pair (*white arrowheads*) as well as the mitochondrial derivative (*orange arrowheads*) are clearly visible and look normal. Scale bar: 200 nm. Error bars represent the S.E.M, significance was assessed using a Mann-Whitney test, ns = not significant.

No significant difference (p = 0.306) was observed between *MKS1*$^{\Delta 1}$ mutants (4.667 eclosed embryos/day $\pm$ 0.652) and WT (6.632 eclosed embryos/day $\pm$ 1.153) males, indicating that there are no gross defects in the flagella of the sperm. Indeed, when the spermatid cysts were qualitatively analysed using TEM, no ultrastructural defects were observed in the

sperm flagella (Figure 3.2 B). The 9-fold symmetry of microtubules was intact, and the central pair of microtubules in the axoneme as well as the mitochondrial derivative that ensure motility were clearly visible.

3.2.5 Behavioural studies of TZ mutations

In addition to male sterility, flies without functional cilia are uncoordinated due to defects in ciliated sensory neurons. Therefore, behavioural studies of $MKS1^{\Delta 1}$ mutant flies were conducted to assess ciliary function in this mutant.

To assess negative gravitaxis, a simple climbing assay was conducted (Hirsch and Tryon, 1956). WT flies climb back to the top of a vial after they have been knocked to the bottom, while flies with defective cilia can not climb properly. An initial climbing assay (Figure 3.3 A and B) showed no clear difference (p = 0.800) in the number of flies that climb above 12 cm in 10 s between $MKS1^{\Delta 1}$mutant (40% $\pm$ 5.774) and WT (33.33% $\pm$ 8.819) flies. It was observed, however, that some $MKS1^{\Delta 1}$ mutant flies seemed to reach higher regions of the tube than the WT flies. Therefore, the climbing assay was repeated and the distance climbed in 7 seconds by individual flies was measured (Figure 3.3 C). A significant increase (p = 0.011) in distance climbed was observed in $MKS1^{\Delta 1}$ mutant flies (495.3 px $\pm$ 35.78) compared to WT (383.8 px $\pm$ 41.23) (Figure 3.3 D). Thus, there are clearly no negative effects on gravitaxis as a result of the $MKS1^{\Delta 1}$mutations. The small increase in gravitaxis is a surprising result, that will be addressed in further behavioural studies.

In order to assess the function of mechanosensory neurons that innervate the fly bristles, the grooming behaviour of the flies was analysed. When covered with dust, flies use their legs to clean their bodies in a highly characteristic way (Phillis et al., 1993). The grooming assay showed a significant increase (p = 0.004) in the cleaned surface of the head after being coated in dust and left to groom for 30 minutes between $MKS1^{\Delta 1}$mutant (90.76% $\pm$ 1.838) and WT flies (76.36% $\pm$ 4.680 in WT). After 60 minutes of grooming there was still a

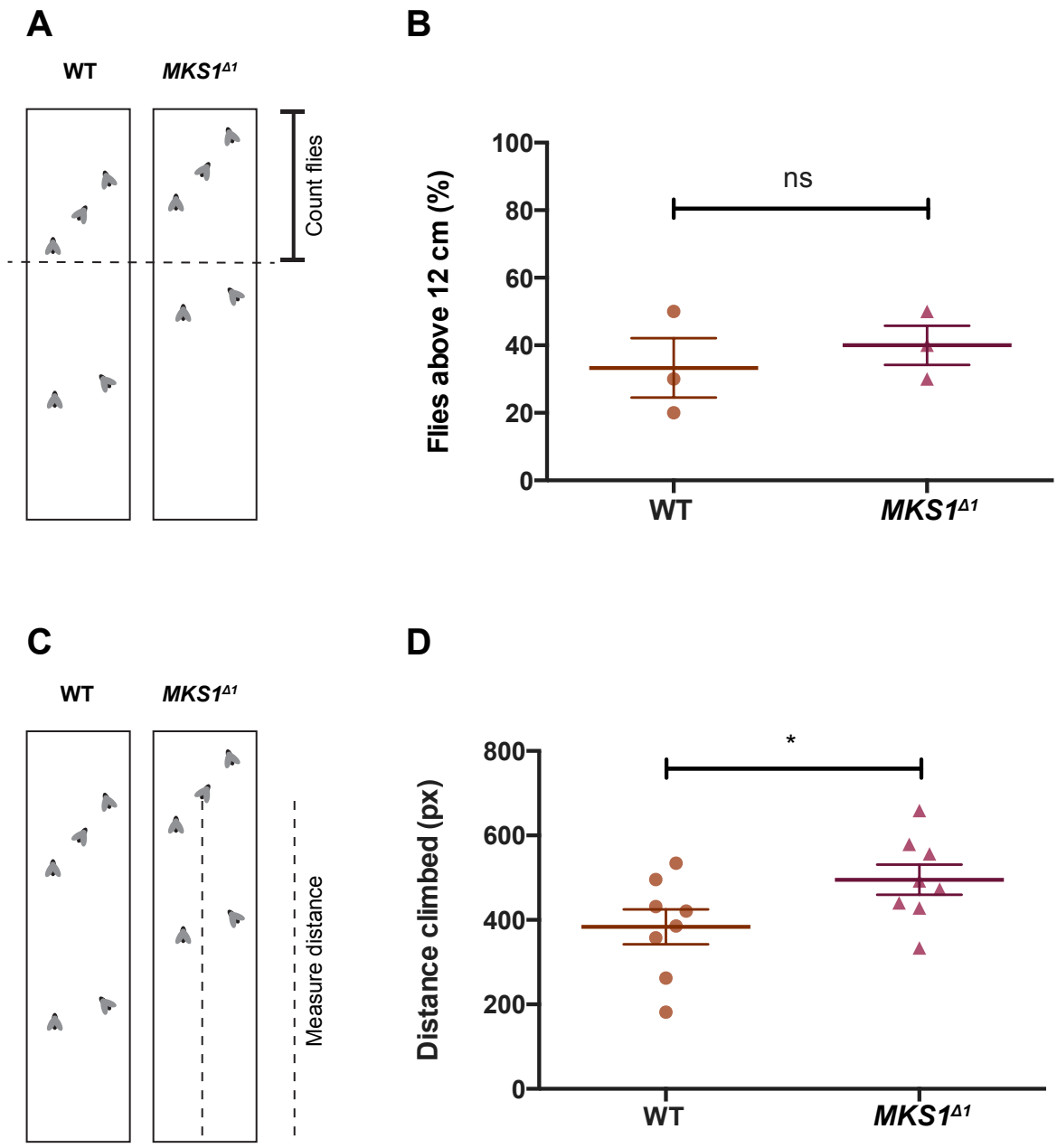

Figure 3.3 Climbing assays in WT and *MKS1*$^{\Delta 1}$ mutant flies. A) Schematic overview of standard climbing assay. B) Quantification of the percentage of flies that climb above 12 cm within 10 seconds. Each data point is an average of 10 flies and 3 replicates. C) Schematic overview of distance climbing assay. D) Quantification the average distance individual flies climb in 7 seconds. Each data point is an average of 10 flies and 5 replicates. Error bars represent the S.E.M, significance was assessed a Mann-Whitney test: ns = not significant, *p<0.01.

significant difference (p = 0.019) in the cleaned surface of the head between *MKS1*$^{\Delta 1}$ mutant flies (92.28% ± 1.453) and WT (88.18% ± 1.679). After 90 minutes of grooming, the flies heads were largely cleaned in both *MKS1*$^{\Delta 1}$ (95.39 ± 1.097) and WT (94.70 % ± 1.497) and no significant (p = 0.548) difference could be observed (Figure 3.4 A).

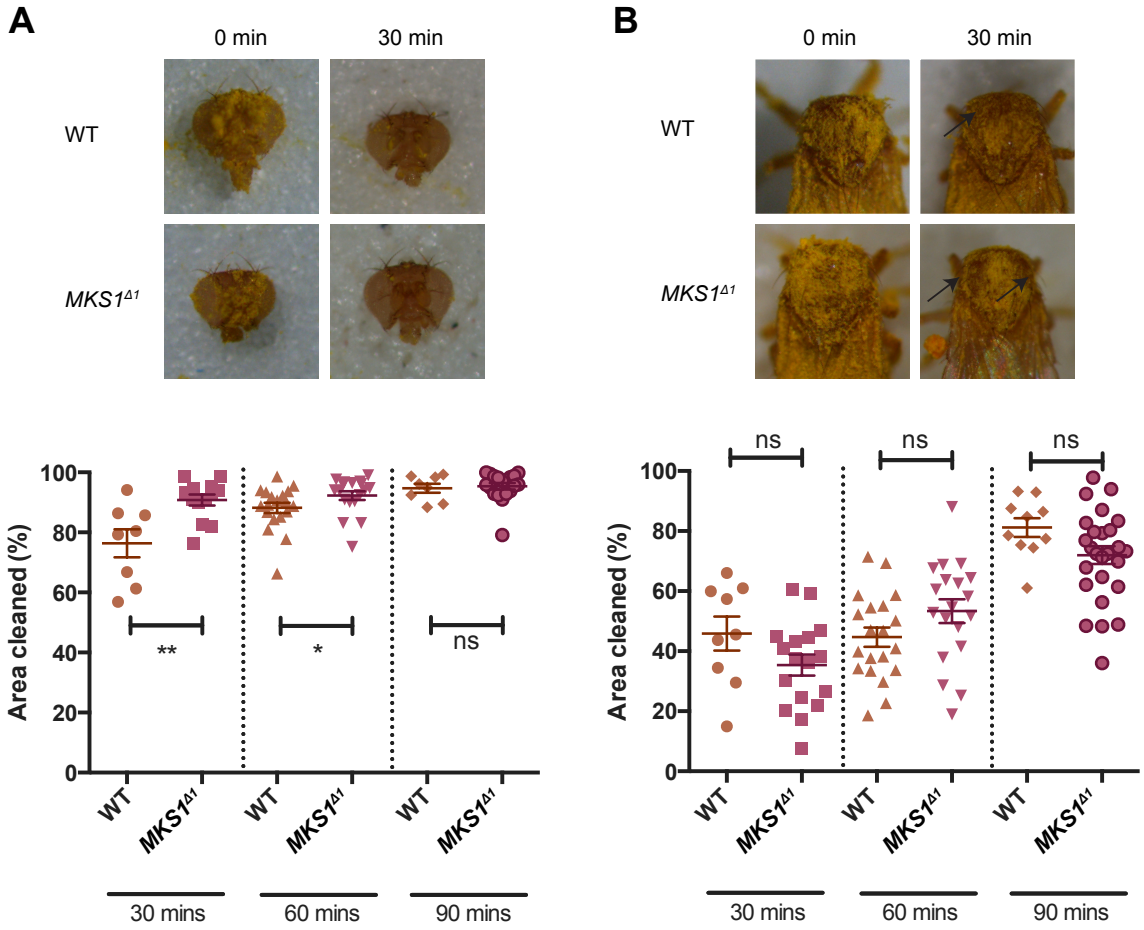

Figure 3.4 Grooming assays in WT and *MKS1*$^{\Delta 1}$ mutant flies. A) Representative images of the head after 0 and 30 minutes of grooming and quantification of the area of the head cleaned after 30, 60 and 90 minutes of grooming WT and *MKS1*$^{\Delta 1}$. B) Representative images of the notum after 0 and 30 minutes of grooming (clean areas are marked with *black arrows*) and quantification of the area of the head cleaned after 30, 60 and 90 minutes of grooming in WT and *MKS1*$^{\Delta 1}$. Error bars represent the S.E.M., significance was assessed using a students t-test: ns = not significant, *p<0.01, **p<00.1, ***p<0.0001.

Interestingly, no difference was observed in the cleaning of the notum at any time point (Figure 3.4 B). After 30 minutes the surface cleaned was not significantly different (p =

0.542) in $MKS1^{\Delta 1}$mutants (35.35% ± 3.513) and WT (45.85% ± 5.683). The surfaces cleaned in $MKS1^{\Delta 1}$mutants (53.34% ± 3.930) and WT (44.67% ± 3.201) were also similar (p = 0.444) after 60 minutes and after 90 minutes (p = 0.178) (81.19 ± 3.107 in WT, 72.00% ± 2.921). It is clear, however, that both $MKS1^{\Delta 1}$mutant and WT flies start cleaning the notum within 90 minutes as the cleaned area increases between 30 and 90 minutes. Taken together, the climbing and grooming assays suggest that there are no obvious defects in cilia function in $MKS1^{\Delta 1}$mutants and there may be a small increase in the sensitivity of $MKS1^{\Delta 1}$mutant *Drosophila* sensory cilia.

3.2.6 Electrophysiology of MKS module mutations

In order to analyse ciliary function more directly, the action potential generated in the sensory neurons in response to a stimulus can be measured using electrophysiology techniques (Kernan et al., 1994). These experiments require specialised equipment and knowledge and were performed by a collaborator (Dr. Joshua Titlow, University of Oxford). Each of the bristles on the notum is innervated by a single ES neuron. By cutting off the tip off the bristle and placing an electrode over it, the transepithelial potential (TEP) can be measured between this electrode and a reference electrode placed in the notum haemolymph (Figure 3.5 A). Upon stimulation of the neuron by bending of the bristle using a piezo stage, ion channels in the ciliary membrane open. This allows ions to flow into the neuron and generate a mechanical response potential (MRP) (Figure 3.5 B). These potentials were measured and quantified in the sensory neurons in WT and $MKS1^{\Delta 1}$, $B9D1^{\Delta 1}$and $CC2D2A^{\Delta 1}$mutants. Plp^5 (Martinez-Campos et al., 2004) was used as a negative control as these flies are known to have severely reduced cilia function and a GFP-MKS1 transgene in the $MKS1^{\Delta 1}$mutant background was also measured (Figure 3.5 C). The average MRP was significantly (p = 0.016) increased in $MKS1^{\Delta 1}$ (13.880 mV ± 1.226) compared to WT (9.554 mV ± 0.793). $B9D1^{\Delta 1}$ also had a significantly (p = 0.004) increased amplitude (14.440 mV ± 1.146) com-

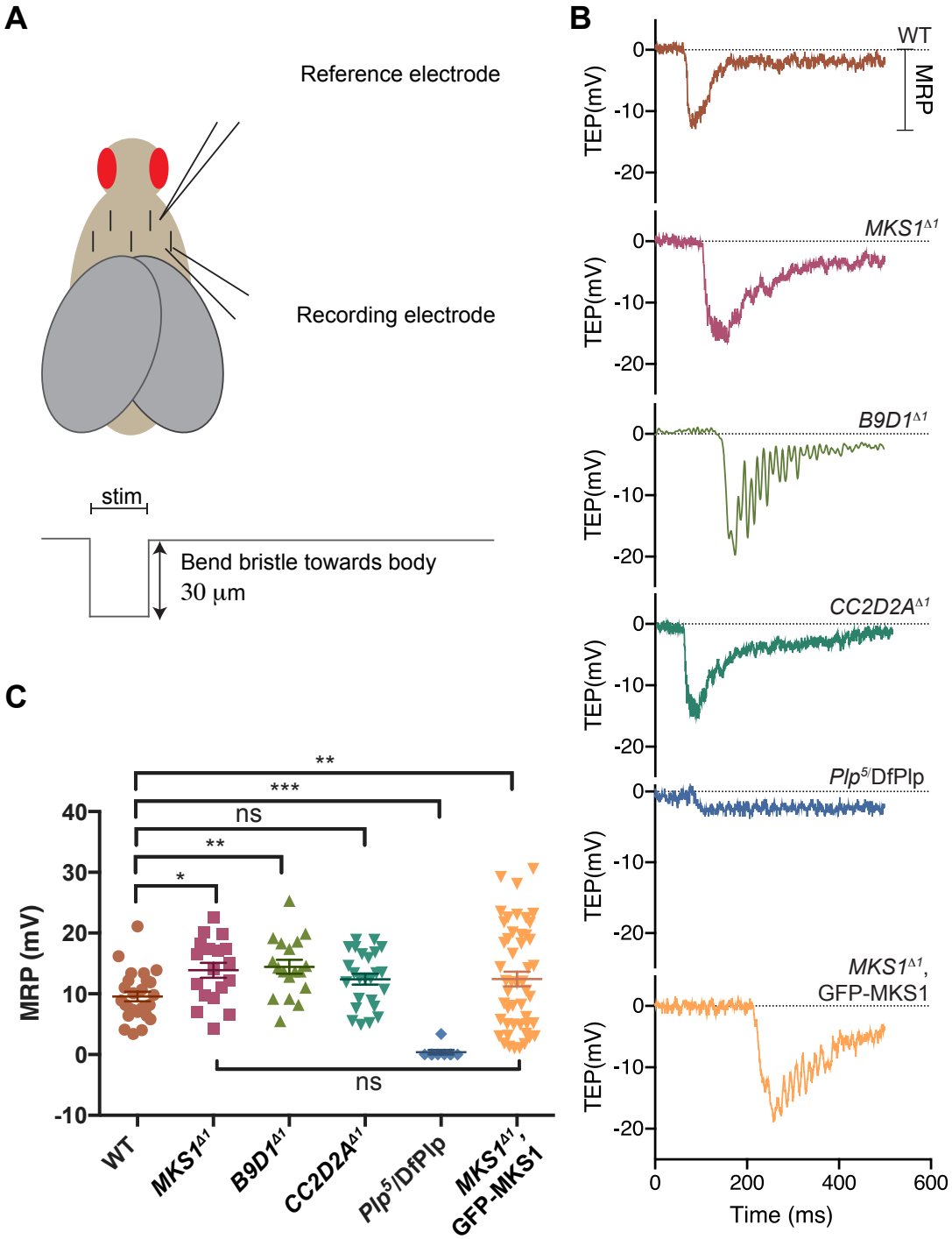

Figure 3.5 Electrophysiology of sensory bristles in WT and TZ mutants. A) Schematic of electrophysiology set-up. B) Representative trans-epithelial electron potential (TEP) traces for WT, *MKS1*$^{\Delta 1}$, *B9D1*$^{\Delta 1}$, *CC2D2A*$^{\Delta 1}$ and, as a negative control, *Plp*^{5}/DfPlp, in which cilia function is known to be severely reduced (Martinez-Campos et al., 2004). A trace from the *MKS1*$^{\Delta 1}$ rescued by GFP-MKS1 is also shown. C) Quantification of the mechanical response potential (MRP) derived from the traces shown in B. Error bars represent the S.E.M, significance was assessed using a one-way ANOVA: ns = not significant, *p<0.01, **p<00.1, ***p<0.0001.

pared to WT, but no difference (p = 0.149) was observed in *CC2D2A*$^{\Delta 1}$ (12.420 $\pm$ 0.903). A small increase (p = 0.106) was also observed in *MKS1*$^{\Delta 1}$, GFP-MKS1 (12.440 mV $\pm$ 1.209), indicating either that the transgene can not fully rescue the effects of the *MKS1*$^{\Delta 1}$mutation or that differences in the genetic background may contribute to the slight increase observed.

3.3 Discussion

Since flies only have cilia in sensory neurons and cells of the sperm lineage, flies lacking functional cilia are male sterile and uncoordinated. Male sterility is the result of a lack of motile sperm, while the uncoordinated phenotype arises from a failure of signal transduction in the mechanosensory neuron, which results in an inability to perceive stimuli and execute coordinated movements. Analysis of male fertility shows that the males mutant for *MKS1*, *B9D1* or *CC2D2A* are all fertile. There was no detectable difference in fertility between *MKS1*$^{\Delta 1}$ mutant and WT males. Furthermore, the ultrastructure of *MKS1*$^{\Delta 1}$mutant sperm axonemes appears normal with intact microtubule structure and 9-fold symmetry. Together, these results indicate that there are no visible defects in the sperm flagella. This is in contrast to mutations in three other TZ genes, *Cep290*, *Chibby* and *Dilatory* (*Dila*) (Basiri et al., 2014; Enjolras et al., 2012; Ma and Jarman, 2011). These mutants all have defects in the sperm flagella, with cells failing to individualise, unstable axonemes and gaps within the spermatid cysts, resulting in reduced male fertility. In addition to male fertility defects, these three mutants also have coordination defects. Both *Cep290*^{mecH} and *dila* flies are fully uncoordinated, as shown by a complete absence of MRP in *Cep290*^{mecH}, and an inability to walk, feed or climb in *dila* (Basiri et al., 2014; Ma and Jarman, 2011). *cby*$^{1/1}$ flies are more mildly uncoordinated, but do show a reduced climbing reflex and MRP (Enjolras et al., 2012). Surprisingly, however, *MKS1*$^{\Delta 1}$, *B9D1*$^{\Delta 1}$and *CC2D2A*$^{\Delta 1}$mutant flies all show no defects in coordination. *MKS1*$^{\Delta 1}$and *B9D1*$^{\Delta 1}$mutants even have a slightly increased MRP, which in the case of *MKS1*$^{\Delta 1}$is consistent with an increase in climbing and grooming re-

flex. This suggests that, if anything, sensory cilia function is slightly increased in MKS module mutants. *CC2D2A*$^{\Delta 1}$mutant MRPs are identical to WT, suggesting that there may be a difference between the *MKS1*$^{\Delta 1}$and *B9D1*$^{\Delta 1}$mutant alleles on the one hand and the *CC2D2A*$^{\Delta 1}$mutant allele on the other. Alternatively, it remains possible that these slight, but significant, differences in electrophysiology and behaviour may reflect genetic background differences between strains. Furthermore, it is possible that the WT strain that was used as a control in these experiments, w^{67}, has a slightly impaired MRP compared to other "wild type" strains such as *OregonR*. Both of these issues could be addressed in the future by back-crossing each mutation into the same genetic background. Several "wild type" strains could be tested prior to back-crossing each mutation in order to identify a strain in which the MRP is robust.

While MKS1, B9D1 and CC2D2A all have been reported to be part of the MKS module, the definition of the TZ modules is not yet very well established and the exact composition of the TZ modules may vary between cell types and species. However, both MKS1 and B9D1 have a B9 domain, while CC2D2A does not. This may indicate that MKS1 and B9D1 are more similar to each other than to CC2D2A. Indeed, as shown in Chapter 4, MKS1 and B9D1 are interdependent for their localisation, while CC2D2A has a slightly different localisation profile.

While the grooming of the head was increased in *MKS1*$^{\Delta 1}$mutant flies, the grooming of the notum was not. Grooming behaviour in flies is highly hierarchical and flies clean their heads first, followed by the abdomen and the wings, and finally clean the notum (Seeds et al., 2014). Since there is a difference in the first, but not the last body part the flies groom, it is possible that *MKS1*$^{\Delta 1}$mutant flies desensitise. This may be because the reservoir of ions is depleted, abolishing any differences in MRP or because behavioural adaptation occurs. Since the MRP was not measured for extended periods of time under constant stimulation, it is not possible to distinguish between these possibilities without further experiments.

Chapter 4

Ultrastructural and localisation studies of spermatocyte cilia

4.1 Introduction

In this Chapter, studies of the localisation of TZ proteins using the *Drosophila* spermatocyte cilia as a model will be described. The same cells are also used to study the effect of mutations in ciliopathy proteins on the localisation of TZ proteins and the ultrastructure of the TZ. Type I sensory neurons will be studied in Chapter 5.

Drosophila sperm are derived from male germ line stem cells (GSC). These cells divide asymmetrically to give rise to spermatogonia (Yamashita et al., 2003). Through four meiotic divisions, each spermatogonium gives rise to 16 spermatocytes. In the spermatocytes, both centrioles dock at the plasma membrane to form a short cilium. The basal bodies and cilia in the spermatocytes are made up of triplet microtubules and lack a central pair of microtubules (Fabian and Brill, 2012; Tates, 1971). Although this cilium is well documented, its function is unknown (Gottardo et al., 2013; Riparbelli et al., 2012; Tates, 1971). During the

subsequent meiotic divisions these cilia remain intact, but are internalised in a deep membrane pocket that translocates to the nucleus; although the centrioles are still organizing a short cilium, they nevertheless recruit PCM and participate in the formation of the meiotic spindles during two rounds of meiotic division that will give rise to 64 haploid spermatids (Riparbelli et al., 2012; Tates, 1971). The spermatids then undergo maturation, individualisation and coiling to develop into mature sperm that is stored in the seminal vesicle until mating (Fabrizio et al., 1998; Phillips, 1970; Tokuyasu et al., 1972b; Tokuyasu et al., 1972a; Tokuyasu, 1974). Mature sperm have a flagellum that is approximately 1.8 mm long (Tates, 1971). Unlike the triplet microtubules of the spermatocyte cilium, the flagellar axoneme is made up of doublet microtubules. Furthermore, the flagellum possesses a central pair of microtubules with associated dynein arms for motility. Nevertheless, TEM analysis of different stages of spermatogenesis and microtubule regrowth assays suggest that the spermatocyte cilium persists throughout spermatogenesis and is extensively remodelled to form the sperm flagellum (Tates, 1971; Gottardo et al., 2014).

In this Chapter, the localisation of TZ proteins in both WT and $MKS1^{\Delta 1}$ mutant spermatocyte cilia are described. The data confirms that ciliopathy proteins localise to the TZ in the spermatocyte cilia, immediately distal to the basal body. Intriguingly, the proteins localise to distinct regions within the TZ, suggesting functional differences. In $MKS1^{\Delta 1}$ mutant cilia, all TZ proteins apart from Cep290 and Chibby fail to localise, suggesting that MKS1 is essential for the formation of a proper TZ. Indeed, electron tomography studies of $MKS1^{\Delta 1}$ mutant spermatocyte cilia reveal that the axoneme fails to extend properly from the basal body and that there is a lack of the electron density at the membrane that is characteristic for the TZ. Deletion of *B9D1* results in the absence of MKS1 at the TZ, confirming the interdependency of MKS module proteins reported in other systems. The ultrastructure of $B9D1^{\Delta 1}$ mutant cilia is very similar to $MKS1^{\Delta 1}$ mutant cilia, with more severe defects in $Cep290^{MecH}$ mutants and less severe defects in $CC2D2A^{\Delta 1}$ mutants. Finally, some of the TZ proteins can be found

extending most of the way along the cilium by 3D-SIM, similarly, the electron density can also be observed extending to, but not including the ciliary tip. This suggests that the spermatocyte cilia do not extend much beyond the TZ so that almost the entire spermatocyte cilium may be considered a modified TZ.

4.2 Results

4.2.1 Ciliopathy proteins localise to distinct regions within the TZ

In order to characterise the TZ, transgenic flies expressing fluorescent fusion proteins of most *Drosophila* TZ proteins were generated. The localisation of these proteins was studied in *Drosophila* primary spermatocytes in late pupal testes. The samples were squashed before immunostaining to achieve a 1 cell layer thick sample for analysis by dual colour 3D SIM super-resolution microscopy. The basal bodies are labelled in red with an antibody against the outer centriolar protein Asl. Asl localises to the basal body wall and so enables the centrioles to be visualized as two orthogonal barrels in 3D-SIM images (Figure 4.1 A).

All TZ proteins except Cep290 form a hollow structure distal to the basal body that varies in width and length and may be open or closed at the distal end. Cep290 also localises distal to the basal body, but it appears to form a rod rather than a barrel. It is possible, however, that this is because Cep290 is localized towards the inner region of the cilia and so any barrel structure may be below the resolution of the 3D-SIM system ($\sim$ 120 nm) and would be visualized as a rod. The length (Figure 4.1 C), width of the rod or barrel wall (Figure 4.1 D) and diameter of the barrel (Figure 4.1 E) were all measured (Figure 4.1 B shows a schematic of the measurements taken). The Asl labelling at the basal body wall has an average circumference of 0.37 µm and average length of 1.3 µm. Cep290 forms a rod with a diameter of 0.33 µm and a length 0.53 µm. The rod appears distal to the basal body and localises to the middle of the axoneme, where the microtubules are. Chibby forms the

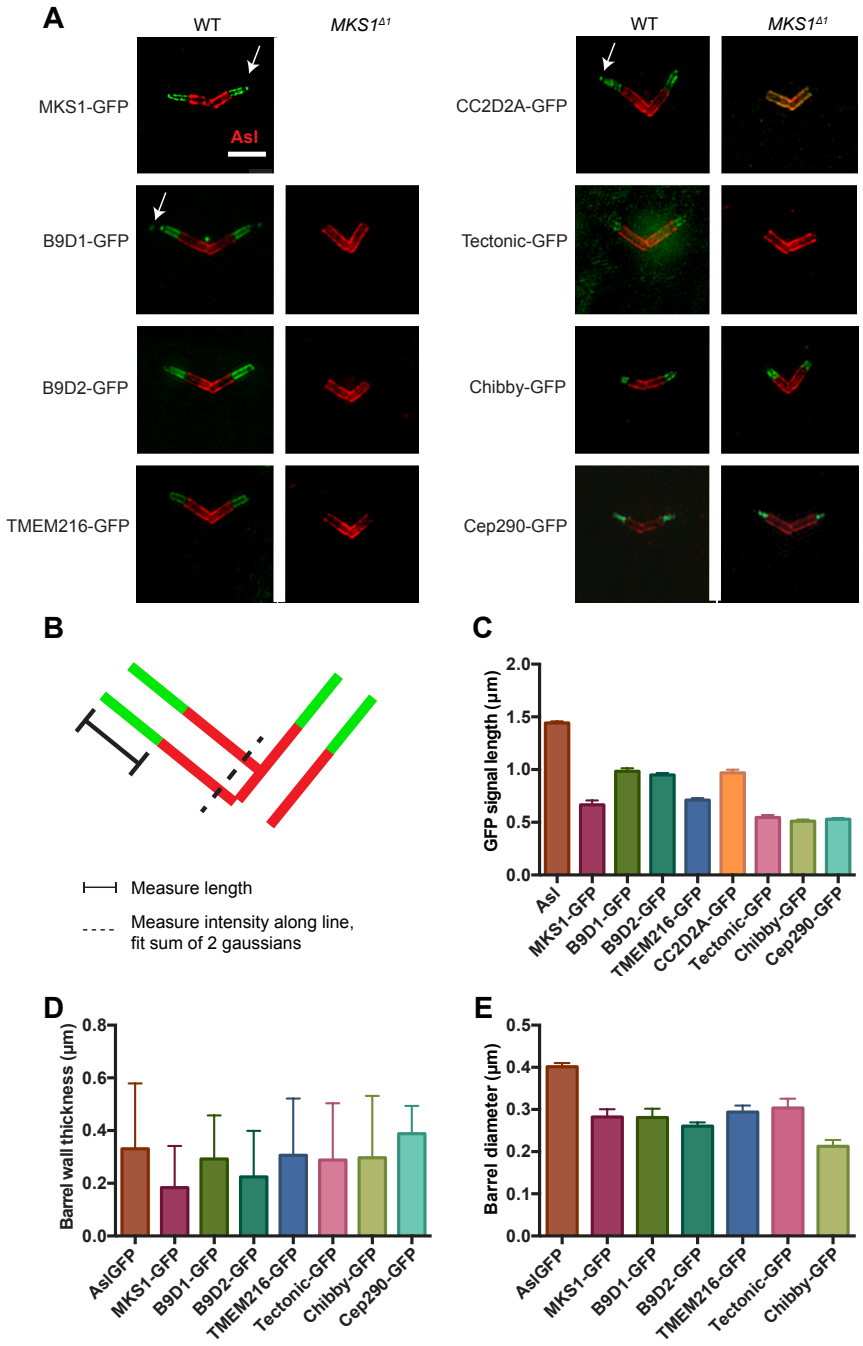

Figure 4.1 Localisation of TZ proteins in WT and *MKS1*$^{\Delta 1}$ mutant spermatocyte cilia. A) Representative 3D-SIM images of *Drosophila* spermatocyte cilia showing the localisation of GFP-tagged TZ proteins (*green*) in relation to the basal body in WT (left panels) and *MKS1*$^{\Delta 1}$ (right panels). The basal body is labelled with an antibody against Asterless (Asl). B) Schematic of measurements taken in C-E. C) Quantification of the length of the Asl and TZ proteins. Isolated dots were observed in some cases, but disregarded for these measurements. D) Thickness of the wall for Asl and TZ proteins that form a hollow tube, or the rod in the case of Cep290. E) Quantification of the diameter of the barrel formed by Asl and various TZ GFP fusion proteins. n>30 images, n>15 cilia for all measurements. Scale bar 2µm. Error bars represent the S.E.M.

tightest barrel-like structure with a width of 0.21 µm, the signal extends 0.51 µm from the basal body. MKS1, B9D1, Tectonic and TMEM216 all have similar widths of 0.28-0.29 µm, but their lengths range from 0.54 µm for Tectonic to 0.98 µm for B9D1. MKS1 extends 0.67 µm and TMEM216 extends 0.71 µm from the centriole. Interestingly, in some images, a "dot" of MKS1, B9D1, B9D2 and CC2D2A could also be visualised at the tip of the cilium (Figure 4.1, *arrows*).

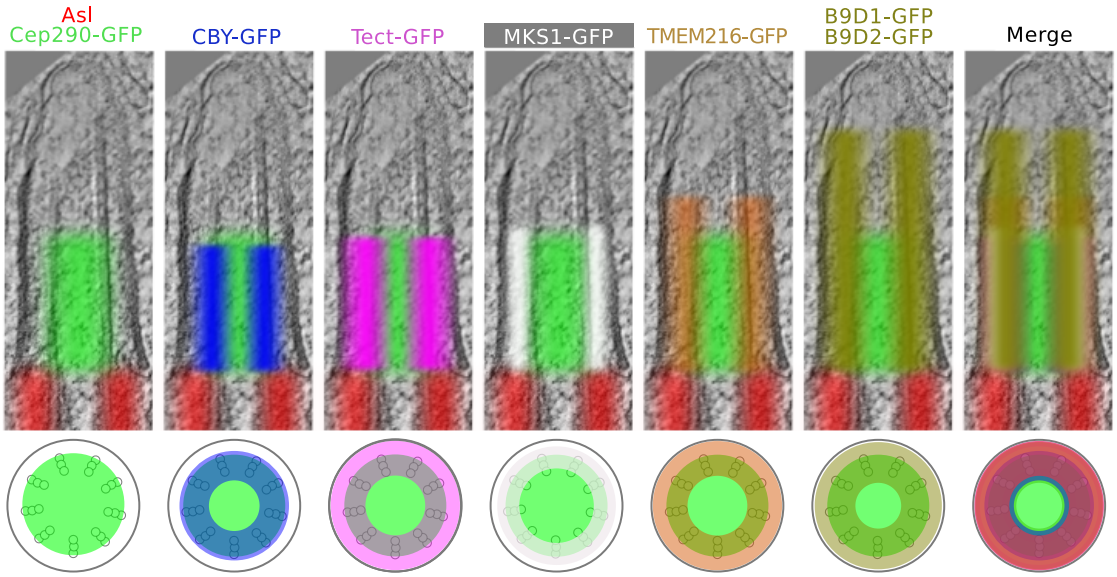

Figure 4.2 Compound electron tomography and 3D-SIM images. Images were created by generating intensity maps from the measurements in Figure 4.1 C-E and scaling and aligning the Asl to the basal body wall.

In an attempt to better understand the relationship between the TZ and the basal body, the axonemal microtubules and the ciliary membrane, "compound" images were created by overlaying the average 3D-SIM distribution of each of the TZ proteins upon an electron tomogram of a typical primary spermatocyte cilium (Figure 4.2). Since some distortion of the tissue is likely during the fixation and processing of the EM samples, these compound images must be interpreted with caution. Nevertheless, these images suggest that Cep290 localises to the lumen of the axoneme, overlapping with the axonemal microtubules. Chibby forms a barrel that overlaps with both Cep290 and the axonemal microtubules, but not the

membrane. Tectonic, MKS1, TMEM216, B9D1 and B9D2 all form barrels that seem to bridge the microtubules and the membrane. Interestingly, the distance the proteins extend from the basal body ranges from halfway for Chibby, to the tip of the axonemal microtubules for B9D1 and B9D2. These observations are consistent with the notion that the cilium does not extend much beyond the TZ and that the spermatocyte cilium may largely comprise a modified TZ.

4.2.2 Key ciliopathy proteins fail to localise in *MKS1*$^{\Delta 1}$ cilia

In order to study the effect of the lack of MKS1 on the localisation of other TZ proteins, the fluorescently labelled TZ proteins were crossed into the *MKS1*$^{\Delta 1}$ mutant background and analysed as described above (Figure 4.1 A). In *MKS1*$^{\Delta 1}$ mutant spermatocytes, B9D1, B9D2, TMEM216 and Tectonic were not detectable in the cilium, indicating that these proteins depend on MKS1 for their localisation to the cilium. In contrast, the localisation of Cep290 and Chibby appears largely unperturbed in *MKS1*$^{\Delta 1}$ mutant spermatocytes, suggesting that these proteins are higher up in the hierarchy of ciliogenesis than MKS1.

Interestingly, CC2D2A is not detectable at the cilium in *MKS1*$^{\Delta 1}$ mutant spermatocytes, but a fraction of the protein appeared to co-localise with Asl at the outer centriole wall. CC2D2A is therefore able to localise to the centriole independently of MKS1, but it requires the presence of MKS1 to either enter the cilium or be retained there. These experiments show that MKS1 is required for the correct localisation of key TZ proteins.

4.2.3 Localisation defects in *B9D1*$^{\Delta 1}$ mutant cilia

Since proteins of the MKS module have been reported to depend on each other for localisation to the cilium in worms, MKS1-GFP and B9D2-GFP were crossed into the *B9D1*$^{\Delta 1}$ mutant background and analysed using 3D-SIM as described above (Williams et al., 2008). MKS1 and B9D2 were not detectable at the cilium in *B9D1*$^{\Delta 1}$ mutant spermatocytes (Figure 4.3),

indicating that MKS1 and B9D1 are interdependent for their localisation in *Drosophila*. Since MKS1 is required to efficiently localize all other TZ proteins tested, except Chibby and Cep290, the loss of MKS1 from the cilia in the B9D1 mutant strongly suggests that the cilia localization of most TZ proteins will be perturbed in the $B9D1^{\Delta 1}$ mutant background.

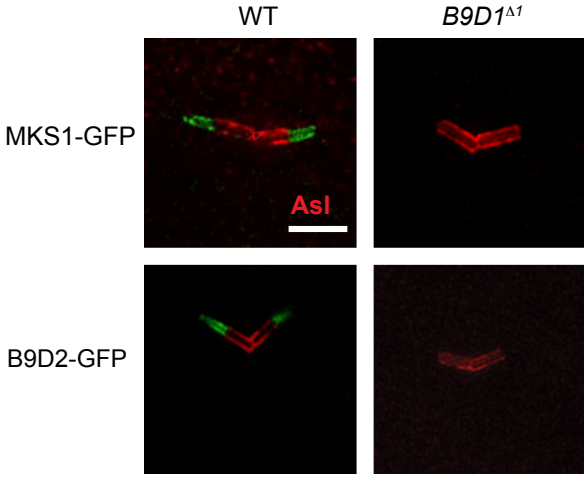

Figure 4.3 Localisation of MKS1 and B9D2 in WT and $B9D1^{\Delta 1}$ spermatocyte cilia. Representative 3D-SIM images of MKS1-GFP and B9D2-GFP (*green*) in WT (left panels) and $B9D1^{\Delta 1}$ (right panels) spermatocyte cilia, where the basal body is labelled with Asl (*red*). n>30 images.

4.2.4 Ultrastructural abnormalities in $MKS1^{\Delta 1}$, $B9D1^{\Delta 1}$ and $CC2D2A^{\Delta 1}$ mutant spermatocyte cilia

Since the localisation of most TZ proteins to the cilium is perturbed in $MKS1^{\Delta 1}$ mutant spermatocytes, electron tomography was carried out on the primary spermatocytes to study the ultrastructure of the cilium in WT, $MKS1^{\Delta 1}$ mutant and $MKS1^{\Delta 1}$ rescued by GFP-MKS1 (Figure 4.4 A). While the length of the basal body is not affected by the $MKS1^{\Delta 1}$ mutation (Figure 4.4 B), the axoneme is reduced in length from $\sim$ 500 nm to $\sim$ 150 nm (Figure 4.4 C). Consequently, the ratio of the axoneme to the basal body is reduced in $MKS1^{\Delta 1}$ mutant cilia (Figure 4.4 D). Furthermore, the characteristic electron density that indicates the presence of proteins or lipids at the ciliary membrane in the WT, was not observed in $MKS1^{\Delta 1}$ mutant

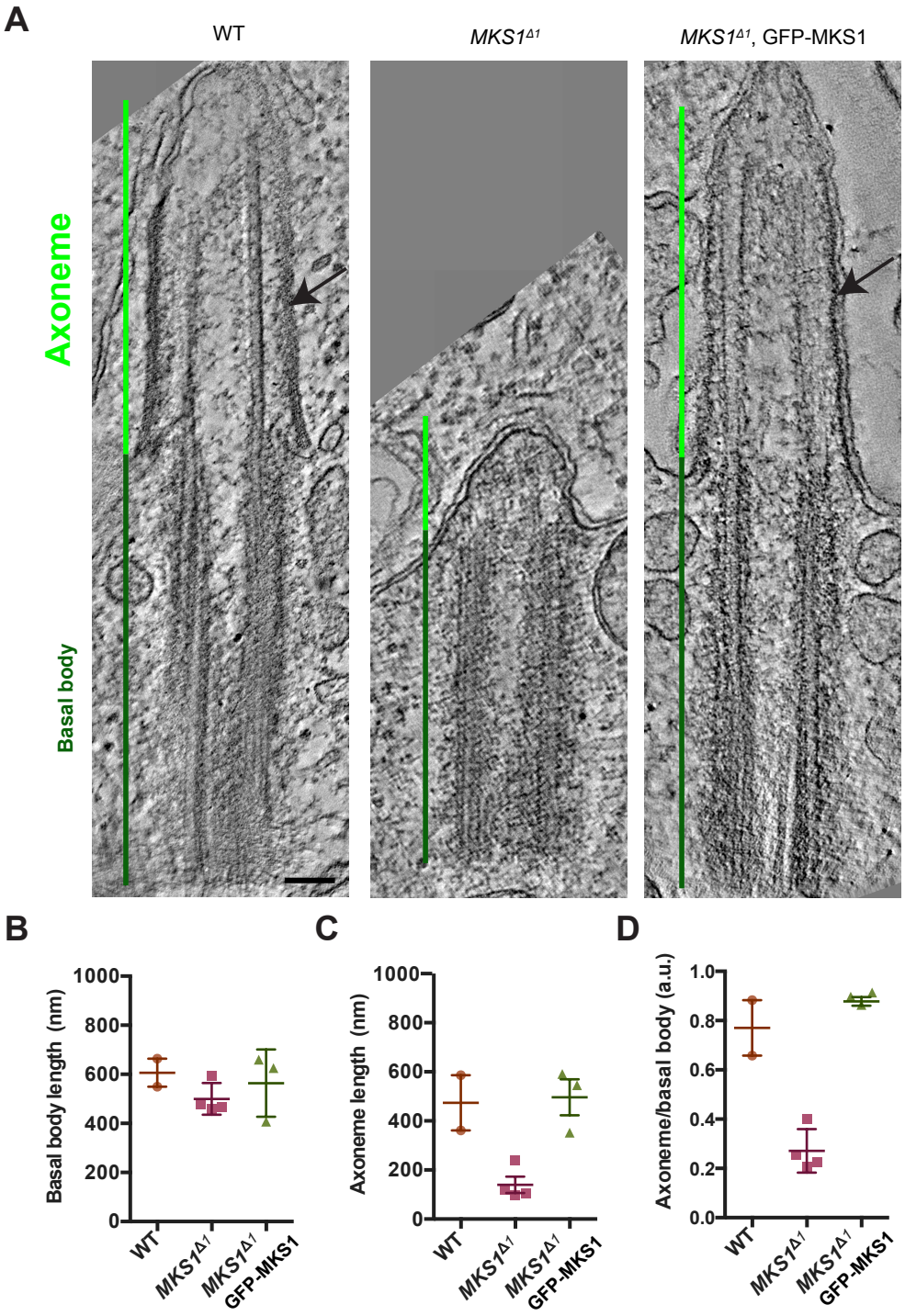

Figure 4.4 Electron microscopy of WT, *MKS1*$^{\Delta 1}$ mutant, and *MKS1*$^{\Delta 1}$, GFP-MKS1 spermatocyte cilia. A) Electron tomograms of WT, *MKS1*$^{\Delta 1}$ mutant, and *MKS1*$^{\Delta 1}$, GFP-MKS1 spermatocyte cilia showing the basal body (*dark green line*), axoneme (*bright green line*) and the electron density characteristic for the TZ (*arrows*) that is missing in *MKS1*$^{\Delta 1}$ cilia. B) Quantification of the length of the basal body C) Quantification of the length of axoneme D) Quantification of the ratio of the length of the axoneme and the basal body. Scale bar: 100 nm. Error bars represent the S.D. No statistical analysis was performed on these results as the *n* is too small. However, more cilia from different flies were observed by eye and the phenotype appeared highly reproducible.

spermatocytes (Figure 4.4 A, *arrows*). Importantly, the defects in both the length and the electron density of the axoneme are rescued by the expression of the GFP-MKS1 transgene in the $MKS1^{\Delta 1}$mutant background, indicating that the defects are specific to the loss of MKS1. Together with the localisation studies described in Section 4.2.2, these electron micrographs suggest that the TZ is severely compromised in $MKS1^{\Delta 1}$ mutant spermatocyte cilia.

Importantly, the $B9D1^{\Delta 1}$mutant phenotype recapitulates the $MKS1^{\Delta 1}$ mutant phenotype, as the cilium is reduced to $\sim$ 175 nm and no electron density was observed at the ciliary membrane (Figure 4.5). This result is consistent with the interdependency of MKS1 and B9D1 for their localisation to the cilium (described in Section 4.2.3). Interestingly, $CC2D2A^{\Delta 1}$ are also reduced in length at $\sim$ 350 nm, however, this reduction is less severe than the reduction observed in both $MKS1^{\Delta 1}$and $B9D1^{\Delta 1}$mutants. Centriolar microtubules extend to form a short axoneme in this mutant and some electron density can be observed at the ciliary membrane. A difference between the phenotype of $CC2D2A^{\Delta 1}$ mutants and the phenotype of $MKS1^{\Delta 1}$ and $B9D1^{\Delta 1}$mutants was also observed in electrophysiology experiments (described in Section 3.2.6). Taken together, these results suggest there is less overlap in the phenotypes of the $MKS1^{\Delta 1}$ and $CC2D2A^{\Delta 1}$ mutant alleles than in the phenotypes of the $MKS1^{\Delta 1}$ and $B9D1^{\Delta 1}$mutant alleles. $Cep290^{MecH}$(Basiri et al., 2014) mutant centrioles were found at the membrane, but did not extended their microtubules to form an axoneme in spermatocytes (Figure 4.5).

Together, these results suggest that MKS1 is required for proper TZ formation. The defects observed in $MKS1^{\Delta 1}$mutants are fully rescued by expressing GFP-MKS1 in the $MKS1^{\Delta 1}$mutant background. B9D1 appears to have a very similar role to MKS1, while Cep290 seems to be completely essential for TZ formation. In the absence of CC2D2A, the axoneme is shortened, but not to the same extent as in the absence of either MKS1 or B9D1. In all cases $\sim$ 3 tomograms were acquired, although more cilia from different flies

were always observed. Note that the processing of samples for TEM tends to result in some shrinkage of the tissue and that length measurements should therefore not be compared across EM and fluorescence microscopy.

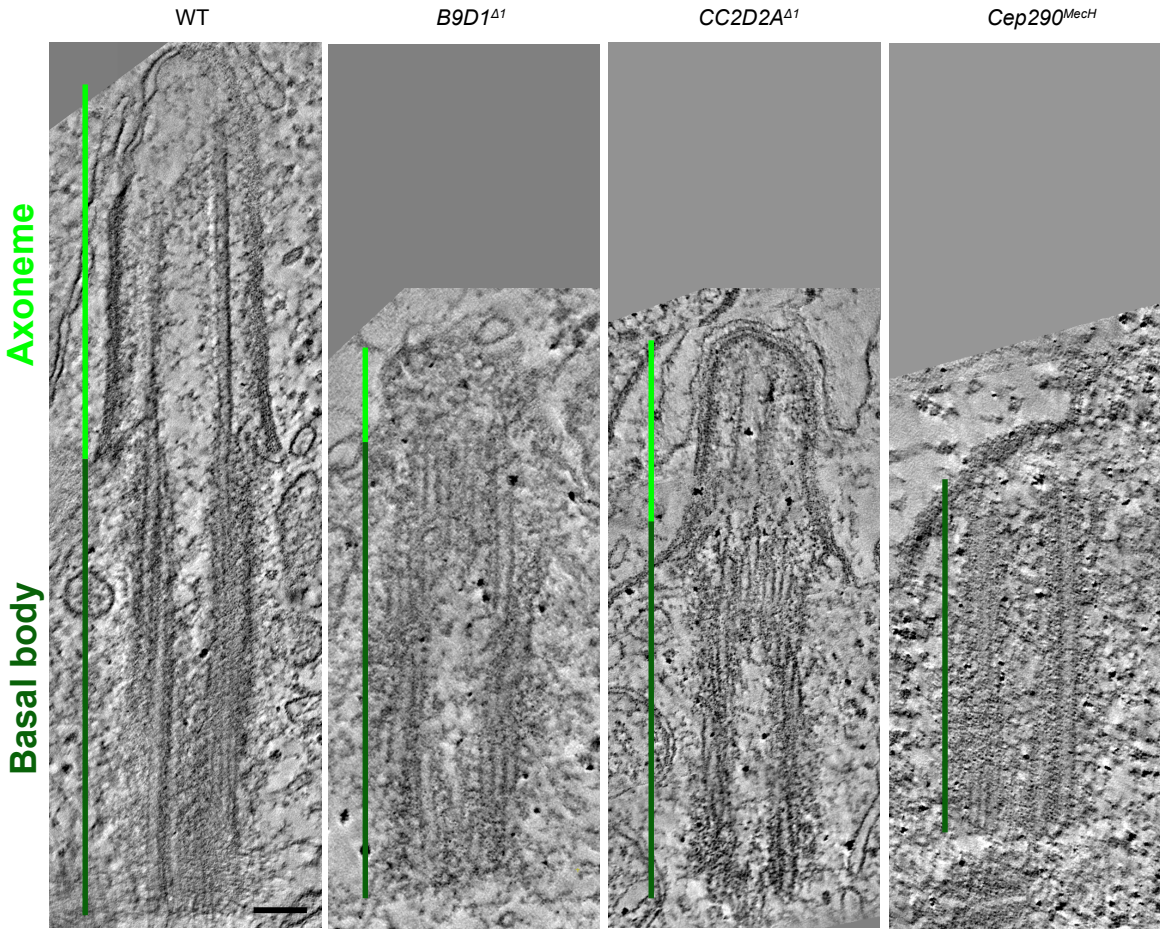

Figure 4.5 Electron microscopy of WT, *B9D1*$^{\Delta 1}$, *CC2D2A*$^{\Delta 1}$, *Cep290*^{MecH} mutant spermatocyte cilia. Electron tomograms of WT, *MKS1*$^{\Delta 1}$mutant, and *MKS1*$^{\Delta 1}$, GFP-MKS1 spermatocyte cilia showing the basal body (*dark green line*), axoneme (*bright green line*). The axoneme is shortened from $\sim$ 500 nm in WT to $\sim$ 175 nm in *B9D1*$^{\Delta 1}$and $\sim$ 175 nm in *CC2D2A*$^{\Delta 1}$mutant cilia. In *Cep290*^{MecH}(Basiri et al., 2014), no axonemes were observed. Scale bar: 100 nm.

4.3 Discussion

The resolution of conventional light microscopy is limited to the wavelength of light to $\sim$ 200 nm. The size of centrioles ranges from $\sim$ 100 nm in wing discs to $\sim$ 800 nm in spermatocytes, with WT spermatocyte axonemes measuring $\sim$ 700 nm (Franz et al., 2013). Since these dimensions are very close to the resolution limit of conventional fluorescent microscopy, super-resolution microscopy is revolutionising the fields of centrioles, centrosomes and cilia. 3D-SIM confirmed that *Drosophila* orthologues of ciliopathy proteins indeed localise to the TZ, in agreement with data from other model systems (Reiter et al., 2012). Interestingly, the proteins do not localise to the same structures or regions within the TZ, as was also recently observed for a subset of TZ proteins in RPE-1 cells (Yang et al., 2015). As in the RPE-1 cells, Cep290 localises to the centre of the axoneme in *Drosophila* spermatocytes, most likely overlapping with the microtubules. This localisation is consistent with reports that Cep290 forms a central cylinder that acts as a scaffold for the rest of the TZ (Schouteden et al., 2015). Indeed, Chibby overlaps with Cep290 to form a tight barrel. This is consistent with reports of Chibby localisation in mouse embryonic fibroblasts (MEFs) (Lee et al., 2014). Chibby is recruited to the basal body and TZ by Cep164 and required for the recruitment of Rabin 8 as well as Ahi1 and Arl13b (Burke et al., 2014; Lee et al., 2014). All other TZ proteins overlap with these two proteins, but the barrels they form are wider and appear to overlap with the ciliary membrane. The length of the barrel also varies between proteins, with the longest barrels extending almost to the top of the cilium. Since the spermatocyte cilium is very short, it is likely that it does not extend much beyond the TZ, although these cilia are slightly unusual and it is also possible that the entire cilium is a modified TZ that may have a role in the formation of the flagellum in the mature sperm.

Deletion of *MKS1* abolishes the ciliary localisation of all proteins except for Cep290 and Chibby, which shows that MKS1 is required for proper TZ assembly. Conversely, deletion

of *B9D1* disrupts the localisation of MKS1, suggesting that proteins of the MKS module are interdependent for their localisation and form a functional unit within the TZ. While CC2D2A fails to localise to the axoneme in $MKS1^{\Delta 1}$ mutant cilia, it localises to the basal body wall, where it overlaps with the Asl labelling. While CC2D2A is able to localise to the basal body in the absence of MKS1, it does rely on MKS1 either to localise to the cilium directly or to build a cilium or TZ that is competent to recruit CC2D2A. It is currently unclear whether CC2D2A has a role at the centriole/basal body in *Drosophila*. In the mouse, CC2D2A is known to localise to the mother centriole where it promotes the assembly of subdistal appendages (Veleri et al., 2014). In mammals, structures like the subdistal appendages distinguish the mother and daughter centriole and enable the mother, but not the daughter to dock at the plasma membrane and form the base of a cilium (Anderson, 1972; Tanos et al., 2013). Flies lack subdistal appendages, so the role of CC2D2A cannot be exactly the same. It is possible, however, that CC2D2A primes the centriole for cilia biogenesis in some way as, unlike in the mouse, it localises to both the mother and daughter centrioles in flies and these will be both go on to form cilia in spermatocytes.

While the axoneme in $CC2D2A^{\Delta 1}$ mutant cilia is dramatically shortened, it does extend, unlike $MKS1^{\Delta 1}$ and $B9D1^{\Delta 1}$ mutant cilia. This suggests that, while CC2D2A clearly has a role in TZ formation, there is less functional overlap between CC2D2A and MKS1 than between B9D1 and MKS1 in *Drosophila* spermatocytes. As described in Section 3.2.6, $CC2D2A^{\Delta 1}$ did not have any effect on the MRP of the sensory bristle cilia, while an increase in MRP was observed in both $MKS1^{\Delta 1}$ and $B9D1^{\Delta 1}$ mutants. Together, these results suggest that CC2D2A is not as closely related to MKS1 as B9D1 is. As mentioned before (Section 3.3), the different modules of the TZ have not been very well established and may vary between species and cell types. However, further experiments will be required to determine whether CC2D2A is a true MKS module protein.

In agreement with the lack of TZ protein localisation in $MKS1^{\Delta 1}$ and $B9D1^{\Delta 1}$ mutant

cilia, there is a lack of the electron density that can be observed at the membrane of the WT TZ. Furthermore, the axoneme fails to extend in both of these mutants. Although the function of these cilia are unknown, the results described in this Chapter and the previous Chapter suggest that the absence of these cilia does not result in any obvious defects in the flies. Most importantly, the defects in the spermatocyte cilia described above do not appear to lead to substantial defects in the sperm axonemes, even though it is widely assumed that these cilia will ultimately form the sperm axoneme (Fabian and Brill, 2012; Gottardo et al., 2013; Riparbelli et al., 2012; Tates, 1971). Importantly, the assembly of the sperm flagellum axoneme is independent of IFT (Avidor-Reiss and Leroux, 2015; Basiri et al., 2014). Since the TZ forms early in ciliogenesis, a role for the TZ in regulating IFT in the developing cilium has been proposed (Deane et al., 2001; Garcia-Gonzalo et al., 2011; Garcia-Gonzalo and Reiter, 2016). It seems possible, therefore, that the lack of defects in the mature sperm flagellum is because IFT is not required to build this flagellum. The relationship between MKS1, the TZ and IFT in other ciliated cells will be discussed in more detail in 5.

Chapter 5

Ultrastructural and localisation studies of sensory cilia

5.1 Introduction

In Chapter 3, it was observed that the $MKS1^{\Delta 1}$ mutation does not negatively affect cilia function, while in Chapter 4, extensive defects in the ultrastructure and protein localisation of spermatocyte TZ were described. In this Chapter, the ultrastructure and protein localisation of cilia present on the only other ciliated cell type in flies, the Type I sensory neurons, will be described.

The peripheral nervous system (PNS) of *Drosophila* comprises ciliated type I and non-ciliated type II neurons (Brewster and Bodmer, 1995; Kernan, 2007). Type I neurons each have a single dendrite with a cilium at the distal end. They are surrounded by three to four support cells, that each have a specialised role. The neuron and its support cells are all derived from a single ectodermal sensory organ precursor (SOP) cell (Brewster and Bodmer, 1995). In contrast, type II neurons have multiple dendrites and are not associated with

support cells. Type I neurons may have either external sensory (ES) structures in the cuticle or internally located stretch receptors, known as chordotonal (Ch) organs (Kernan, 2007).

ES organs may be either mechanosensory or chemosensory. The chaete, or sensory bristles are the most abundant ES organs. Located externally on the notum of the fly, they are also among the most accessible and amenable to imaging and functional studies. The SOP undergoes a series of highly stereotypical divisions to form the neuron and three other cells, the thecogen, tormogen and trichogen (Hartenstein, 1988; Hartenstein and Posakony, 1989). The thecogen forms the support cell most closely associated with the neuron, the sheath cell, while the trichogen (sometimes called hair cell) secretes the bristle shaft and the tormogen forms the socket.

Genetic screens have identified a number of genes required for sensory bristle ciliary function in *Drosophila* (Kernan et al., 1994; Willingham and Keil, 2004). These include two genes that are required for IFT: reduced mechanoreceptor potential A (RempA) and no mechanoreceptor potential B (NompB). NompB (IFT88 in humans) is a member of the IFT-B complex, which is primarily associated with anterograde transport, while RempA (IFT140 in humans) is part of the predominantly retrograde IFT-A complex (Han et al., 2003; Lee et al., 2008). In addition, these screens identified NompA, NompC, NompD and NompH. NompA physically attaches the cilium to the bristle and is required for the transduction of the mechanic stimulus to the neuron (Chung et al., 2001). To generate the action potential in response to the stimulus, ion channels in the membrane open. NompC encodes a transient receptor potential (TRP) channel in the bristle (Walker et al., 2000). NompH encodes a cytochrome P450 that is only expressed in sensory bristles, while the function of NompD is unknown (Kernan et al., 1994; Willingham and Keil, 2004).

The results described in this Chapter suggest that while there are initially substantial defects in $MKS1^{\Delta 1}$mutant cilia, these defects are largely rescued over time. In developing $MKS1^{\Delta 1}$mutant cilia, there are striking defects in both the microtubules and the

membrane. These are largely rescued by the time the cilia appear fully developed. However, while the TZ does form, it is shorter in mature $MKS1^{\Delta 1}$mutant cilia. Furthermore, a membrane surrounded volume could be observed in cilia at this stage in development. In $MKS1^{\Delta 1}$cilia, this volume is larger than in WT. Live cell imaging of NompA revealed that while $MKS1^{\Delta 1}$mutant cilia initially grows more slowly, the final signal does not seem different from WT.

5.2 Results

5.2.1 Ultrastructure of sensory cilia

In order to gain insight into the architecture of the sensory organs, serial block-face scanning electron microscopy (SBF-SEM) was used. With this technique, the block is automatically sectioned by an ultramicrotome within the microscope and the whole block face is then scanned after each section. Consequently, much larger volumes can be imaged by SBF-SEM than by TEM. The data described in this section were performed by Dr. Hélio Roque.

The ultrastructure of sensory cilia was analysed by SBF-SEM at two different time points; 48 and 72 hours after pupa formation (APF). At 48 hours APF, the cuticle is not formed yet. Since the cuticle is a barrier for EM stains, it is easier to observe the ultrastructure at this point in development (Figure 5.1). At this time point, the sensory organ extends into an electron dense bristle that extends away from the epithelium of the notum. Within the bristle cell, many microtubules and small mitochondria can be observed. The neuron extends into the hair cell, reaching the base of the bristle (Figure 5.1 A and C). The cilium is at the tip of the sensory process, protruding out of the hair cell into the void and elongating along the bristle (Figure 5.1 B and C, *magenta*). A thin, electron dense protrusion can be observed extending away from the ciliary tip (Figure 5.1 C, *dark blue*). This structure has not been described before, but may be important for cilia function. Strikingly, the ciliated

neuron (Figure 5.1 A and C, *cyan*) seems to be entirely encapsulated in hair cell (Figure 5.1 A, dark stained cell) and the support cell (Figure 5.1 A, *yellow dashed line*), with the sensory process protruding through hair cell and the support cell and emerging on the other side (Figure 5.1 A and C, *cyan dashed line*).

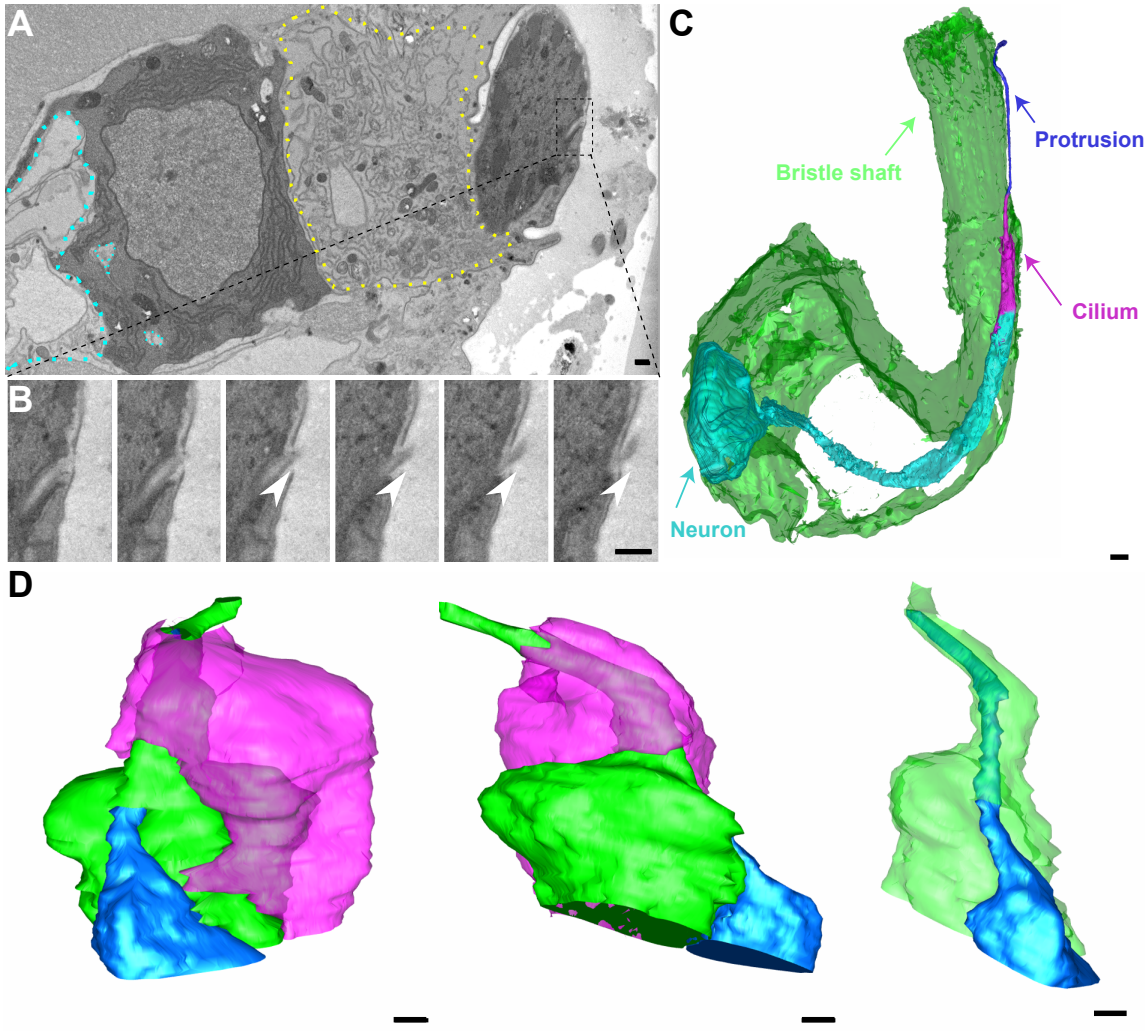

Figure 5.1 SBF-SEM of WT sensory bristle cilia. A) Electron micrograph showing a single slice of a 3D dataset giving an overview of the organisation of the neuron (outlined in *cyan dashed line*) hair cell (dark stained) and support cell (outlined in *yellow dashed line*). B) A higher magnification view of 6 z slices showing the ciliary tip and the protrusion extending into the void (*white arrowheads*). C) A 3D rendered model of this complete dataset, showing the arrangement of the hair cell (*green*), neuron (*cyan*), cilium (*magenta*) and ciliary protrusion (*dark blue*). D) Three views of the arrangement of the neuron (*cyan*), hair cell (*green*) and socket cell (*magenta*). Scale bars: 300 nm.

While it has been suggested the cilium is surrounded by the support cells or products secreted by these cells, how exactly this arrangement is formed is not fully understood (Hartenstein, 1988; Kernan, 2007). Drawings based on electron microscopy studies suggest that the hair (trichogen) and socket (tormogen) cells wrap "mesaxon-like processes" around the sheath (thecogen) cell and the neuron (Hartenstein, 1988). The term mesaxon-like is based on Schwann cells, which wrap around axons and secrete myelin (Monk et al., 2015). The, to my knowledge novel, 3D-reconstruction performed here, however, suggests the neuron is closely associated with the sheath cell and both the neuron and the sheath cell then form a "tunnel" through the volume of the socket cell. A time series of serial EM studies of Ch organs suggest that support cells, in this case the scolopale, can form a fissure and subsequently a cavity that allows the dendrite to extend into the cell (Carlson et al., 1997). A similar process could contribute to the formation of the ES organ, although time series like the ones described for Ch organs will be required to confirm this.

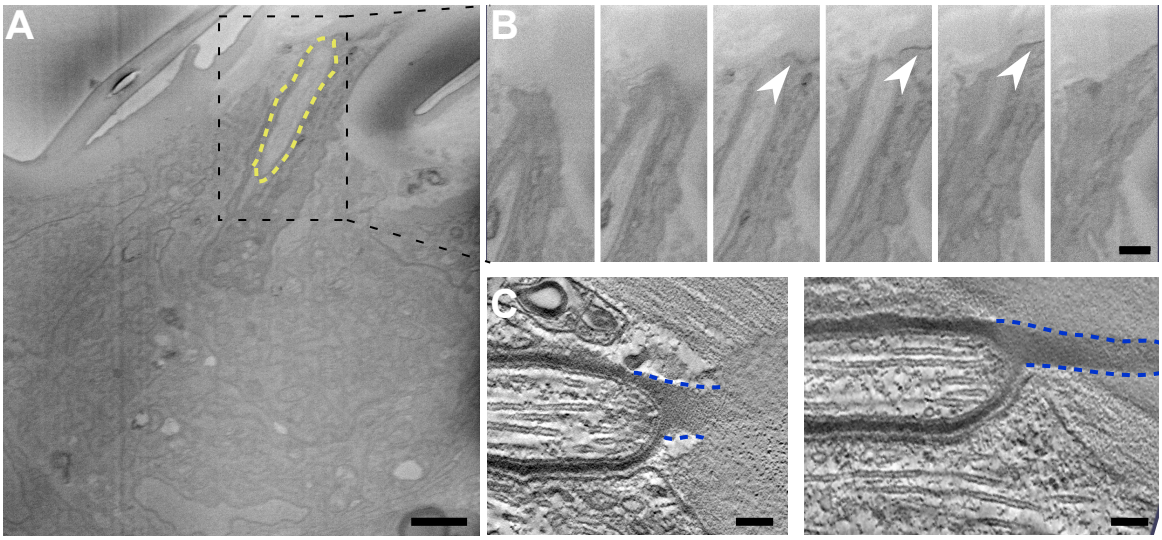

Figure 5.2 SBF-SEM and electron tomography of WT sensory bristly cilia. A) Overview of the cilium (*yellow dashed line*) within the sensory organ by SBF-SEM. B) Higher magnification 6 SBF-SEM z slices through the cilia volume at the ciliary tip and the electron dense protrusion extending into the cuticle (*white arrowheads*). C) Electron tomograms of two examples of the electron dense protrusion (*blue dashed lines*) extending from the ciliary tip into the cuticle. Scale bars A-B: 300 nm, C: 100 nm.

At 72 hours APF, the organisation of the sensory organ is largely unchanged (Figure 5.2). The cuticle is now deposited and the ciliary tip terminates at the cuticle barrier of the bristle. The electron dense protrusion is more difficult to observe within the cuticle. However, careful electron tomography shows that this protrusion is still present at 72 hours APF and extends into the cuticle, physically linking the ciliary tip to the bristle (Figure 5.2 C). These experiments have revealed a highly unusual tissue architecture, with the ciliated neuron essentially entirely surrounded by the support cell. This means the support cell has a donut shape, with a channel passing through it. Furthermore, the data shows that the tip of the cilium is physically connected to the cuticle via an electron dense protrusion.

5.2.2 Ultrastructural abnormalities in *MKS1*$^{\Delta 1}$ mutant sensory cilia

After establishing an overview of the sensory organ by SBF-SEM, electron tomography was performed to achieve increased magnification and resolution of key structures, focusing in particular on the cilium. The experiments in this section were performed in collaboration with Dr. Hélio Roque. At 48 hours APF, a clear disorganisation of the membrane and microtubules can be observed in *MKS1*$^{\Delta 1}$ mutant sensory cilia compared to WT cilia (Figure 5.3 A and B). The WT ciliary membrane is straight and organised tightly around an axoneme. The axoneme is composed of 9 doublet microtubules originating from the basal body. However, in the *MKS1*$^{\Delta 1}$ mutant cilia, very few microtubules extend from the basal body into the axoneme (Figure 5.3 E), the cilium is less regular and cylindrical and the ciliary membrane is more loosely organised (Figure 5.3 A and B). Specific defects can also be observed at the tip (Figure 5.3 C) and base (Figure 5.3 D and F) of the cilium. In WT cilia, there is electron density at the membrane of the ciliary tip and this part of the membrane is closely associated with the membrane of the support cell. In *MKS1*$^{\Delta 1}$mutant cilia, this electron density and the association with the support cell is less well organised (Figure 5.3 C). At the base of the WT cilium, the TZ can be distinguished immediately distal to the basal body as an area of

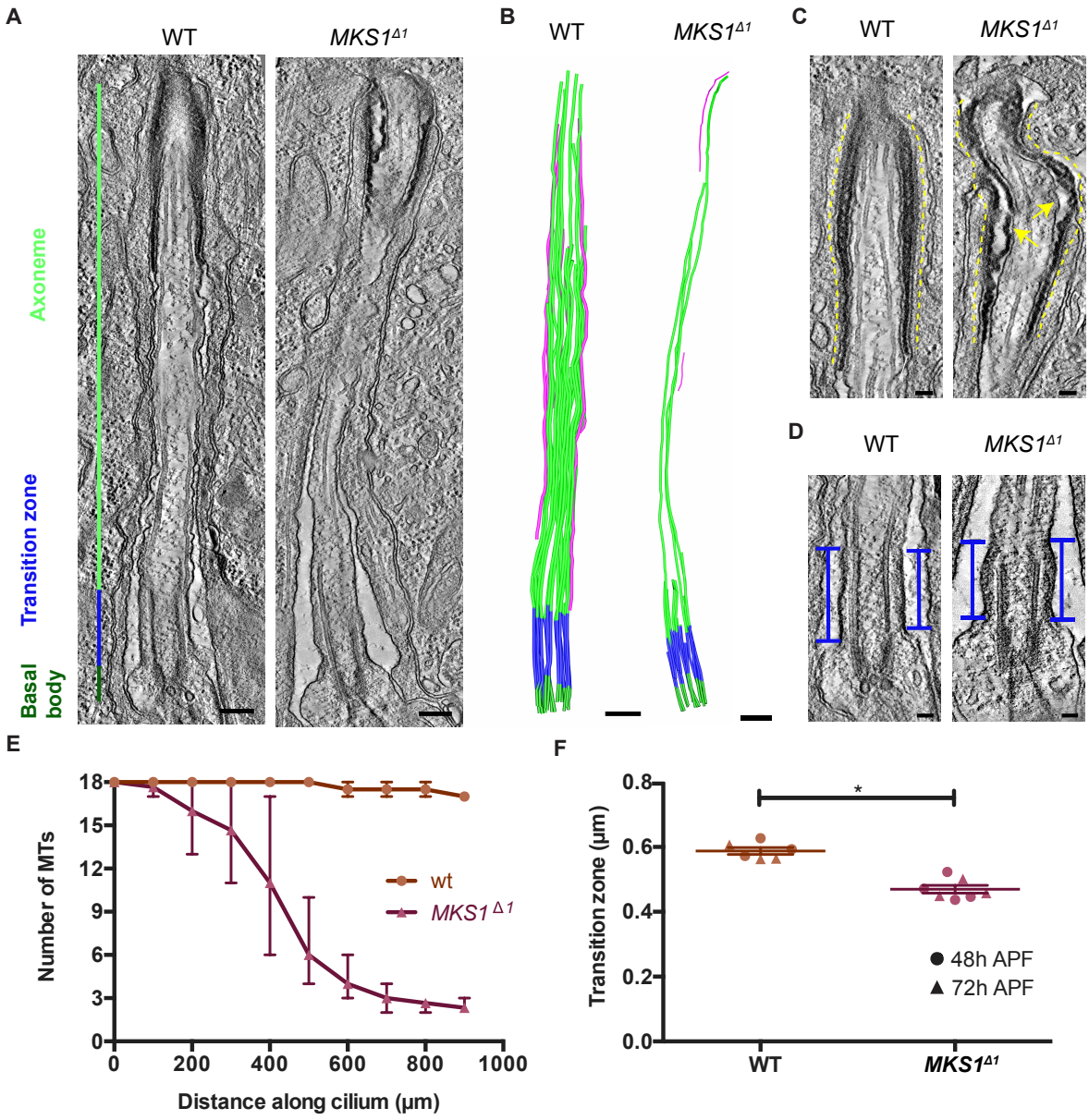

Figure 5.3 Electron tomography of sensory bristle cilia at 48 hours APF. A) Electron tomograms of WT and *MKS1*$^{\Delta 1}$ mutant sensory bristle cilia showing the basal body (*dark green line*), TZ (*blue line*) and axoneme (*bright green line*) at 48 hours APF. B) 3D models of the cilia shown in (A). Microtubules not attached to the basal body are labelled in *magenta*. C) Higher magnification electron tomograms of ciliary tip. In *MKS1*$^{\Delta 1}$ mutant cilia gaps (*yellow arrows*) are present between the ciliary membrane and the sheath cell membrane (*dashed yellow line*), and the electron-dense crystalline array normally found between the cells appears disordered. D) Higher magnification electron tomograms of the TZ (*blue capped lines*). The *MKS1*$^{\Delta 1}$ mutant TZ is shorter and the electron dense material at the membrane appears more diffuse. E) Quantification of the number of axonemal microtubules derived from the basal body present at various lengths along the cilium. F) Quantification of TZ length. Note that as there was no difference in the TZ between 48 and 72 hours APF, some data is taken from tomograms at 72 hours APF. Scale bars A-B: 500 nm, C-D: 100 nm. Error bars represent the S.D. Significance was assessed using a Wilcoxon test, *p<0.01.

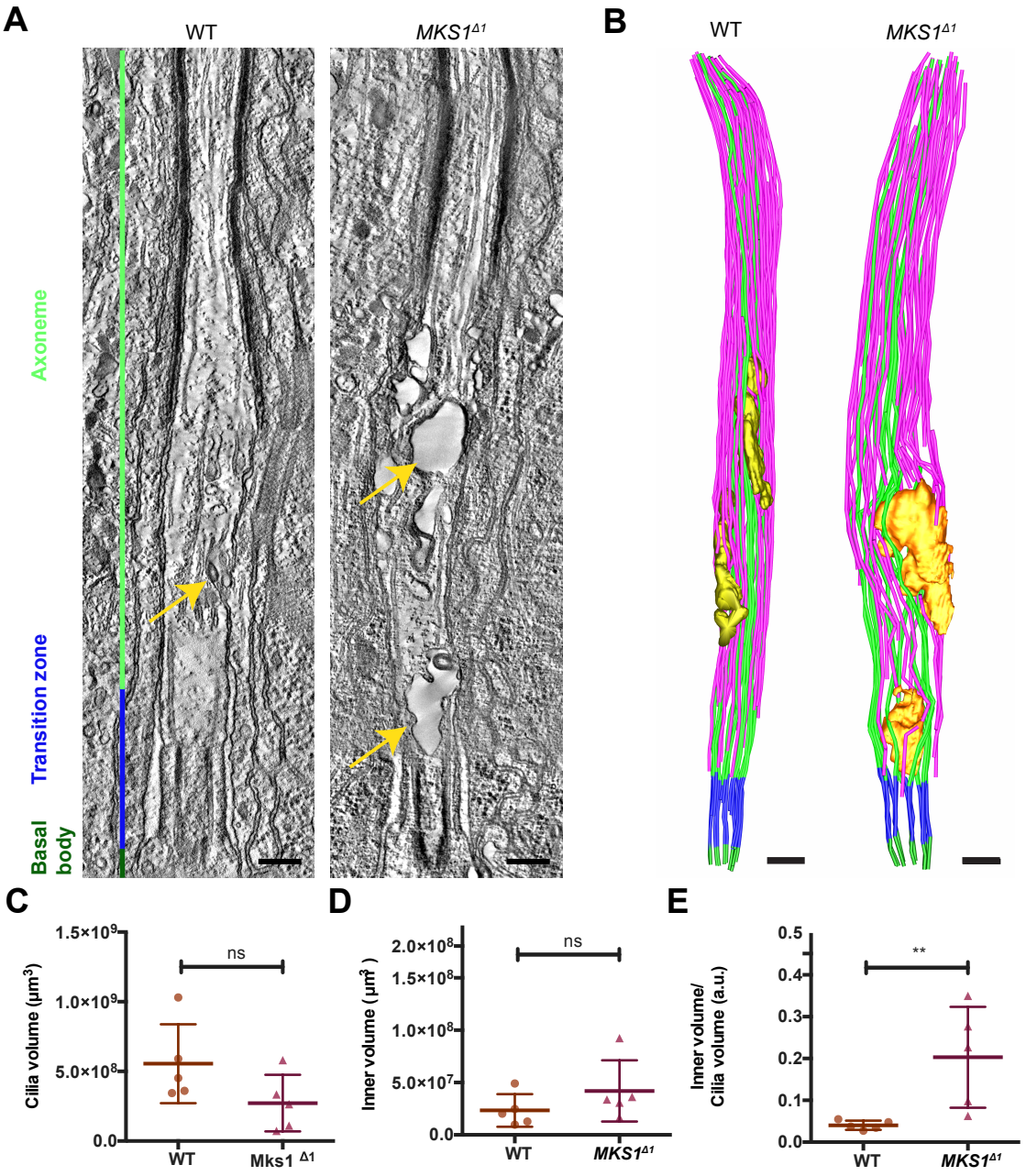

Figure 5.4 Electron tomography of sensory bristle cilia at 72 hours APF. A) Electron tomograms of WT and *MKS1*$^{\Delta 1}$ sensory bristle cilia showing the basal body (*blue line*), TZ (*dark green line*) and axoneme (*bright green line*) at 72 hours APF. A membrane surrounded volume can be observed within the cilium (*gold arrows*) and this is larger in *MKS1*$^{\Delta 1}$. B) 3D models of A, showing microtubules not attached to the basal body (*magenta*), the inner membrane surrounded volume (*gold*) in addition to the basal body, TZ and axonemal microtubules. C) Quantification of the total acquired cilia volume in WT and *MKS1*$^{\Delta 1}$ mutants. D) Quantification of the inner volume in WT and *MKS1*$^{\Delta 1}$ mutants. E) Quantification of the ratio of the inner volume to the total acquired cilia volume in WT and *MKS1*$^{\Delta 1}$ mutants. Since the inner volume is slightly, but not significantly larger and the total volume is slightly, but not significantly smaller, the inner volume is proportionally larger in *MKS1*$^{\Delta 1}$ mutant cilia. Scale bar: 500 nm. Error bars represent the S.D., significance was assessed using a students t-test, p*<0.01, p**<0.001.

the membrane that is relatively straight and electron dense. In $MKS1^{\Delta 1}$ mutant cilia, the TZ is still present, but is significantly (p = 0.031) smaller (0.469 ± 0.012 µm) than the WT TZ (0.587 ± 0.011 µm). Note that the TZ did not change between 48 and 72 hours APF and the measurements of the TZ at 72 hours were also included in the analysis presented in Figure 5.3 F. At 72 hours APF, the number of microtubules in $MKS1^{\Delta 1}$ mutant cilia is closer to the number of microtubules in WT cilia (Figure 5.4 A and B). The membrane structure also resembles the WT cilium more closely. At this stage in development, a large membrane-surrounded volume can be observed within the cilium (Figure 5.4 A, *yellow arrows* and B, *gold*). This volume is larger in $MKS1^{\Delta 1}$ mutant cilia (Figure 5.4 D), although

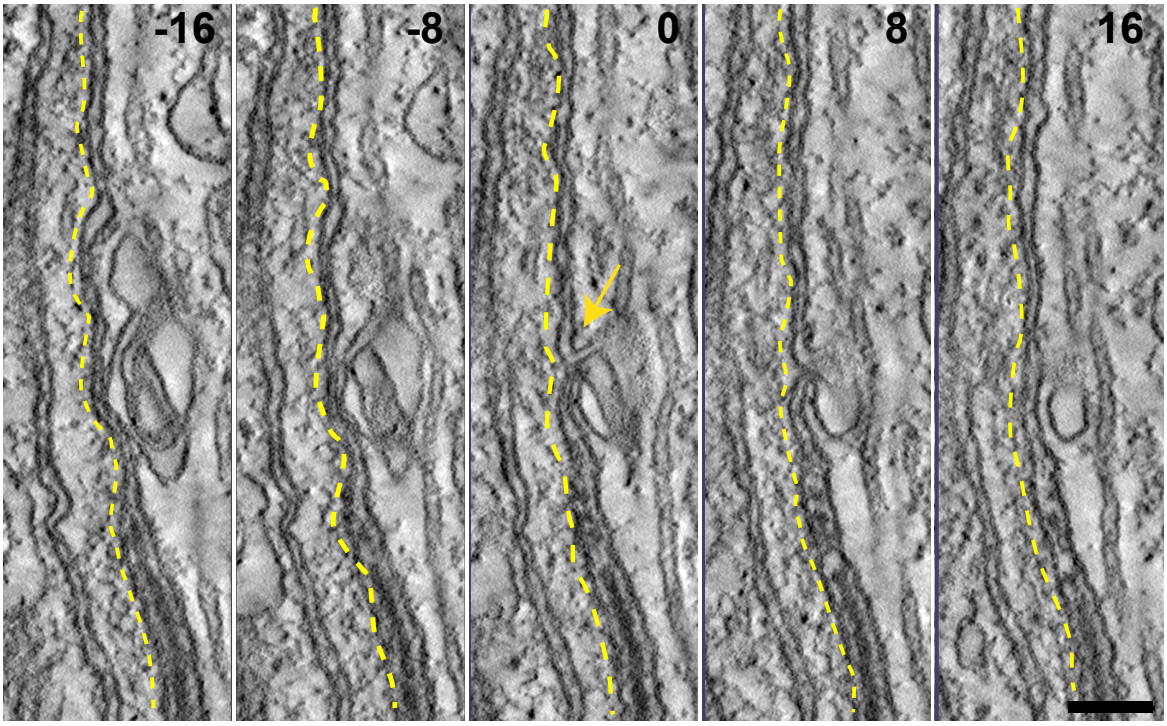

Figure 5.5 Electron tomography of sensory bristle cilia membrane surrounded inner volume. Electron micrographs of serial sections of the same sample show that the inner volume is connected to the extracellular environment via a narrow channel in the ciliary membrane (*gold arrow*, in section 0), the sheath membrane is marked with *dashed yellow line*. Scale bar: 100 nm.

significance is not reached. This may be in part due to the small *n*, but since the total ciliary volume is smaller (Figure 5.4 C, again not significant) the inner membrane surrounded volume clearly is proportionally larger in $MKS1^{\Delta 1}$ mutant cilia (Figure 5.4 E). Interestingly, this

inner membrane surrounded volume appears to be connected to the extracellular environment via a narrow channel in the ciliary membrane (Figure 5.5). This membrane surrounded volume has not been observed before and its functional significance is therefore unknown.

In summary, while there are clear defects in the microtubules and the membrane of sensory cilia at 48 hours APF, these defects appear to be largely corrected by 72 hours. At 72 hours APF $MKS1^{\Delta 1}$ mutant cilia can only be distinguished from WT by the slightly shorter TZ and the proportionally increased membrane surrounded volume within the cilium.

5.2.3 Larval behaviour assays

While no severe defects were observed in $MKS1^{\Delta 1}$ mutant sensory cilia at 72 hours APF, the ciliary structure is perturbed at 48 hours APF, as described above (Section 5.2.2). This result is consistent with the observations that adult $MKS1^{\Delta 1}$ mutant flies exhibit few, if any defects in ES cilia function and associated behaviours (see Sections 3.2.5 and 3.2.6) but this does not exclude the possibility that the $MKS1^{\Delta 1}$ mutation affects the function of Ch organs. In the larva, Ch organs are required for normal hearing and crawling. Therefore, preliminary studies of these behaviours were conducted on third instar larvae, just before pupa formation.

First, a hearing assay, adapted from previous studies in *Drosophila*, was performed (Styczynska-Soczka and Jarman, 2015). WT larvae startle in response to sound, which can be observed as a retraction, which may be followed by a change of direction or a prolonged absence of movement (freeze) (Wu et al., 2011). Larvae were played 500 Hz tones and their behaviour was scored. Higher scores indicate stronger responses. Interestingly, the $MKS1^{\Delta 1}$ mutant larvae do have a significantly ($p = 0.036$) reduced response to sound (1.780 ± 0.062) compared to WT (2.320 ± 0.167) (Figure 5.6 A). This is in contrast to behaviour studies in adults, which showed an increased response to stimuli (Section 3.2.5).

To investigate whether the reduced response to sound was indicative of a general reduc-

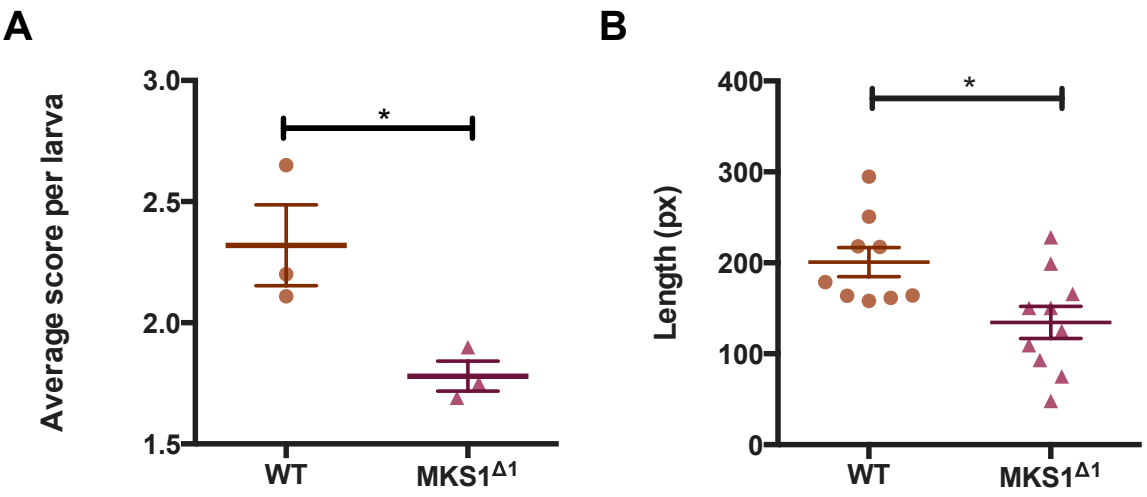

Figure 5.6 Quantification of behaviour in WT and *MKS1*$^{\Delta 1}$ mutant larvae. A) Quantification of the average response per larva to a pure 500 Hz tone. Each data point is an average of 10 larvae over 10 tones. B) Quantification of the distance crawled by individual larvae in 2 minutes. Error bars represent the S.E.M., significance was assessed using a Mann-Whitney test (A) or using a students t-test (B), p*<0.01.

tion in ciliary function, analysis of larval crawling behaviour was performed (Styczynska-Soczka and Jarman, 2015). WT larvae crawl around freely, whereas defects in proprioception cause flies with defective cilia to move less (Caldwell et al., 2003b). WT and *MKS1*$^{\Delta 1}$ mutant larvae were placed on an apple juice-agar plate and imaged while crawling freely for 2 minutes. *MKS1*$^{\Delta 1}$ mutant larvae covered significantly (p = 0.013) less distance (134.5 px $\pm$ 17.60) than WT larvae (200.9 px $\pm$ 16.02) (Figure 5.6 B), suggesting that these larvae have defects in proprioception. While the sound and crawling experiments are preliminary, they do suggest that there may be small, but significant, defects in ciliary function in *MKS1*$^{\Delta 1}$ mutant larvae. This is clearly in contrast to behaviour and electrophysiology in adults, which, if anything, show a slight increase in ciliary function in *MKS1*$^{\Delta 1}$ mutant flies.

5.2.4 NompA and NompC localise normally in *MKS1*$^{\Delta 1}$

Although most ultrastructural defects in *MKS1*$^{\Delta 1}$ mutant cilia appear to be "rescued" by 72 hours APF, it seemed possible that the localisation of other ciliary proteins may be affected

by the mutation. To study the localisation of NompA, which is thought to form a mechanical link that is required for transduction of stimuli, a NompA-GFP trap cassette in the WT and $MKS1^{\Delta 1}$mutant backgrounds was imaged at 72 hours APF (Chung et al., 2001). In both WT and $MKS1^{\Delta 1}$mutant cilia, NompA-GFP localised strongly to the base of the cilium with a thin and much dimmer protrusion extending into the sensory process (Figure 5.7 B, *arrowhead*). No significant difference (p = 0.667) was observed in the length of this protrusion in $MKS1^{\Delta 1}$mutants (14.12 nm $\pm$ 0.827) compared to WT (14.79 nm $\pm$ 0.800).

Quantification of the fluorescence signal (Figure 5.7 C) showed that the amount of NompA is not significantly different (p = 0.310) in $MKS1^{\Delta 1}$mutant (4109 a.u. $\pm$ 311.2) and WT cilia (5442 a.u. $\pm$ 835.1). To study the localisation of TRP ion channel NompC, expression of a UAS-NompC-GFP transgene was driven by NompC-Gal4 in the WT and $MKS1^{\Delta 1}$mutant backgrounds and imaged at 72 hours APF (Walker et al., 2000). NompC-GFP localised to the base of the cilium as a single dot in both WT and $MKS1^{\Delta 1}$mutant sensory cilia (Figure 5.7 E). The quantity of NompC-GFP appears not significantly different (p = 0.859) in $MKS1^{\Delta 1}$mutant cilia (4790 a.u. $\pm$ 1341) and WT (4317 a.u. $\pm$ 1015), indicating that the distribution of this ion channel is not perturbed in $MKS1^{\Delta 1}$mutant cilia (Figure 5.7 F). Together, these results suggests there are no changes in the NompC ion channel or the mechanical link between the cilium and its support cells.

5.2.5 Changes in IFT in $MKS1^{\Delta 1}$ mutant sensory cilia

To assess whether IFT is affected by the loss of MKS1, a GFP tagged version of NompB (IFT88, required for anterograde transport) and a YFP tagged version of RempA (IFT140, required for retrograde transport) were expressed in WT and $MKS1^{\Delta 1}$ mutant backgrounds and imaged in sensory bristles at 72 hours APF (Han et al., 2003; Lee et al., 2008). In both WT and $MKS1^{\Delta 1}$ mutant cilia, NompB-GFP forms an elongated structure at the base of the cilium (Figure 5.8 B-D). Interestingly, the signal is significantly (p = 0.008) more

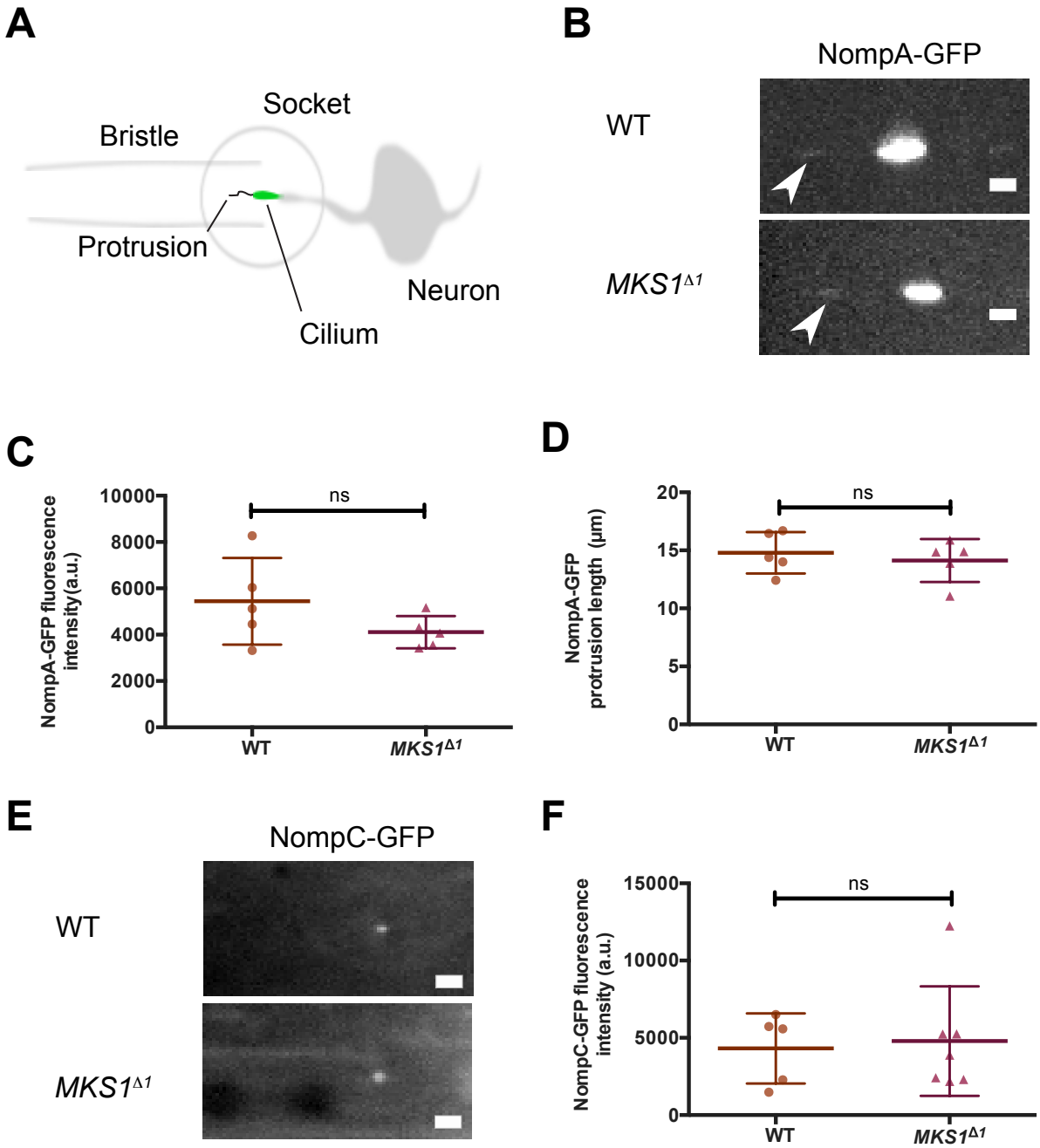

Figure 5.7 Localisation of NompA and NompC in WT and *MKS1*$^{\Delta 1}$ mutant cilia. A) Schematic overview of the cilium in the sensory bristle. B) Representative image of NompA-GFP in WT and *MKS1*$^{\Delta 1}$ mutant cilia. NompA localises strongly to the base of the cilium and a thin protrusion with lower fluorescence intensity (*white arrowheads*) extends into the sensory process. C) Quantification of the fluorescence intensity of NompA-GFP in WT and *MKS1*$^{\Delta 1}$ mutant cilia. D) Quantification of the distance from the tip of the protrusion to the base of the cilium in WT and *MKS1*$^{\Delta 1}$ mutant cilia. E) Representative images of NompC-GFP in WT and *MKS1*$^{\Delta 1}$ mutant cilia. F) Quantification of the fluorescence intensity of NompA-GFP in WT and *MKS1*$^{\Delta 1}$ mutant cilia. Error bars represent the S.E.M., significance was assessed using a Mann-Whitney test, ns = not significant. Scale bar: 2µm.

elongated in $MKS1^{\Delta 1}$ mutant cilia (3.072 nm ± 0.247), than in WT (2.299 nm ± 0.091), while intensity of the signal appears similar (p = 0.802) in $MKS1^{\Delta 1}$mutant (955.6 a.u. ± 86.28) cilia and in WT (1056 a.u. ± 275.5). Together, these results show there is more NompB-GFP present at the base of the cilium in $MKS1^{\Delta 1}$ mutant cilia than in WT cilia.

RempA-YFP forms a dot at the base of the cilium in both WT and $MKS1^{\Delta 1}$mutants (Figure 5.8 E). The intensity of RempA-YFP, however, appears significantly (p = 0.008) lower in $MKS1^{\Delta 1}$ mutants (800.1 a.u. ± 93.34) than in WT (1287 a.u. ± 67.35) (Figure 5.8 F). This suggests that the localisation of IFT-B complex components to the base of the cilium is increased, while the localisation of IFT-A complex components is decreased.

IFT complexes have be visualised by electron microscopy as "trains" travelling along the microtubules in *Chlamydomonas* and some human cells (Marshall, 2013; Rogowski et al., 2013; Stepanek and Pigino, 2016; Vannuccini et al., 2016). Interestingly, in electron tomograms of the fly sensory cilia, electron dense particles can be observed along the microtubules at the base of the cilium (Figure 5.8 F, *orange arrows*). The appearance of these particles is consistent with IFT particles observed in the literature (Marshall, 2013; Rogowski et al., 2013; Stepanek and Pigino, 2016; Vannuccini et al., 2016). Moreover, while in the WT the putative IFT trains are short and interspersed, in $MKS1^{\Delta 1}$mutant cilia the IFT trains are longer and are almost continuous, potentially in agreement with the increase in NompB-GFP observed at the base of the cilium (Figure 5.8 A).

Surprisingly, however, in sensory cilia these putative IFT particles are located on the inside of the microtubules. In examples in the literature, which are mostly obtained from *Chlamydomonas*, the IFT trains are on the outside of the axoneme, between the microtubules and the membrane. Although further experiments will be required to test whether these electron dense particles really are IFT complexes, this result raises the possibility that IFT particles may be assembled and transported on either the luminal side of the axoneme or the membrane facing side, depending on the cell type and organism.

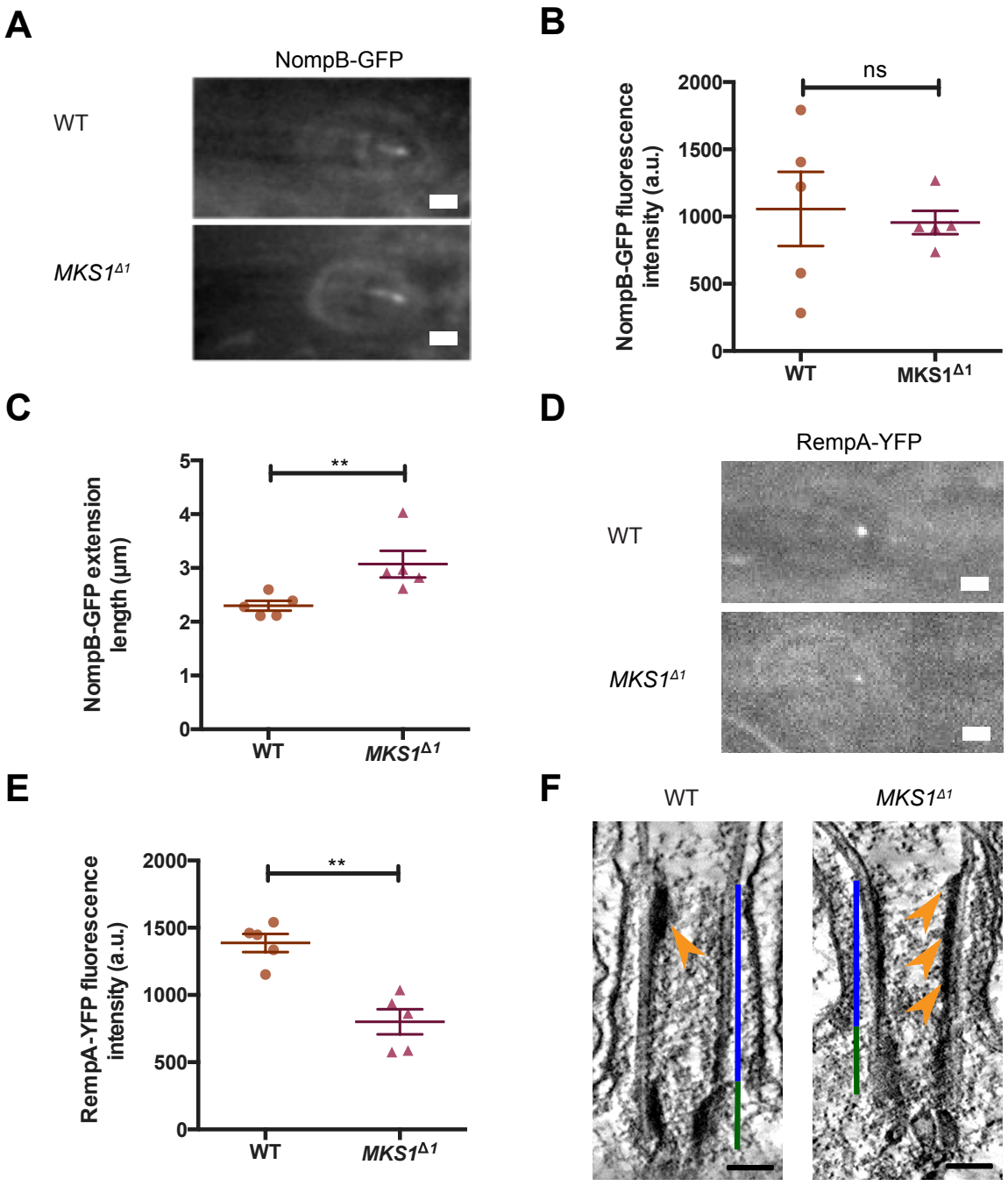

Figure 5.8 IFT in WT and *MKS1*$^{\Delta 1}$ mutant sensory bristle cilia. A) Representative images of NompB-GFP in WT and *MKS1*$^{\Delta 1}$ mutant cilia. B) Quantification of the intensity of the NompB-GFP signal in A. C) Quantification of the length of the NompB-GFP signal in A. D) Representative images of RempA-YFP in WT and *MKS1*$^{\Delta 1}$ mutant cilia. E) Quantification of the intensity of the RempA-YFP signal in D. F) Putative electron dense IFT trains (*orange arrows*) in the TZ (*blue line*) of sensory bristle cilia. Each data point represents the average of all cilia in the field of view per pupa. Significance was assessed using a Mann-Whitney test, ns = not significant, p*<0.01, p**<0.001. Scale bars A and D: 2 µm, F: 100 nm.

5.2.6 Live-cell imaging of ciliogenesis

In order to gain more dynamic insight into the process of ciliogenesis, a live cell imaging protocol was established. Fluorescently labelled RempA, NompA, NompB and NompC were tested as ciliary markers. These fluorescent constructs were expressed in a WT background. NompC-GFP expression was driven by the NompC-Gal4 driver, while all other fusion proteins were expressed under the endogenous promoter. The fluorescent proteins were imaged in developing sensory bristles in the *Drosophila* pupal notum over extended periods of time on an Andor spinning disk system. The pupal notum is well established for live cell imaging (Zitserman and Roegiers, 2011). Of the potential cilia markers, only NompA-GFP was present at early enough stages and at sufficient fluorescence levels to allow imaging the growing cilium over long periods of time (up to 24 hours).

To image NompA-GFP, the pupal case was partially removed from pupae at 30 hours APF. Pupae were then imaged for 22 hours on a spinning disk system. Both in WT and $MKS1^{\Delta 1}$ cilia, NompA-GFP showed a highly unusual dynamic profile (Figure 5.9 A-B). Initially, protein localized as small dot that then extended in length in a linear fashion to a size of $\sim$ 25 µm in both WT and $MKS1^{\Delta 1}$ cilia. After a short plateau phase, the signal abruptly dropped to $\sim$ 4 µm. Although the the final length of the NompA-GFP signal does not appear to be significantly (p = 0.1130) different in $MKS1^{\Delta 1}$ mutant cilia (3.915 $\pm$ 0.239) compared WT (4.471 $\pm$ 0.225) (Figure 5.9 B), the initial rate of NompA extension is slightly, but significantly (p = 0.011) lower in $MKS1^{\Delta 1}$ mutants (0.008 $\pm$ 0.001) compared to in WT (0.012 $\pm$ 0.001) (Figure 5.9 C). However, NompA-GFP appears to form both a bright dot and a much dimmer protrusion (see Section 5.2.4). This protrusion possibly corresponds to the electron dense protrusion observed in SBF-SEM and electron tomography studies of the sensory bristle cilium (see Sections 5.2.1 and 5.2.2). Therefore, it seems likely that NompA-GFP does not just label the cilium.

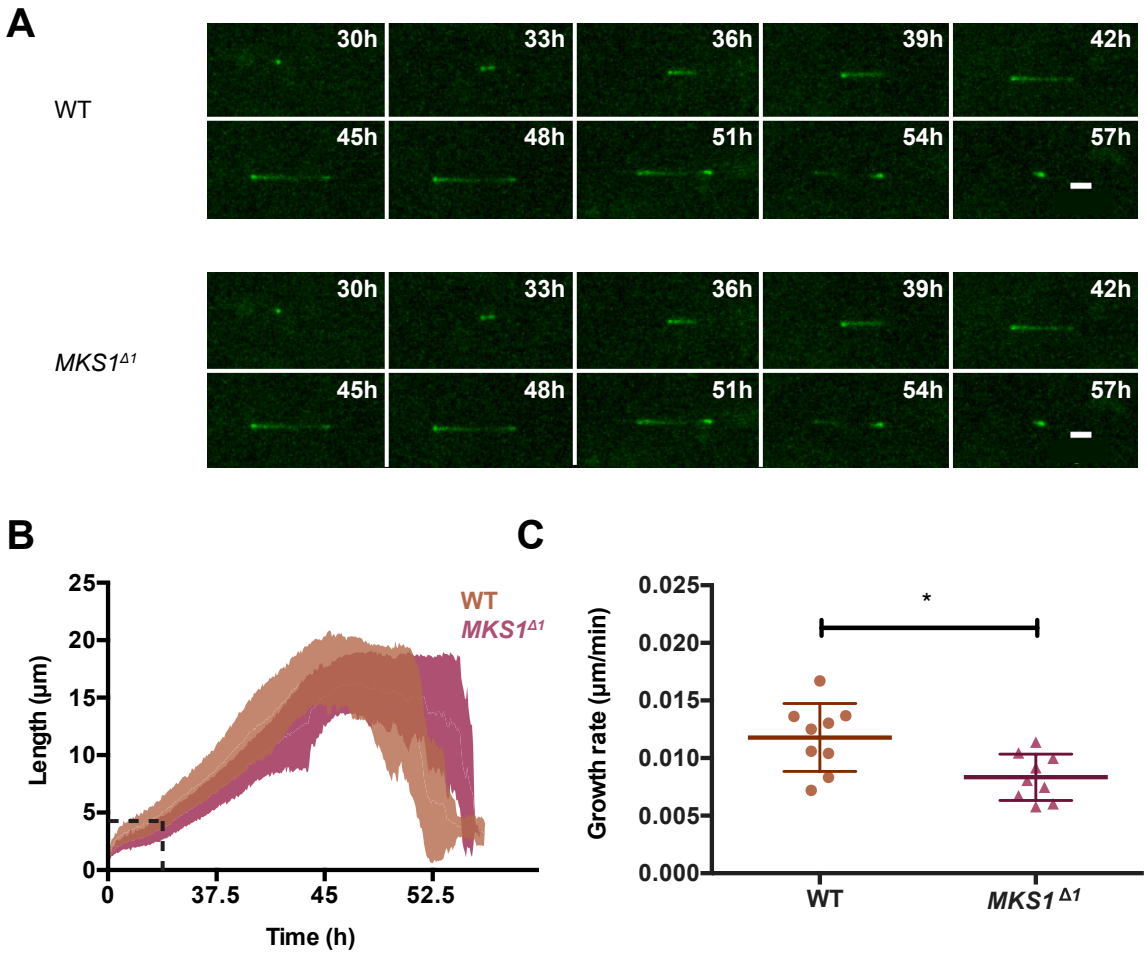

Figure 5.9 Live cell imaging of NompA-GFP in bristle cilia. A) Stills from representative cilia in WT (top panel) and *MKS1*$^{\Delta 1}$(bottom panel). B) Quantification of NompA-GFP incorporation in sensory bristle cilia in WT and *MKS1*$^{\Delta 1}$mutant cilia over $\sim$ 25 25 hours. Data is presented as all cilia in the field of view of 9 flies of each genotype $\pm$ the S.E.M. C) Quantification of the initial rate of NompA-GFP incorporation in WT and *MKS1*$^{\Delta 1}$mutant sensory bristle cilia. Scale bar: 5 µm. Error bars represent the S.E.M., significance was assessed using a students t-test, *p<0.01.

More detailed analysis of NompA-GFP, such as co-expression with other fluorescent cilia proteins, will be required to determine which structures are labelled by the constructs and what the significance of the drop in the length of the NompA-GFP signal is. Moreover, further fluorescent constructs (or combinations thereof) could be tested in this set-up. What is clear, however, is that the cilia in the pupal notum can be imaged successfully over up to 24 hours, provided the fluorescent signal is bright enough.

5.3 Discussion

Each bristle on the notum of the fly is associated with an ES organ that consists of a ciliated neuron and its support cells, all of which are derived from one SOP. The divisions and differentiation of the SOP and its progeny are highly stereotypical and well described (Brewster and Bodmer, 1995; Ghysen and Dambly-Chaudiere, 1989; Ghysen et al., 1993; Kernan, 2007). Their location on the outside of the body makes the sensory bristles suitable for fluorescence (live-)imaging as well as electron microscopy. To my knowledge, the arrangement of the ES organ within the tissue is studied both on a larger scale (using SBF-SEM) and in more detail (using electron tomography) than previously. Both techniques offer 3D analysis of the cilia and the surrounding tissue and reveal a highly unusual tissue architecture. The dendrite of the ciliated neuron extends through the support cell, which envelops the neuron entirely. This arrangement is present at both 48 and 72 hours APF and, to my knowledge, has not been observed in 3D and at this level of detail before. To form such a "tunnel" through the support cell, the ES neuron dendrite must either extend into the support cell from the basal side and exit at the apical side, with concomitant rearrangement of the support cell membrane to allow the formation of a tunnel or the support cell must envelop the growing dendrite and fuse to form a hollow. While this is a fascinating question, it may be difficult to answer. The ES organ develops between $\sim$ 30 and $\sim$ 72 hours APF and during this period the tissue moves as the pupa develops. Therefore, to get good quality live-imaging data, the tissue would have to be imaged over long periods of time and the z-stacks would have to be large enough to ensure the relevant cells stay in focus, or the microscope should be able to reliably focus on the tissue automatically. This means that fluorescent markers have to be bright and photostable. It may also be difficult to resolve the different cells. One possibility could be to express different wavelength UAS reporter constructs driven by cell type specific Gal4 drivers, although most Gal4 drivers tend to be

expressed in multiple cell types of the sensory organs (Nicholson et al., 2008). Another possibility is to perform SBF-SEM on a series of timed pupae. Since the sample preparation, image acquisition and image reconstruction are all time consuming, this will be very labour intensive, depending on the time resolution required to build an accurate model.

The combination of SBF-SEM and electron tomography also revealed an electron dense protrusion that physically connects the ciliary tip to the cuticle. This is likely required for the transmission of mechanical force from the hair to the mechanosensory neuron. Previously, it was shown that the *Drosophila* ciliary protein NompA localises to sensory organs and is required for the connection between the sensory cilium and cuticular structures (Chung et al., 2001). In my hands, NompA-GFP localises to a bright dot at the base of the bristle and extends into the bristle as a thin (and much dimmer) protrusion at 72 hours APF. This suggests that NompA may localise to, or be part of the electron dense protrusion mechanically links the bristle and the ciliated neuron. This hypothesis could be addressed by immunogold labelleling.

Electron tomography at 48 and 72 hours APF showed while there are defects in the organisation of $MKS1^{\Delta 1}$mutant cilia, the ultrastructure of the cilium is largely normal by 72 hours APF. At 48 hours APF, most of the basal body microtubules extend to form the axoneme in the WT cilium. The cilium as a whole is relatively straight and the membrane is organised tightly around the microtubules. In $MKS1^{\Delta 1}$mutant cilia, however, only a few of the basal body microtubules have extended at this time point. The cilium lacks structure and the membrane is less organised. At 72 hours, however, these defects are largely rescued. Both the WT and the $MKS1^{\Delta 1}$basal bodies have now extended all their microtubules to form the axoneme. In addition to these microtubules, both have a comparable density of microtubules that are wholly contained within the cilium. In studies of *Drosophila* campaniform sensilla and studies of bristle sensilla in other insects have shown a tubular body (Keil, 1997; Liang et al., 2011; Liang et al., 2013b). It seems possible that this tubular body corre-

sponds to the extra-axonemal microtubules described here. However, since there is limited data on the tubular body and this data was acquired in other systems, further investigation will be required to confirm this. Tubular bodies or other non-axonemal microtubules may provide additional structure and rigidity to the cilium, or act as the microtubules with which NompC Ankyrin repeats associate in order to form a gating spring in the cilium, similar to the gating spring that has been described in campaniform sensilla (Liang et al., 2011; Zhang et al., 2015a). At 72 hours APF, both WT and $MKS1^{\Delta 1}$ cilia are very straight with the ciliary membrane appearing highly organised and associated tightly to both the microtubules and the plasma membrane of neighbouring support cells. Interestingly, the localisation of two IFT proteins is perturbed in $MKS1^{\Delta 1}$ mutant cilia. The levels of RempA, part of the IFT-A complex predominantly associated with retrograde transport, is decreased at the base of the cilium, while the levels of NompB, part of the IFT-B complex predominantly associated with anterograde transport, is increased. Interestingly, mutations in RempA result in an increase in NompB in the chordotonal organs (Lee et al., 2008). This suggests that an initial defect in RempA localization might lead to a subsequent defect in NompB localization in the $MKS1^{\Delta 1}$ mutant cilia. Moreover, IFT was recently shown to influence microtubule growth as IFT-54, another component of the IFT-B complex, modulates the expression of microtubule associated protein 4 (MAP4) (Bizet et al., 2015). MAP4 is known to localise to the cilium where it negatively regulates ciliary growth (Ghossoub et al., 2013). This may explain why microtubules do not elongate as efficiently in $MKS1^{\Delta 1}$ mutant axonemes as in WT axonemes. Perhaps as a result of the lack of microtubules, the structure of the membrane is also affected by the $MKS1^{\Delta 1}$ mutation.

Both RempA-YFP and NompB-GFP mostly localise to the base of the cilium. RempA-YFP forms a single dot, while the NompB-GFP signal is elongated along the cilium. Interestingly, electron density was observed along the microtubules in the TZ. This electron density resembles IFT trains observed in other systems and may correspond to the NompB-

GFP signal. In support of this hypothesis both the electron density and the NompB-GFP signal is more elongated in *MKS1*$^{\Delta 1}$mutant cilia, although immunogold labelling will be the only way to confirm it. If these electron dense particles are indeed IFT trains, immunogold labelling in both cross-section and longitudinal sections of the cilium will also show whether the IFT-A and IFT-B complex travel on different microtubules, as was recently shown in *Chlamydomonas* (Stepanek and Pigino, 2016). Intriguingly, the electron densities are found facing the lumen of the axoneme. So far, all IFT trains have been observed on the outside of the axoneme, between the microtubules and the ciliary membrane. However, studies have mostly been done in *Chlamydomonas*, which has a motile flagellum. It is possible that the central pair of microtubules and the dynein arms that are characteristic of motile cilia would make it more favourable for the IFT trains to travel on the outside of the microtubules. In *Drosophila*, nothing in the literature provides a compelling reason for IFT trains to travel on the outside of the axoneme. There may be important species and cell type differences in IFT. In the dataset described here, IFT-like particles were only observed in the TZ, not in the axoneme. A possible explanation is that the chances of encountering IFT trains at the base of the cilium are higher than in the axoneme since IFT trains tend to accumulate at the base of the cilium (Follit et al., 2009; Qin et al., 2004). However, it is important to note that without conclusive immunogold labelling of NompB and/or RempA, describing the electron dense particles found in the TZ as IFT trains is speculative and this hypothesis is likely to be controversial.

As described in Section 3.2.6, the action potential in mature *MKS1*$^{\Delta 1}$mutant sensory cilia seems to have a slightly larger amplitude. In agreement with this, *MKS1*$^{\Delta 1}$mutant flies seem to respond slightly more strongly to some stimuli. These results could indicate that more ions flood into the cell upon stimulation. The quantity and distribution of ion channel NompC does not, however, appear to be affected in *MKS1*$^{\Delta 1}$mutant cilia. Although it is possible that other ion channels may be present and negatively affected by the loss of MKS1,

this seems unlikely as MRPs are undetectable in NompC mutant bristles (Kernan et al., 1994). Another possibility is a larger amount of ions entering the cell because the concentration in the extracellular environment is higher. The larger membrane surrounded volume found within $MKS1^{\Delta 1}$ mutant sensory cilia at 72 hours APF may make more ions available to the cilium, which may result in a larger amplitude of the action potential. Further experiments will be required to investigate this hypothesis. For example, it could be informative to directly image the flow ions in response to stimuli by using Ca^{2+} sensitive dyes or reporter constructs (Riemensperger et al., 2012). Furthermore, it will be interesting to see how WT and $MKS1^{\Delta 1}$ mutant neurons react to continuous stimulation. If the membrane surrounded volume is the source of ions, it would be expected that while the initial response to stimuli is increased in $MKS1^{\Delta 1}$ mutant flies, the response will gradually be reduced and as the stores of ions in the volume are depleted, resulting in a similar response in WT and $MKS1^{\Delta 1}$ mutant neurons, or potentially an even lower response in $MKS1^{\Delta 1}$ mutant flies as the ions may be more diluted in the larger membrane surrounded volume. Conversely, as described above, at 48 hours APF there are considerable defects in the $MKS1^{\Delta 1}$ mutant cilium. This suggests that there may be defect in ciliary function at earlier stages. Furthermore, it is possible that there are defects in other types of cilia, such as the Ch organs. To address this possibility, some preliminary experiments were conducted in third instar larvae. WT larvae normally crawl around freely when left on agar. Larvae with defects in proprioception as a result of mutations in cilia related genes cover less distance under the same circumstances. Furthermore, such larvae would be predicted to show less of a "startle-response" after a sound or touch stimulus. Indeed, $MKS1^{\Delta 1}$ mutant larvae crawl less far than WT larvae if left undisturbed for two minutes. Furthermore, when played a 500 Hz tone or when touched with a single brush hair, the $MKS1^{\Delta 1}$ mutant larvae have a reduced startle response compared to WT larvae. This suggests that, in contrast to $MKS1^{\Delta 1}$ mutant adults, $MKS1^{\Delta 1}$ mutant larvae have defects in proprioception. Since these experiments measure only some behaviours and

larval Ch cilia have not been studied by imaging techniques or electrophysiology, these results are very preliminary. Without further study, these experiments are somewhat difficult to interpret. Since there are defects in $MKS1^{\Delta 1}$ mutant sensory bristles at 48 hours APF, but not 72 hours APF it is also possible that the $MKS1^{\Delta 1}$ mutation affects larval cilia at a certain point in development, but not necessarily throughout the larval stage. In this scenario, it is possible that the larvae were analysed at a stage of development where there are defects in the $MKS1^{\Delta 1}$ mutant cilia. More extensive analysis of larval sensory neurons at different time using behavioural studies combined with electrophysiology, fluorescence microscopy and electron tomography experiments similar to those described for pupal ES organs in this thesis will be required to determine whether the behavioural defects observed in $MKS1^{\Delta 1}$ mutant larvae observed in these preliminary studies are indicative of a real defect in larval Ch cilia. Furthermore, such experiments will provide mechanistic insight into any defect.

As shown in this Chapter and Chapter 4, axonemes that are largely functional and ultrastructurally relatively normal will eventually form in both the Drosophila sensory cilia and sperm lineages in $MKS1^{\Delta 1}$ mutant flies. This suggests that flies can compensate for the loss of MKS1 and build and maintain a largely normal TZ without it. Indeed, a TZ can clearly be distinguished in electron tomograms taken at 48 and 72 hours APF. Although the morphology of the TZ is relatively normal in $MKS1^{\Delta 1}$ mutant cilia, the TZ is shorter than the WT TZ at both time points. Between 48 and 72 hours APF the lack of mictrotubules in the axoneme and the wavy structure of the ciliary membrane are largely rescued. Similarly, while spermatocytes do not form the short cilia that are thought to be precursors of the sperm flagellum, sperm flagella do eventually form and have no obvious defects in morphology or function. This is in contrast to mutations in *Cep290*, *Chibby* and *dila* (Basiri et al., 2014; Enjolras et al., 2012; Ma and Jarman, 2011). In the absence of either of these proteins, both types of cilia have clear functional defects. Evidently, Cep290, Chibby and Dila are

able to build a functional TZ in *Drosophila* sensory neurons in the absence of MKS1, but this is not possible in the absence of Cep290, Chibby or Dila. The relatively mild defects in MKS deficient cilia in other systems, most notably *C.elegans*, is thought to be due to a redundancy with proteins of the NPHP module (Williams et al., 2008; Williams et al., 2011; Yee et al., 2015). However, in flies, no orthologues of core NPHP proteins have been discovered to date (Basiri et al., 2014; Barker et al., 2014). Therefore, the mild phenotype of the $MKS1^{\Delta 1}$mutation is perhaps surprising. It seems possible that there are functional orthologues of NPHP proteins in flies that have not yet been discovered, or that MKS1 is redundant with another TZ protein. Perhaps the most likely candidates for this redundancy are Chibby, Dila or proteins of the BBSome. Mutations in the latter complex were recently shown to modulate the phenotypes of Cep290, MKS and NPHP module mutations in other systems (Barbelanne et al., 2015; Yee et al., 2015; Zhang et al., 2014). However, not much is known about the BBSome in flies.

Many of the defects observed in patients or mammalian models of ciliopathies, such as defects in L-R asymmetry, neural tube defects and defects in limb patterning are likely to be the result of perturbation of signalling pathways such as the Hedgehog pathway (described in more detail in Section 1.5.3). Depending on the tissue, defects in the cilia structure range from perturbations of cilia length and a reduction in the number of cilia in the node and kidney of *MKS1* mutant mice and rats, to no visible defects in the lungs and bile ducts of *MKS1* mutant mice (Tammachote et al., 2009; Weatherbee et al., 2009). The cilium of *Drosophila* sensory neurons could be a cell type that is similarly capable of building a largely normal cilium without MKS1. The structure of *MKS* mutant mammalian cells has, however, been less extensively studied by fluorescence or electron microscopy than *Drosophila* $MKS1^{\Delta 1}$mutant cilia in this thesis. Finally, it is important to note that *Drosophila* are relatively simple organisms. Flies without centrosomes, for example, develop almost normally (Basto et al., 2006). The timing of their eclosure is near normal and with the exception of ciliated cells,

the flies are morphologically normal. In higher eukaryotes, however, centrosomes are indispensable and the absence of centrosomes triggers p53 mediated arrest in G_1-phase or apoptosis (Bazzi and Anderson, 2014; Lambrus et al., 2015; Lerit and Poulton, 2016). Fly cells lacking centrosomes do not arrest or die, suggesting that cell cycle checkpoints may not be as stringent as in vertebrates (Basto et al., 2006). It is possible that defects in the cilium are also less likely to trigger responses such as apoptosis, potentially providing a developmental window in which defects can be rescued.

Chapter 6

Cep104

6.1 Introduction

In this Chapter, efforts to characterise a recently identified cilia associated gene, *Cep104*, are described. A CRISPR indel mutation ($Cep104^{\Delta 1}$) was generated, and mutant flies are both male and female sterile, which appears to be caused by extensive defects in the flagellar ultrastructure in males. An analysis of this mutant allele, however, suggests that this allele may affect other genes or gene regulatory regions. Because this project was started relatively recently and the genetics of the $Cep104^{\Delta 1}$ mutant allele appear to be complicated, all results presented in this Chapter are preliminary.

Cep104 was first identified in a screen for microtubule plus-end tracking proteins (+TIPs) (Jiang et al., 2012). Like many +TIPs, Cep104 has an SxIP motif (Jakobsen et al., 2011; Jiang et al., 2012). This motif facilitates the binding of +TIPs to microtubule end binding (EB) proteins (Honnappa et al., 2009). At the centriole, the protein interacts with Cep97 through its N-terminus and with CP110 through its C-terminus (Jiang et al., 2012). Like Cep104, both of these proteins localise to the distal end of the centriole where they are

thought to regulate centriole length and or ciliogenesis (Franz et al., 2013; Schmidt et al., 2009; Spektor et al., 2007; Tsang et al., 2006). Studies in *Chlamydomonas* showed that Cep104 also localises to the ciliary tip (Satish Tammana et al., 2013). In ciliated mammalian cells (RPE-1 cells), Cep104 localises both to the ciliary tip and the distal end of the daughter, but not the mother centriole. Knock-down of Cep104 in RPE-1 cells showed marked defects in ciliogenesis, consistent with the phenotypes observed in *Cep104* mutants in *Chlamydomonas* (Satish Tammana et al., 2013). Consistent with a role in ciliogenesis, mutations in Cep104 were recently linked to human JBTS (Srour et al., 2015). In addition to the Cep97 and CP110 interaction sites, a collaborator at the University of Cambridge, Dr. Mark van Breugel, recently identified and solved the crystal structure of a TOG domain in human Cep104, and showed that this domain interacts with tubulin *in vitro* (Mark van Breugel, personal communication). These results are in agreement with *in vitro* studies of human Cep104 and a crystal structure of chicken Cep104 that has since been published by another group (Rezabkova et al., 2016). The interaction between the TOG domain and tubulin is hitherto unconfirmed *in vivo* or *in crystallo*. Indeed, since the gene was identified so recently, not much is known about the role of Cep104 in either centrosomes or cilia *in vivo*.

In this Chapter, the localisation of Cep104 was studied in both *Drosophila* spermatocyte cilia and *Drosophila* embryos. In the spermatocytes, Cep104 localises to the center of the cilium in a punctate fashion. In the embryo, analysis of the localisation of GFP-tagged Cep104 mRNA constructs relative to the centriolar protein Asl suggest that a domain at the far N-terminus is required for centrosomal localisation of Cep104, while the far C-terminus on its own localises to the mitotic spindle, rather than the centrosomes. Although studies of Cep104 were hampered by lack of time and the complicated genetics of the $Cep104^{\Delta 1}$ allele, results in other systems suggests the protein has an interesting role and future studies will likely yield interesting results.

6.2 Results

6.2.1 Identification of key domains in *Cep104*

The *Drosophila* orthologue of *Cep104* was identified through n->n Uniprot BLAST as *CG10137*. *CG10137* is a 12.6 kbp (941 amino acids) gene located on the second chromosome. Secondary structure prediction using COILs, FFAS and PsiPRED identified 4 structured domains. In addition to verifying 3 domains identified previously from bioinformatical and structural studies (Mark van Breugel, personal communication), a potential coiled-coil domain was identified at amino acids 200-285. At the N-terminus (amino acid position 1-171), a domain predicted to be similar to APC10 can be found, a predicted TOG domain at amino acids 463-732, and a Zinc-finger domain at amino acids 802-934 (Figure 6.1).

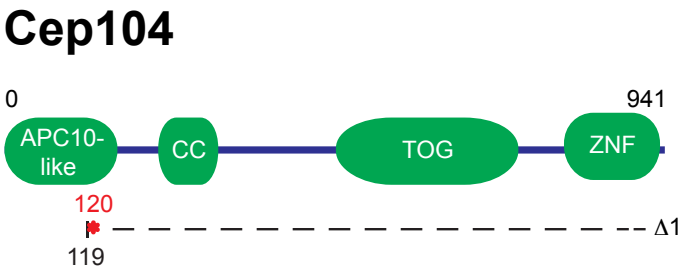

Figure 6.1 Schematic overview of Cep104. Domains (*green*) and mutations (*capped lines and asterisk*) are marked on the schematic. The 4 bp insertion in Cep104 induces a frameshift at amino acid 119, leading to miss sense codons (*dashed capped line*) and a premature stop codon (*red asterisk*) at amino acid 120.

6.2.2 Localisation of Cep104 in spermatocytes

In order to study the localisation of Cep104 in ciliated cells, transgenic flies expressing Cep104-GFP were created. The localisation of Cep104-GFP was studied in *Drosophila* spermatocytes using 3D-SIM as described in Chapter 4. Cep104 localises to the center of

the cilia, immediately distal to the basal bodies which are labelled in red with an antibody against Asl (Figure 6.2 A). The protein does not form a continuous signal along the cilium, but forms dots. The localisation to the center of the cilium suggests that Cep104 may be closely associated with the axonemal microtubules. Cep104-GFP also localises to the flagella where it forms an elongated structure distal to the basal body (Figure 6.2 B). It is unclear what the function of Cep104 in the flagella may be. It is important to note that Cep104-GFP is overexpressed and these results should therefore be interpreted with caution.

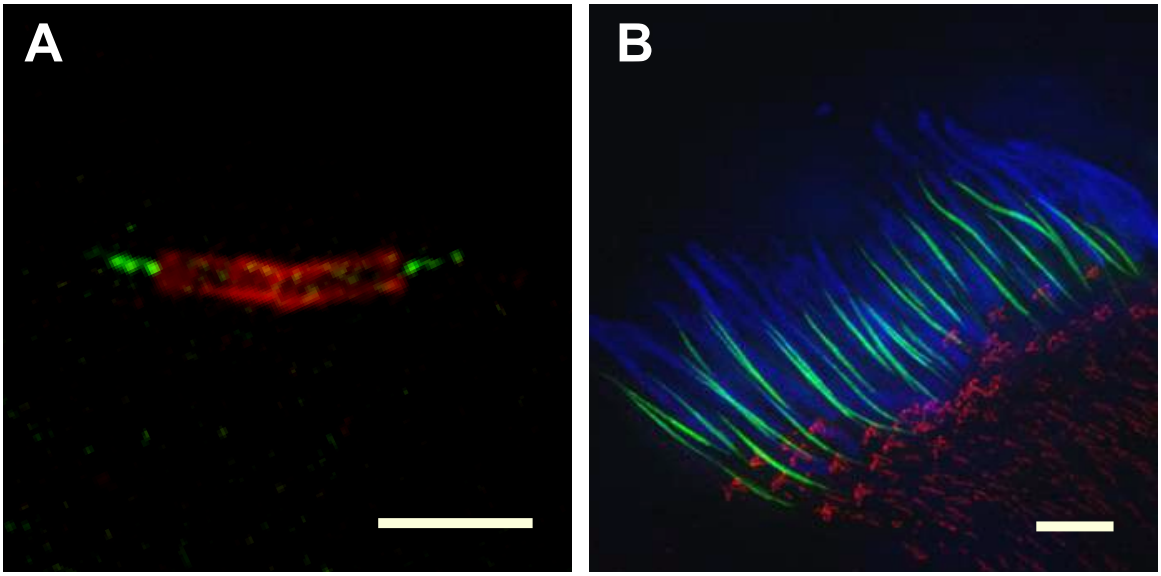

Figure 6.2 Localisation of Cep104-GFP in testes. A) Representative 3D-SIM image of *Drosophila* spermatocyte cilia showing the localisation of GFP-tagged Cep104 (*green*) in relation to the basal body. The basal body is labelled with an antibody against Asl (*red*). B) Representative 3D-SIM image of *Drosophila* spermatid flagella showing the localisation of GFP-tagged Cep104 (*green*) in relation to the basal body (*red*) and the DNA (*blue*). Scale bars: 2 µm.

6.2.3 Microinjections of Cep104 mRNA constructs into living embryos

In order to gain insight into the role of the domains identified above (Section 6.2.1), various GFP tagged Cep104 constructs were injected into *Drosophila* embryos as mRNA to assess their localisation. The domains were sequentially deleted by progressively trimming back from either the N- or C-terminus. All constructs were fluorescently labelled with GFP. For

this assay, the mRNA was generated *in vitro* and injected into living *Drosophila* embryos by part II student Zhai Gen Tan under my supervision. Once the mRNA had been translated and the protein had been folded and matured, the embryos were imaged and the localisation pattern was assessed. To assess the localisation of the constructs relative to the centrosomes and to enable quantification of the GFP signal at the centrosomes, the constructs were injected into embryos expressing Asl-mCherry. A Fiji macro was written by Dr. Hélio Roque to quantify the levels of Cep104 at the centrosome in an automated and unbiased fashion. Briefly, the centrosomes were located using the Asl-mCherry channel, before measuring the Cep104 signal in the GFP channel. The levels of GFP surrounding the centrosome were also measured and subtracted from the level at the centrosome to correct for background fluorescence. Cep104 levels were scored as "strong" when the signal was more than two standard deviations above background, "moderate" when between one and two standard deviations above background and "undetectable" when within one standard deviation of the background.

Constructs that are labelled with GFP at the N-terminus (GFP-Cep104) appear to localise poorly, compared to constructs labelled at the C-terminus (Figure 6.3). A possible explanation could be that the GFP is preventing the N-terminal portion of Cep104 from folding properly, which might interfere with its localisation. This hypothesis is supported by the fact that the construct lacking the N-terminal APC10 domain (Cep104$^{\Delta APC}$-GFP) localises less strongly to the centrosomes (0% strong localisation, 7 % moderate localisation) than Cep104^{FL}-GFP (90 % strong localisation, 7 % moderate localisation). Removing the first linker, L1 (Cep104-GFP$^{\Delta APC\text{-}L1}$), as well as L1 and the coiled-coil Cep104-GFP$^{\Delta APC\text{-}CC}$ result in undetectable localisation in 100 % of embryos. Also deleting the second linker, L2 Cep104-GFP$^{\Delta APC\text{-}L2}$, seems to result in some moderate localisation (26 %). Finally, deleting the TOG domain Cep104-GFP$^{\Delta APC\text{-}TOG}$ or the TOG domain and the third linker, L3 Cep104-GFP$^{\Delta APC\text{-}L3}$, in addition to the domains previously mentioned, resulted some

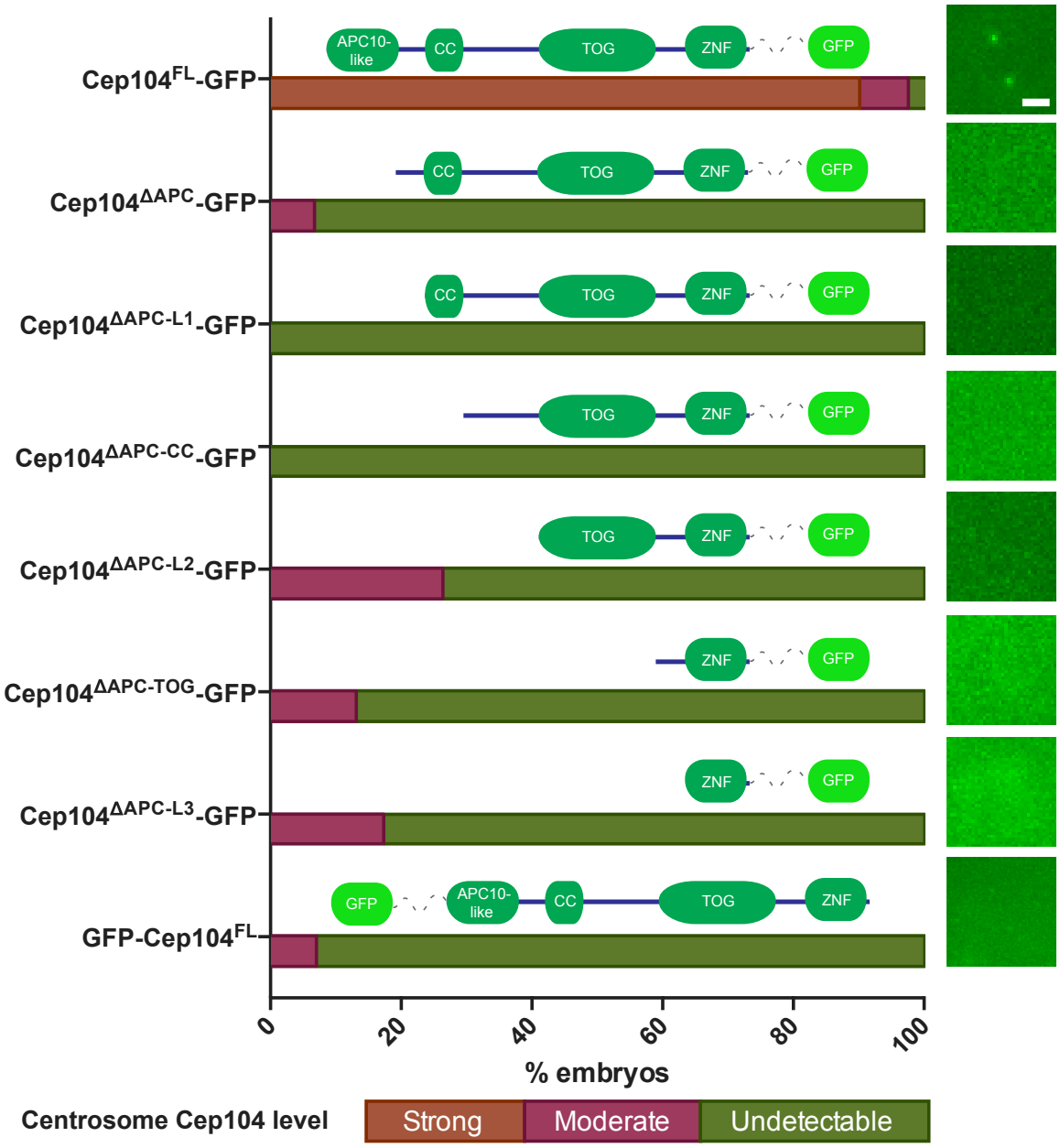

Figure 6.3 Localisation of Cep104-GFP in embryos. Quantification of progressively trimmed back Cep104-GFP constructs (left panel). Localisation of all Cep104-GFP constructs at the centrosome is classified in strong (*orange*), moderate (*pink*) or undectectable (*green*). Representative images of each construct are also depicted (right panel). Scale bars: 2 µm.

moderate localisation (26 % and 13 %, respectively). These two constructs have a more diffuse localisation and appear to localise to the spindle in mitosis. Since GFP-Cep104^{FL} was not robustly detected at the centrosomes (0 % strong localisation, 7 % moderate localisation), quantitative analysis of the deletion constructs with an N-terminal GFP-tag was not informative.

6.2.4 Generation of an Cep104 mutant allele, Cep104$^{\Delta 1}$

In order to study the role of Cep104 *in vivo*, a new mutant allele was generated in *Drosophila*. CRISPR genome engineering was used to generate the mutant allele, similar to the generation of the *B9D1*$^{\Delta 1}$ and *CC2D2A*$^{\Delta 1}$ mutant alleles (described in Section 3.2.3). Two gRNAs (see Table 2.3) were cloned into the pCDF3-dU6:3gRNA vector and microinjected into *Drosophila* embryos expressing the Cas9 gene under the Nanos promoter. A 4 bp insertion at position 151 of the third exon (amino acid 119) was obtained (Figure 6.1), which results in a frameshift and a premature stop codon at amino acid 120 and will be referred to as *Cep104*$^{\Delta 1}$.

6.2.5 *Cep104*$^{\Delta 1}$ mutant flies are male and female sterile

Flies homozygous for *Cep104*$^{\Delta 1}$ are viable, but do not produce any offspring (data not shown). Crossing individual *Cep104*$^{\Delta 1}$ males and females to 3 wild type flies of the opposite sex revealed that both male and female *Cep104*$^{\Delta 1}$ flies were sterile. Since male sterility may be due to defects in the sperm flagella, cross sections of sperm flagella were analysed by TEM. Indeed, there are a variety of ultrastructural defects in the sperm (Figure 6.4 A). The axonemes themselves have abnormal structures (*green arrows*). Furthermore, there are defects in the arrangement of the axonemes and the mitochondrial derivatives (*orange arrowheads*). Finally, the cells appear to fail to individualise properly as some cells contain multiple axonemes and mitochondrial derivatives. Interestingly, the structure of

Cep104$^{\Delta 1}$ mutant spermatocyte cilia appears to be normal. This is the opposite phenotype of the *MKS1*$^{\Delta 1}$ mutation, where spermatocyte cilia are strongly perturbed, but the flagella appear normal and functional (Chapter 4. Together, these results suggest that there are severe defects in spermatogenesis in *Cep104*$^{\Delta 1}$ mutant males. These defects were observed in multiple samples obtained from multiple flies.

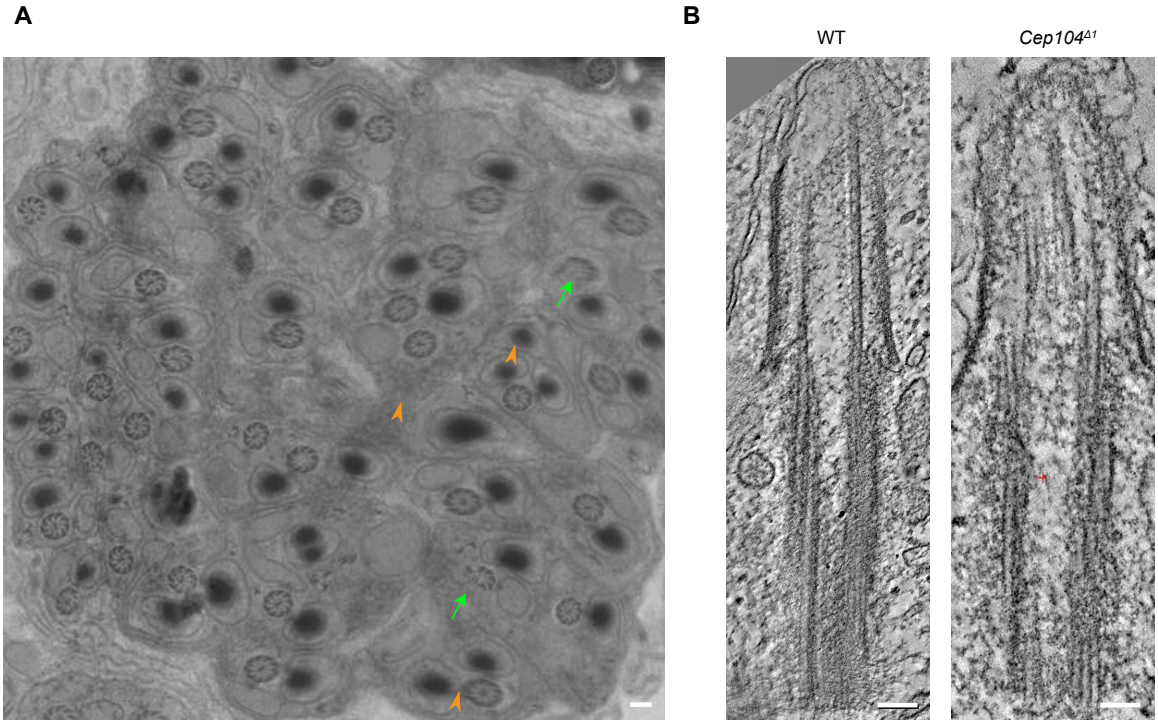

Figure 6.4 Electron micrograph of *Cep104*$^{\Delta 1}$ mutant sperm axonemes. A) Cross-section of mature sperm in *Cep104*$^{\Delta 1}$, some flagella do not have the normal 9-fold symmetry (*green arrows*). Furthermore, some mitochondrial derivatives are arranged abnormally (*orange arrowheads*) and there are disorganised regions within the cyst. B) Electron tomograms of WT (*left panel*) and *Cep104*$^{\Delta 1}$ mutant (*right panel*) spermatocyte cilia. Scale bars A: 200 nm, B: 100 nm.

Importantly, neither male nor female sterility could be rescued by expressing Cep104-GFP in the *Cep104*$^{\Delta 1}$ mutant background. Therefore, no efforts were made to understand the mechanism of female sterility. While GFP-tagged transgenes do not always rescue the mutant phenotype, this might also indicate a secondary mutation, a dominant negative effect of the mutation or another genetic abnormality. Moreover, the mutant phenotype could not be recapitulated by crossing the *Cep104*$^{\Delta 1}$ mutant allele to either of two strains carrying

different deficiencies that included the *Cep104* gene. Together, these results suggest that the phenotype described above may not be a true *Cep104* mutant phenotype. Most likely, the mutation affects either another gene or a gene regulatory region. A potential problem with CRISPR-Cas9 genome engineering is the risk of inducing off-target DSBs (Fu et al., 2013; Zhang et al., 2015b). Another potential candidate for a secondary mutation is *CG10165*. This gene is located in the same position on the second chromosome on the antisense strand (see Figure 6.5). There are five isoforms of CG10165, the exons of all isoforms are positioned between exons 1 and 2. It is possible that the 4 bp insertion in *Cep104* affects either *CG10165* or its regulatory regions.

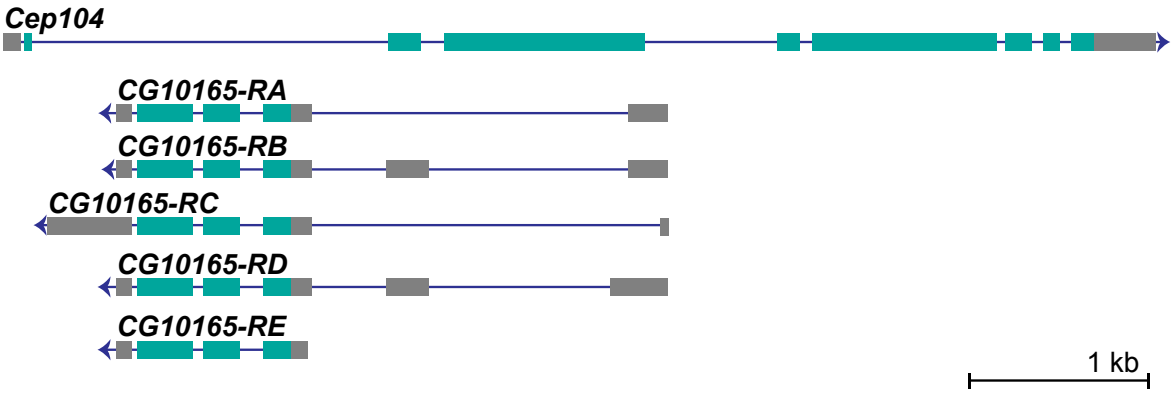

Figure 6.5 Relative positions of *Cep104* and *CG10165*. Position of *Cep104* (*top*) and five isoforms of *CG10165* (*bottom, CG10165A-E*). Exons are labelled in *aquamarine*, untranslated regions are labelled in *grey*.

Furthermore, it is possible that alternative splicing may result in a (partially) active Cep104 protein. Further experiments, such as rescue experiments with CG10165, sequencing of the genes most likely to affected by off-target DSBs and analysis of Cep104 at the protein level by western blot or IF will be required to fully characterise the $Cep104^{\Delta 1}$ allele.

6.3 Discussion

In vitro studies had previously suggested that human Cep104 interacts with microtubules through the TOG domain. Other proteins with a TOG domain include ch-TOG and CLASP, which are both important regulators of cytoplasmic microtubules (Al-Bassam et al., 2007; Al-Bassam and Chang, 2011; Slep and Vale, 2007). Recently, a novel TOG domain containing protein family was identified (Das et al., 2015). This family of proteins, Crescerins, is highly conserved and the TOG domain of mammalian Crescerin1 also binds microtubules and promotes microtubule polymerisation *in vitro*. In *C. elegans*, the Crescerin family is required for the development of sensory cilia, linking TOG domain containing proteins to ciliogenesis. In addition to the TOG domain, Cep104 also contains an APC10-like domain and a ZNF. Futhermore, a putative coiled-coil domain was identified. In order to study the role of these domains *in vivo*, progressively trimmed back, GFP-labelled versions of Cep104 were injected into living *Drosophila* embryos. This is a rapid way of studying the effects of deleting domains on the localisation of a protein. Centrosomal localisation was much reduced in full length GFP-Cep104 compared to full length Cep104-GFP. Furthermore, deleting the APC10-like domain at the far N-terminus also resulted in a reduction of Cep104 at the centrosome. Together, these results suggest that an intact and accessible APC10-like domain are important for the centrosomal localisation of Cep104. Interestingly, removing the TOG domain as well, thus leaving only the ZNF intact, means the protein is no longer enriched at the centrosome and instead seems to bind to the mitotic spindle. Interestingly, this part of the protein interacts with CP110 (Jiang et al., 2012; Rezabkova et al., 2016). CP110 localises to the centrioles (Franz et al., 2013; Schmidt et al., 2009; Spektor et al., 2007; Tsang et al., 2006). The localisation of this construct to the microtubules is therefore perhaps surprising. However, in human Cep104, the EB binding SxIP motif is also found in this part of the protein (Jiang et al., 2012; Rezabkova et al., 2016). Although no SxIP

motif was found in the *Drosophila* sequence, it is possible that a similar EB binding motif is present at the C-terminus of *Drosophila* Cep104, which could explain the localisation of the Cep104 ZNF to the spindle microtubules. It is important to realise that the constructs were injected into WT embryos. Therefore, it is possible that mutant Cep104 forms a complex with WT Cep104 and may thus be able to translocate by "piggybacking" on the WT protein. In spermatocyte cilia, Cep104-GFP forms a punctate rod immediately distal to the basal body. The protein localises to the center of the cilium, suggesting that it may associate closely with the microtubules. Cep104 is also found in flagella, where it forms an elongated structure distal to the basal body. It is not known how the protein localises to these structures and what its role might be.

In order to study the role of *Cep104 in vivo*, a Cep104 mutant allele ($Cep104^{\Delta 1}$) was generated using CRISPR genome engineering. Sequencing suggests that a 4 bp insertion results in scrambled code and a premature stop codon at the start of the third exon. The $Cep104^{\Delta 1}$mutation is associated with sterility in both male and female flies. Male sterility seems to be the result of aberrant flagellar assembly. The axonemes of $Cep104^{\Delta 1}$mutant spermatids appear unstable and there is a high degree of disorganisation in the spermatid cyst. However, neither male sterility nor female sterility can be rescued by expressing Cep104-GFP in the mutant background. Furthermore, neither the male or female sterility phenotypes can be recapitulated when the $Cep104^{\Delta 1}$allele is made hemizygous with either of two separate deficiency lines that lack the *Cep104* gene. Cep104 has a large intron between the first and second exon, and an uncharacterised gene, *CG10165*, is present within this intron on the antisense strand. It is possible that the $Cep104^{\Delta 1}$mutation disrupts *CG10165* or its regulatory regions, thus explaining why Cep104-GFP does not rescue the $Cep104^{\Delta 1}$phenotype. This does however not explain why the phenotype of the Cep104 deficiency is not comparable to the $Cep104^{\Delta 1}$phenotype. Furthermore, without a clear mutant phenotype that can be rescued by expressing Cep104 in the $Cep104^{\Delta 1}$mutant back-

ground, the possibility that a (partially) functional version of the protein is expressed, can not be ruled out. Without further analysis, it is not possible to be certain whether the defects observed in *Drosophila* are due to the absence of functional Cep104 or a secondary effect of the $Cep104^{\Delta 1}$ mutation. Analysis of the $Cep104^{\Delta 1}$ mutant allele could include careful sequencing of both CG10165 and the most likely CRISPR off-target genes. Off-target mutations on other chromosomes could be crossed out by crossing the $Cep104^{\Delta 1}$ allele to WT flies several times (backcrossing), while mutations in genes on the same chromosome (including in *CG10165*) could be rescued transgenically. In order to determine whether any functional Cep104 is still present, western blot or IF with antibodies against Cep104 could be carried out. Ultimately, it may be better to generate another mutant allele that is a clean deletion of *Cep104*. A good possibility would be to delete the entire *Cep104* gene without affecting *CG10165*. This could be done replacing the *Cep104* gene region by a construct with an intact copy of *CG10165* by CRISPR homologous recombination. The $Cep104^{\Delta 1}$ allele, however, is homozygous viable and the $Cep104^{\Delta 1}$ mutation over a Cep104 deficiency is even viable. The $Cep104^{\Delta 1}$ allele can therefore be studied *in vivo*. With a better understanding of the genetics of Cep104, the $Cep104^{\Delta 1}$ allele could become relevant to the characterisation of Cep104. For example, comparing a future clean deletion of Cep104 with the $Cep104^{\Delta 1}$ frameshift could be informative.

The localisation data in embryos and spermatocytes, in combination with localisation data in other systems, suggest that Cep104 has a potentially interesting localisation pattern. The protein is found both in centrosomes, where it localises to the distal end of the centriole, and in cilia. In RPE-1 cells, Cep104 localises to the tip of both centrioles prior to ciliogenesis (Satish Tammana et al., 2013). Once the cell starts to form a cilium, the protein can be found at the tip of the daughter centriole and at the tip of the growing cilium, but it disappears from the distal end of the mother centriole. Furthermore, Cep104 interacts with Cep97 and CP110, which have been implied in the regulation in ciliogenesis in some systems, al-

though this remains controversial and likely cell type specific (Franz et al., 2013; Schmidt et al., 2009; Spektor et al., 2007; Tsang et al., 2006). Together, these results suggest that Cep104 may have a function in the conversion of the mother centriole into the ciliary basal body. It will be interesting to investigate where Cep104 localised during ciliogenesis in the *Drosophila* pupal notum and whether ciliogenesis in the sensory neurons or spermatocytes is affected by deletion of *Cep104*.

Chapter 7

General discussion

7.1 General discussion

7.1.1 Establishing the TZ in *Drosophila*

The ciliary TZ is essential for proper cilia function (Czarnecki and Shah, 2012; Reiter et al., 2012). Recent studies in worms and mice show that three protein modules, the MKS, NPHP and Cep290 modules, are required to establish the TZ (Basiri et al., 2014; Schouteden et al., 2015; Williams et al., 2008; Williams et al., 2011; Yee et al., 2015). All of these modules require RGRIP1L (also known as MKS5 or NPHP8) to localise to the TZ (Li et al., 2016; Schouteden et al., 2015; Yang et al., 2015). At the TZ, Cep290 builds a scaffolding structure that is required for the rest of the TZ to form. (Li et al., 2016; Schouteden et al., 2015). The MKS and NPHP modules act partly redundantly to form the Y-links (Jensen et al., 2015; Williams et al., 2011). While six potential members of the MKS module have been identified in *Drosophila*, the NPHP module appears to be largely absent (Barker et al., 2014; Basiri et al., 2014).

Drosophila spermatocytes have short cilia of $\sim$ 700 nm. All conserved TZ proteins

studied in this thesis localise immediately distal to the basal body in this cilium. Cep290 localises to the center of the cilium. Cep290 is required for establishing the TZ (Basiri et al., 2014). The other proteins, including the MKS module, form a hollow tube that varies in both length and width, consistent with studies of sub sets of these TZ proteins in different systems (Lambacher et al., 2015; Lee et al., 2014; Yang et al., 2015). Furthermore, these results fit with reports that proteins of the MKS module are required to form the Y-links, together with the NPHP module (Jensen et al., 2015; Williams et al., 2011).

In both $MKS1^{\Delta 1}$ and $B9D1^{\Delta 1}$ mutant cilia, all other proteins of the MKS module appear to be absent from the TZ, in agreement with findings in *C. elegans* (Bialas et al., 2009; Williams et al., 2008). Furthermore, all proteins except Cep290 and Chibby seem to fail to localise to the TZ in $MKS1^{\Delta 1}$. Cep290 and Chibby both appear to localise normally, suggesting that these proteins are higher up than MKS1 in the hierarchy of ciliogenesis. Consistent with the localisation defects, there are defects in the ultrastructure of the TZ in spermatocyte cilia. The axoneme does not extend properly, reducing the length of cilium from $\sim$ 700 nm to $\sim$ 200 nm. Furthermore, the electron density that can be observed in the WT TZ membrane is absent in $MKS1^{\Delta 1}$ mutant cilia. Since fertility appears unaffected in male $MKS1^{\Delta 1}$ flies, the axoneme must eventually extend to make a functional flagellum. No defects were observed in the ultrastructure of $MKS1^{\Delta 1}$ mutant sperm flagella in cross section. Consistent with the hypothesis that a functional TZ forms in $MKS1^{\Delta 1}$ mutant sperm, the TZ does form in $MKS1^{\Delta 1}$ mutant sensory neurons. Although the TZ is shorter in $MKS1^{\Delta 1}$ mutant sensory neurons, it appears otherwise morphologically normal. It should be acknowledged, however, that the fertility assay used here is quite crude, as it may be that a significant drop in sperm motility or viability does not translate into a significant drop in the number of progeny generated in this type of mating assay. Furthermore, the EM analysis of the sperm axoneme may well have missed subtle defects, particularly since the length of the flagellum was not examined.

Nevertheless, the data presented in this thesis helps to define a TZ hierarchy as it appears that sperm flagella and sensory cilia can eventually compensate for the lack of MKS proteins, while this is not the case for proteins like Cep290, Chibby and Dila, implying these proteins play a different, more essential part in TZ assembly. An important task for the future would be to test these mutations (on their own and in combination) at the same time, in the same lab and in the same assay, as, currently, each mutation has been assayed in different labs in slightly different ways, making it difficult to draw reliable comparisons.

7.1.2 IFT and cilia function

As described above (Section 7.1.1), cilia on the spermatocytes are dramatically shortened and many TZ proteins appear to be absent from these shortened cilia in the $MKS1^{\Delta 1}$mutant. While function of these short spermatocyte cilia is unknown, it appears that the axonemes of these cilia can be dramatically perturbed without any obvious effect on the fly. It therefore remains unclear why proteins of the MKS module proteins are highly expressed in testes. It is possible that these proteins contribute to the formation or function of cilia/flagella function in cells of the sperm lineage, but that this function is not apparent in the assays described in this thesis.

Behavioural and electrophysiology tests show no defect in the function of sensory neurons as a result of the $MKS1^{\Delta 1}$mutation. If anything, a slight increase in ciliary function was observed. While neither the quantity or the localisation of the ion channel protein NompC was not detectably perturbed in $MKS1^{\Delta 1}$mutant sensory neurons, there where some ultrastructural changes. In addition to the reduced length of the TZ mentioned above (Section 7.1.1), the ratio of an inner membrane surrounded volume to the total cilium volume was increased in $MKS1^{\Delta 1}$mutant neurons. This internal membrane surrounded volume is in contact with the extracellular environment and appears to be formed by invagination of the cilia membrane. At present, it is unclear what causes the relative increase in this volume

in $MKS1^{\Delta 1}$mutant cilia. The lack of axonemal microtubules and the looser organisation of the ciliary membrane that was observed in developing $MKS1^{\Delta 1}$mutant cilia may contribute to this increase. The membrane surrounded volume in sensory neurons has not been previously described and is of unknown function. One intriguing possibility is that this volume is a reservoir of ions required for the action potential, or it extends the membrane surface and as such the ion channels in the membrane. Potentially, this may explain why the amplitude of the action potential and, downstream, the response to stimuli is increased in $MKS1^{\Delta 1}$mutant flies. However, the differences between the WT and $MKS1^{\Delta 1}$mutant flies are small and may be due to differences in the genetic background of the flies. In addition to these ultrastructural changes, the localisation and distribution of IFT proteins was also subtly perturbed. The IFT-B protein NompB signal appears to be more elongated in $MKS1^{\Delta 1}$mutant cilia, while there appears to be less of the IFT-A protein RempA. Since NompB is also reported to accumulate in RempA mutant flies (Lee et al., 2008). Therefore, it seems likely that MKS1 initially affects the localization of RempA, which leads to the abnormal accumulation of NompB in turn. Interestingly, more extensive electron dense particles were observed at the base of the cilium in $MKS1^{\Delta 1}$mutant cilia than in WT cilia. These particles strongly resemble IFT trains, although they localise on the inside of the axoneme, rather than between the axoneme and the membrane as has been reported in other systems, most notably *Chlamydomonas* (Rogowski et al., 2013; Stepanek and Pigino, 2016; Vannuccini et al., 2016). Further analysis, such as immunogold labelling, of these particles will be required in order to confirm that they are indeed IFT trains.

While the ultrastructure of mature cilia appeared only mildly perturbed, much more extensive defects were observed in developing cilia. Most strikingly, very few of the microtubules extend from the basal body into the cilium. This may be due to the increase in NompB, as another component of the IFT-B complex has been shown to influence ciliary microtubule growth by negatively regulating the microtubule stabilising protein MAP4

(Bizet et al., 2015). Furthermore, the membrane appears relatively loosely organised, especially at the ciliary tip. Thus, while MKS1 seems to be important for establishing proper cilia structure, when given enough developmental time, flies appear to be able to build and maintain a largely normal cilium.

Together with previous studies in flies, the results presented in this thesis support a model of sequential assembly of the TZ (Basiri et al., 2014; Enjolras et al., 2012; Ma and Jarman, 2011). Through a not fully understood mechanism, the basal body docks at the plasma membrane and triggers the recruitment of TZ components. No orthologue of RGRIP1L has been identified in *Drosophila*, but Cep290 is essential for establishing a functional TZ (Basiri et al., 2014). Chibby and Dila also play important roles in this process, but do not appear to be essential (Enjolras et al., 2012; Ma and Jarman, 2011). While *cby* and *dila* mutants show reduced mechanosensation and male fertility, no such defects were observed for *MKS1* mutant flies, despite extensive abnormalities in the short axoneme present on spermatocytes. In *C. elegans*, the relatively mild defects of mutations in MKS1 are explained by a redundancy with NPHP (Williams et al., 2008; Williams et al., 2011; Yee et al., 2015). In flies, most of the NPHP module appears to be lacking (Basiri et al., 2014; Barker et al., 2014). It is possible there are unidentified functional orthologues of the NPHP module, or that MKS1 is redundant with another protein. Possible candidates for this redundancy are Chibby or proteins of the BBSome. Perturbing the BBSome was recently shown to modulate the phenotypes of mutations in the Cep290, MKS and NPHP modules in other systems (Barbelanne et al., 2015; Yee et al., 2015; Zhang et al., 2014). To date, the BBSome is poorly characterised in flies.

7.2 Future perspectives

At the outset of this project, the aim was to establish flies as a useful model to study TZ assembly. In one sense, the mild phenotypes of the mutations described here might be con-

sidered disappointing. The more extensive defects observed in human ciliopathies may be explained both by defects in cilia dependent Hh signalling, which does not occur in flies, and by the fact that flies are relatively simple organisms with few cilia and may therefore be resistant to a less efficient mode of TZ assembly and ciliogenesis in a way that higher eukaryotes are not. On the other hand, this could be considered a major advantage. Although it will be time consuming, it should be possible to analyse the phenotypes described here to establish how they arise. For example, it will be interesting to determine why there are fewer axonemal microtubules in $MKS1^{\Delta 1}$ mutant cilia at early time points and whether this is related to the increase in the membrane surrounded volume. There may be subtle, but potentially informative, differences between the phenotypes caused by mutations in different TZ genes that could be worth exploring. The fact that the $MKS1^{\Delta 1}$ mutation affects the formation of structures of which the function is unknown, such as the spermatocyte cilium and the hitherto undescribed membrane surrounded volume within the sensory cilium could provide clues to the formation and function of these structures in the future. The relatively normal development of flies with TZ mutations will make it much easier to try to answer these questions. Moreover, it must be recognised that some of the assays of cilia function that used here are relatively crude. It seems likely that more sensitive assays will reveal subtle defects that can be studied. One possible explanation for the relatively mild defects observed in mature cilia/flagella, in contrast to developing cilia, is redundancy of MKS1 with another protein, possibly Chibby, the BBSome or a yet unidentified component of the NPHP module. This hypothesis is worth exploring further and analysing combinations of mutations will potentially help to refine the hierarchy and redundancy of TZ assembly. Finally, it will be interesting to further investigate whether the small increase in ciliary function is indeed an effect of the $MKS1^{\Delta 1}$ mutation, rather than an effect of differences in the genetic background of the flies. If the amplitude of the action potential is indeed increased as a direct effect of mutations in MKS1, it will be interesting to see the short and long term

effects on the sensory neurons. Hyperexcitability has been linked to neurodegeneration in diseases such as Alzheimer's disease and amyotrophic lateral sclerosis (ALS), although this connection is not fully understood (Bae et al., 2013; Leroy et al., 2014; Siskova et al., 2014).

Some interesting new features were identified in WT sensory cilia, including non-axonemal ciliary microtubules, the membrane surrounded volume that is connected to the extracellular environment and electron dense particles on the luminal side of the axonemal microtubules that resemble IFT trains. In future studies, it will be important to study the origin and function of these structures. Perhaps the first step would be to address whether these particles are IFT trains. Since cilia are now widely studied in a range of model systems, it seems likely that more information will emerge about the species and cell type differences in cilia in general. For example, in *MKS1* mutant mice, cilia in the node and kidney are sparser and shorter, while cilia in the lung and bile duct appear to be unaffected (Weatherbee et al., 2009). Adding further complexity, fibroblasts derived from patients with MKS1-related JBTS have been reported to be longer than control fibroblasts, as have cilia in the kidneys of *MKS1* mutant rats (Slaats et al., 2015; Tammachote et al., 2009). Although significant advances have been made in understanding ciliogenesis over the past decade, it is clear that challenges remain to fully understand the process and the implications of defects in ciliogenesis in ciliopathies and acquired diseases that have a link to cilia, such as cancer. Clearly, not all of these can be studied in *Drosophila*, but studies in flies may help to bridge the gap between *ex vivo* studies in mammalian cells and defects observed in ciliopathy patients.

Bibliography

Abdul-Majeed, S. and Nauli, S. M. 2011. Calcium-mediated mechanisms of cystic expansion. *Biochimica et Biophysica Acta*. 1812(10):1281–90.

Al Jord, A., Lemaître, A.-I., Delgehyr, N., Faucourt, M., Spassky, N., and Meunier, A. 2014. Centriole amplification by mother and daughter centrioles differs in multiciliated cells. *Nature*. 516(7529):104–7.

Andersen, M. K. and Sandholt, C. H. 2015. Recent Progress in the Understanding of Obesity: Contributions of Genome-Wide Association Studies. *Current Obesity Reports*. 4(4):401–410.

Anderson, R. G. 1972. The three-dimensional structure of the basal body from the rhesus monkey oviduct. *The Journal of Cell Biology*. 54(2):246–65.

Ando, J. and Yamamoto, K. 2013. Flow detection and calcium signalling in vascular endothelial cells. *Cardiovascular Research*. 99(2):260–268.

Auber, B., Burfeind, P., Herold, S., Schoner, K., Simson, G., Rauskolb, R., and Rehder, H. 2007. A disease causing deletion of 29 base pairs in intron 15 in the MKS1 gene is highly associated with the campomelic variant of the Meckel-Gruber syndrome. *Clinical Genetics*. 72(5):454–9.

Avasthi, P. and Marshall, W. F. 2012. Stages of ciliogenesis and regulation of ciliary length. *Differentiation*. 83(2):S30–S42.

Avidor-Reiss, T. and Leroux, M. R. 2015. Shared and Distinct Mechanisms of Compartmentalized and Cytosolic Ciliogenesis. *Current Biology*. 25(23):R1143–50.

Babu, D. and Roy, S. 2013. Left-right asymmetry: cilia stir up new surprises in the node. *Open Biology*. 3(5):130052.

Bae, J. S., Simon, N. G., Menon, P., Vucic, S., and Kiernan, M. C. 2013. The puzzling case of hyperexcitability in amyotrophic lateral sclerosis. *Journal of Clinical Neurology*. 9(2):65–74.

Barakat, M. T., Humke, E. W., and Scott, M. P. 2010. Learning from Jekyll to control Hyde: Hedgehog signaling in development and cancer. *Trends in Molecular Medicine*. 16(8):337–348.

Barbelanne, M., Hossain, D., Chan, D. P., Peränen, J., and Tsang, W. Y. 2015. Nephrocystin proteins NPHP5 and Cep290 regulate BBSome integrity, ciliary trafficking and cargo delivery. *Human Molecular Genetics*. 24(8):2185–200.

Barish, S. and Volkan, P. C. 2015. *Mechanisms of olfactory receptor neuron specification in Drosophila*.

Barker, A. R., Renzaglia, K. S., Fry, K., and Dawe, H. R. 2014. Bioinformatic analysis of ciliary transition zone proteins reveals insights into the evolution of ciliopathy networks. *BMC Genomics*. 15(1):531.

Basiri, M. L., Ha, A., Chadha, A., Clark, N. M., Polyanovsky, A., Cook, B., and Avidor-Reiss, T. 2014. A migrating ciliary gate compartmentalizes the site of axoneme assembly in Drosophila spermatids. *Current Biology*. 24(22):2622–2631.

Al-Bassam, J. and Chang, F. 2011. Regulation of microtubule dynamics by TOG-domain proteins XMAP215/Dis1 and CLASP. *Trends in Cell Biology*. 21(10):604–614.

Al-Bassam, J., Larsen, N. A., Hyman, A. A., and Harrison, S. C. 2007. Crystal Structure of a TOG Domain: Conserved Features of XMAP215/Dis1-Family TOG Domains and Implications for Tubulin Binding. *Structure*. 15(3):355–362.

Basten, S. G. and Giles, R. H. 2013. Functional aspects of primary cilia in signaling, cell cycle and tumorigenesis. *Cilia*. 2(1):6.

Basto, R., Lau, J., Vinogradova, T., Gardiol, A., Woods, C. G., Khodjakov, A., and Raff, J. W. 2006. Flies without Centrioles. *Cell*. 125(7):1375–1386.

Bazzi, H. and Anderson, K. V. 2014. Acentriolar mitosis activates a p53-dependent apoptosis pathway in the mouse embryo. *Proceedings of the National Academy of Sciences*. 111(15):E1491–E1500.

Benton, R. 2007. *Sensitivity and specificity in Drosophila pheromone perception*.

Berbari, N. F., O'Connor, A. K., Haycraft, C. J., and Yoder, B. K. 2009. The primary cilium as a complex signaling center. *Current Biology*. 19(13):R526–35.

Bergmann, C., Fliegauf, M., Brüchle, N. O., Frank, V., Olbrich, H., Kirschner, J., Schermer, B., Schmedding, I., Kispert, A., Kränzlin, B., Nürnberg, G., Becker, C., Grimm, T., Girschick, G., Lynch, S. A., Kelehan, P., Senderek, J., Neuhaus, T. J., Stallmach, T., Zentgraf, H., Nürnberg, P., Gretz, N., Lo, C., Lienkamp, S., Schäfer, T., Walz, G., Benzing, T., Zerres, K., and Omran, H. 2008. Loss of Nephrocystin-3 Function Can Cause Embryonic Lethality, Meckel-Gruber-like Syndrome, Situs Inversus, and Renal-Hepatic-Pancreatic Dysplasia. *American Journal of Human Genetics*. 82(4):959–970.

Bialas, N. J., Inglis, P. N., Li, C., Robinson, J. F., Parker, J. D. K., Healey, M. P., Davis, E. E., Inglis, C. D., Toivonen, T., Cottell, D. C., Blacque, O. E., Quarmby, L. M., Katsanis, N., and Leroux, M. R. 2009. Functional interactions between the ciliopathy-associated Meckel syndrome 1 (MKS1) protein and two novel MKS1-related (MKSR) proteins. *Journal of Cell Science*. 122(Pt 5):611–24.

Bisgrove, B. W. and Yost, H. J. 2006. The roles of cilia in developmental disorders and disease. *Development*. 133(21):4131–43.

Bizet, A. A., Becker-Heck, A., Ryan, R., Weber, K., Filhol, E., Krug, P., Halbritter, J., Delous, M., Lasbennes, M.-C., Linghu, B., Oakeley, E. J., Zarhrate, M., Nitschké, P., Garfa-Traore, M., Serluca, F., Yang, F., Bouwmeester, T., Pinson, L., Cassuto, E., Dubot, P., Elshakhs, N. A. S., Sahel, J. A., Salomon, R., Drummond, I. A., Gubler, M.-C., Antignac, C., Chibout, S., Szustakowski, J. D., Hildebrandt, F., Lorentzen, E., Sailer, A. W., Benmerah, A., Saint-Mezard, P., and Saunier, S. 2015. Mutations in TRAF3IP1/IFT54 reveal a new role for IFT proteins in microtubule stabilization. *Nature Communications*. 6:8666.

Blume-Jensen, P. and Hunter, T. 2001. Oncogenic kinase signalling. *Nature*. 411(6835):355–65.

Bobinnec, Y., Moudjou, M., Fouquet, J. P., Desbruyères, E., Eddé, B., and Bornens, M. 1998. Glutamylation of centriole and cytoplasmic tubulin in proliferating non- neuronal cells. *Cell Motility and the Cytoskeleton*. 39(3):223–232.

Bodmer, R., Carretto, R., and Jan, Y. N. 1989. Neurogenesis of the peripheral nervous system in Drosophila embryos: DNA replication patterns and cell lineages. *Neuron*. 3:21–32.

Bornens, M. 2012. The centrosome in cells and organisms. *Science*. 335(6067):422–6.

Boucher, C. and Sandford, R. 2004. Autosomal dominant polycystic kidney disease (ADPKD, MIM 173900, PKD1 and PKD2 genes, protein products known as polycystin-1 and polycystin-2). *European Journal of Human Genetics*. 12(5):347–54.

Brewster, R. and Bodmer, R. 1995. Origin and specification of type II sensory neurons in Drosophila. *Development*. 121(9):2923–36.

Brewster, R. and Bodmer, R. 1996. Cell lineage analysis of the Drosophila peripheral nervous system. *Developmental Genetics*. 18(1):50–63.

Briscoe, J. and Thérond, P. P. 2013. The mechanisms of Hedgehog signalling and its roles in development and disease. *Nature Reviews Molecular Cell Biology*. 14(7):418–431.

Brody, S. L., Yan, X. H., Wuerffel, M. K., Song, S. K., and Shapiro, S. D. 2000. Ciliogenesis and left-right axis defects in forkhead factor HFH-4-null mice. *American Journal of Respiratory Cell and Molecular Biology*. 23(1):45–51.

Brooks, E. R. and Wallingford, J. B. 2014. *Multiciliated Cells*. arXiv: 15334406.

Burke, M. C., Li, F.-Q. F.-Q., Cyge, B., Arashiro, T., Brechbuhl, H. M., Chen, X., Siller, S. S., Weiss, M. A., O'Connell, C. B., Love, D., Westlake, C. J., Reynolds, S. D., Kuriyama, R., and Takemaru, K.-I. K.-I. 2014. Chibby promotes ciliary vesicle formation and basal body docking during airway cell differentiation. *The Journal of Cell Biology*. 207(1):123–137.

Cachero, S., Simpson, T. I., Zur Lage, P., Ma, L., Newton, F., Holohan, E., Armstrong, J. D., and Jarman, A. 2011. The gene regulatory cascade linking proneural specification with differentiation in Drosophila sensory neurons. *PLOS Biology*. 9(1).

Caldwell, J. C., Miller, M. M., Wing, S., Soll, D. R., and Eberl, D. F. 2003a. Dynamic analysis of larval locomotion in Drosophila chordotonal organ mutants. *Proceedings of the National Academy of Sciences of the United States of America*. 100(26):16053–8.

Caldwell, J. C., Miller, M. M., Wing, S., Soll, D. R., and Eberl, D. F. 2003b. Dynamic analysis of larval locomotion in Drosophila chordotonal organ mutants. *Proceedings of the National Academy of Sciences of the United States of America*. 100(26):16053–8.

Campuzano, S. and Modolell, J. 1992. Patterning of the Drosophila nervous system: the achaete-scute gene complex. *Trends in Genetics*. 8(6):202–208.

Carlson, S. D., Hilgers, S. L., and Juang, J. L. 1997. First developmental signs of the scolopale (glial) cell and neuron comprising the chordotonal organ in the drosophila embryo. *Glia*. 19(3):269–274.

Carvajal-Gonzalez, J. M., Roman, A.-C., and Mlodzik, M. 2016. Positioning of centrioles is a conserved readout of Frizzled planar cell polarity signalling. *Nature Communications*. 7:11135.

Carvalho-Santos, Z., Machado, P., Alvarez-Martins, I., Gouveia, S. M., Jana, S. C., Duarte, P., Amado, T., Branco, P., Freitas, M. C., Silva, S. T., Antony, C., Bandeiras, T. M., and Bettencourt-Dias, M. 2012. BLD10/CEP135 Is a Microtubule-Associated Protein that

Controls the Formation of the Flagellum Central Microtubule Pair. *Developmental Cell*. 23(2):412–424.

Carvalho-Santos, Z., Machado, P., Branco, P., Tavares-Cadete, F., Rodrigues-Martins, A., Pereira-Leal, J. B., and Bettencourt-Dias, M. 2010. Stepwise evolution of the centriole-assembly pathway. *Journal of Cell Science*. 123(9):1414–1426.

Caspary, T., Larkins, C. E., and Anderson, K. V. 2007. The Graded Response to Sonic Hedgehog Depends on Cilia Architecture. *Developmental Cell*. 12(5):767–778.

Chapman, A. B., Stepniakowski, K., and Rahbari-Oskoui, F. 2010. *Hypertension in Autosomal Dominant Polycystic Kidney Disease*.

Chavali, P. L. et al. 2014. Small organelle, big responsibility: the role of centrosomes in development and disease. *Philosophical Transactions of the Royal Society of London. Series B, Biological sciences*. 369(1650):422–426.

Chen, J., Knowles, H. J., Hebert, J. L., and Hackett, B. P. 1998. Mutation of the mouse hepatocyte nuclear factor/forkhead homologue 4 gene results in an absence of cilia and random left-right asymmetry. *The Journal of Clinical Investigation*. 102(6):1077–82.

Chih, B., Liu, P., Chinn, Y., Chalouni, C., Komuves, L. G., Hass, P. E., Sandoval, W., and Peterson, A. S. 2012. A ciliopathy complex at the transition zone protects the cilia as a privileged membrane domain. *Nature Cell Biology*. 14(1):61–72.

Choksi, S. P. et al. 2014. Switching on cilia: transcriptional networks regulating ciliogenesis. *Development*. 141(7):1427–41.

Christensen, S. T., Clement, C. A., Satir, P., and Pedersen, L. B. 2012. Primary cilia and coordination of receptor tyrosine kinase (RTK) signalling. *The Journal of Pathology*. 226(2):172–184.

Chung, Y. D., Zhu, J., Han, Y.-G., and Kernan, M. J. 2001. NompA encodes a PNS-Specific, ZP domain protein required to connect mechanosensory dendrites to sensory structures. *Neuron*. 29(2):415–428.

Cole, D. G., Diener, D. R., Himelblau, A. L., Beech, P. L., Fuster, J. C., and Rosenbaum, J. L. 1998. Chlamydomonas kinesin-II-dependent intraflagellar transport (IFT): IFT particles contain proteins required for ciliary assembly in Caenorhabditis elegans sensory neurons. *The Journal of Cell Biology*. 141(4):993–1008.

Conduit, P. T., Brunk, K., Dobbelaere, J., Dix, C. I., Lucas, E. P., and Raff, J. W. 2010. Centrioles regulate centrosome size by controlling the rate of Cnn incorporation into the PCM. *Current Biology*. 20(24):2178–2186.

Conduit, P. T., Richens, J. H., Wainman, A., Holder, J., Vicente, C. C., Pratt, M. B., Dix, C. I., Novak, Z. A., Dobbie, I. M., Schermelleh, L., and Raff, J. W. 2014. A molecular mechanism of mitotic centrosome assembly in Drosophila. *eLife*. 3:e03399.

Conduit, P. T., Wainman, A., Novak, Z. A., Weil, T. T., and Raff, J. W. 2015a. Re-examining the role of Drosophila Sas-4 in centrosome assembly using two-colour-3D-SIM FRAP. *eLife*. 4(pii: e08483).

Conduit, P. T., Wainman, A., and Raff, J. W. 2015b. Centrosome function and assembly in animal cells. *Nature Reviews Molecular Cell Biology*. 16(10):611–624.

Corbit, K. C., Aanstad, P., Singla, V., Norman, A. R., Stainier, D. Y. R., and Reiter, J. F. 2005. Vertebrate Smoothened functions at the primary cilium. *Nature*. 437(7061):1018–21.

Corbit, K. C., Shyer, A. E., Dowdle, W. E., Gaulden, J., Singla, V., Chen, M.-H., Chuang, P.-T., and Reiter, J. F. 2008. Kif3a constrains beta-catenin-dependent Wnt signalling through dual ciliary and non-ciliary mechanisms. *Nature Cell Biology*. 10(1):70–6.

Cottee, M. A., Raff, J. W., Lea, S. M., and Roque, H. 2011. SAS-6 oligomerization: the key to the centriole? *Nature Chemical Biology*. 7(10):650–653.

Czarnecki, P. G. and Shah, J. V. 2012. The ciliary transition zone : from morphology and molecules to medicine. *Trends in Cell Biology*. 22(4):201–210.

Das, A., Dickinson, D. J., Wood, C. C., Goldstein, B., and Slep, K. C. 2015. Crescerin uses a TOG domain array to regulate microtubules in the primary cilium. *Molecular Biology of the Cell*. 26(23):4248–4264.

Davenport, J. R. and Yoder, B. K. 2005. An incredible decade for the primary cilium: a look at a once-forgotten organelle. *American Journal of Physiology. Renal Physiology.* 289(6):F1159–F1169.

Davis, E. E. and Katsanis, N. 2012. The ciliopathies: a transitional model into systems biology of human genetic disease. *Current Opinion in Genetics & Development*. 22(3):290–303.

Deane, J. A., Cole, D. G., Seeley, E., Diener, D. R., and Rosenbaum, J. L. 2001. Localization of intraflagellar transport protein IFT52 identifies basal body transitional fibers as the docking site for IFT particles.

Delattre, M. and Gönczy, P. 2004. The arithmetic of centrosome biogenesis. *Journal of Cell Science*. 117(9):1619–30.

Delaval, B., Bright, A., Lawson, N. D., and Doxsey, S. 2011. The cilia protein IFT88 is required for spindle orientation in mitosis. *Nature cell biology*. 13(4):461–8.

Dobbelaere, J., Josué, F., Suijkerbuijk, S., Baum, B., Tapon, N., and Raff, J. 2008. A genome-wide RNAi screen to dissect centriole duplication and centrosome maturation in Drosophila. *PLOS Biology*. 6(9):1975–1990.

Doherty, D., Parisi, M. A., Finn, L. S., Gunay-Aygun, M., Al-Mateen, M., Bates, D., Clericuzio, C., Demir, H., Dorschner, M., Essen, A. J. van, Gahl, W. A., Gentile, M., Gorden, N. T., Hikida, A., Knutzen, D., Ozyurek, H., Phelps, I., Rosenthal, P., Verloes, A., Weigand, H., Chance, P. F., Dobyns, W. B., and Glass, I. A. 2010. Mutations in 3 genes (MKS3, CC2D2A and RPGRIP1L) cause COACH syndrome (Joubert syndrome with congenital hepatic fibrosis). *Journal of Medical Genetics*. 47(1):8–21.

Doroquez, D. B., Berciu, C., Anderson, J. R., Sengupta, P., and Nicastro, D. 2014. A high-resolution morphological and ultrastructural map of anterior sensory cilia and glia in Caenorhabditis elegans. *eLife*. 3:e01948.

Eddé, B., Rossier, J., Le Caer, J. P., Desbruyères, E., Gros, F., and Denoulet, P. 1990. Post-translational glutamylation of alpha-tubulin. *Science*. 247(4938):83–85.

Engel, B. D., Ludington, W. B., and Marshall, W. F. 2009. Intraflagellar transport particle size scales inversely with flagellar length: revisiting the balance-point length control model. *The Journal of Cell Biology*. 187(1):81–9.

Enjolras, C., Thomas, J., Chhin, B., Cortier, E., Duteyrat, J.-L., Soulavie, F., Kernan, M. J., Laurencon, A., and Durand, B. 2012. Drosophila chibby is required for basal body formation and ciliogenesis but not for Wg signaling. *The Journal of Cell Biology*. 197(2):313–325.

Fabian, L. and Brill, J. A. 2012. Drosophila spermiogenesis: Big things come from little packages. *Spermatogenesis*. 2(3):197–212.

Fabrizio, J. J., Hime, G., Lemmon, S. K., and Bazinet, C. 1998. Genetic dissection of sperm individualization in Drosophila melanogaster. *Development*. 125(10):1833–43.

Follit, J. A., Xu, F., Keady, B. T., and Pazour, G. J. 2009. Characterization of mouse IFT complex B. *Cell Motility and the Cytoskeleton*. 66(8):457–68.

Forsythe, E. and Beales, P. L. 1993. Bardet-Biedl Syndrome. In: *Molecular Syndromology*. Vol. 7. 2. Karger Publishers: pp. 62–71.

Franz, A., Roque, H., Saurya, S., Dobbelaere, J., and Raff, J. W. 2013. CP110 exhibits novel regulatory activities during centriole assembly in Drosophila. *The Journal of Cell Biology*. 203(5):785–99.

Fu, J., Hagan, I. M., and Glover, D. M. 2015. *The centrosome and its duplication cycle*.

Fu, Y., Foden, J. A., Khayter, C., Maeder, M. L., Reyon, D., Joung, J. K., and Sander, J. D. 2013. High-frequency off-target mutagenesis induced by CRISPR-Cas nucleases in human cells. *Nature Biotechnology*. 31(9):822–6.

Furman, D. P. and Bukharina, T. A. 2012. Morphogenesis of Drosophila melanogaster macrochaetes: cell fate determination for bristle organ. *Journal of Stem Cells*. 7(1):19–41.

Gao, C. and Chen, Y.-G. 2010. Dishevelled: The hub of Wnt signaling. *Cellular Signalling*. 22(5):717–27.

Garcia-Gonzalo, F. R., Corbit, K. C., Sirerol-Piquer, M. S., Ramaswami, G., Otto, E. A., Noriega, T. R., Seol, A. D., Robinson, J. F., Bennett, C. L., Josifova, D. J., García-Verdugo, J. M., Katsanis, N., Hildebrandt, F., and Reiter, J. F. 2011. A transition zone complex regulates mammalian ciliogenesis and ciliary membrane composition. *Nature Genetics*. 43(8):776–84.

Garcia-Gonzalo, F. R. and Reiter, J. F. 2012. Scoring a backstage pass: mechanisms of ciliogenesis and ciliary access. *The Journal of Cell Biology*. 197(6):697–709.

Garcia-Gonzalo, F. R. and Reiter, J. F. 2016. Open Sesame: How Transition Fibers and the Transition Zone Control Ciliary Composition. *Cold Spring Harbor Perspectives in Biology*.

Gerdes, J. M., Davis, E. E., and Katsanis, N. 2009. The Vertebrate Primary Cilium in Development, Homeostasis, and Disease. *Cell*. 137(1):32–45.

Ghossoub, R. et al. 2013. Septins 2, 7 and 9 and MAP4 colocalize along the axoneme in the primary cilium and control ciliary length. *Journal of Cell Science*. 126(Pt 12):2583–94.

Ghysen, A. and Dambly-Chaudiere, C. 1989. Genesis of the Drosophila peripheral nervous system. *Trends in Genetics*. 5(C):251–255.

Ghysen, A., Dambly-Chaudière, C., Jan, L. Y., and Jan, Y. N. 1993. Cell interactions and gene interactions in peripheral neurogenesis. *Genes and Development*. 7(5):723–733.

Gillespie, P. G. and Walker, R. G. 2001. Molecular basis of mechanosensory transduction. *Nature*. 413(6852):194–202. arXiv: 0035855845.

Gilula, N. B. and Satir, P. 1972. The ciliary necklace. A ciliary membrane specialization. *The Journal of Cell Biology*. 53(2):494–509.

Goetz, S. C. and Anderson, K. V. 2010. The primary cilium: a signalling centre during vertebrate development. *Nature Reviews Genetics*. 11(5):331–44.

Gong, Z. 2004. Two Interdependent TRPV Channel Subunits, Inactive and Nanchung, Mediate Hearing in Drosophila. *Journal of Neuroscience*. 24(41):9059–9066.

Gonnissen, A., Isebaert, S., and Haustermans, K. 2015. Targeting the Hedgehog signaling pathway in cancer: beyond Smoothened. *Oncotarget*. 6(16):13899–913.

Göpfert, M. C. and Robert, D. 2003. Motion generation by Drosophila mechanosensory neurons. *Proceedings of the National Academy of Sciences of the United States of America*. 100(9):5514–5519.

Gottardo, M., Callaini, G., and Riparbelli, M. G. 2013. The cilium-like region of the Drosophila spermatocyte: an emerging flagellum? *Journal of Cell Science*. 126(Pt 23):5441–52.

Gottardo, M., Callaini, G., and Riparbelli, M. G. 2014. Procentriole assembly without centriole disengagement: a paradox of male gametogenesis. *Journal of Cell Science*. 127:3434–3439.

Graser, S., Stierhof, Y.-D., Lavoie, S. B., Gassner, O. S., Lamla, S., Le Clech, M., and Nigg, E. A. 2007. Cep164, a novel centriole appendage protein required for primary cilium formation. *The Journal of Cell Biology*. 179(2):321–30.

Gratz, S. J., Cummings, A. M., Nguyen, J. N., Hamm, D. C., Donohue, L. K., Harrison, M. M., Wildonger, J., and O'Connor-Giles, K. M. 2013. Genome engineering of Drosophila with the CRISPR RNA-guided Cas9 nuclease. *Genetics*. 194(4):1029–1035.

Greenspan, R. J. 2004. *Fly pushing: The Theory and Practice of Drosophila Genetics*.

Gresh, L., Fischer, E., Reimann, A., Tanguy, M., Garbay, S., Shao, X., Hiesberger, T., Fiette, L., Igarashi, P., Yaniv, M., and Pontoglio, M. 2004. A transcriptional network in polycystic kidney disease. *The EMBO journal*. 23(7):1657–68.

Gundersen, G. G. and Bulinski, J. C. 1986. Microtubule arrays in differentiated cells contain elevated levels of a post-translationally modified form of tubulin. *European Journal of Cell Biology*. 42(2):288–94.

Habbig, S., Bartram, M. P., Müller, R. U., Schwarz, R., Andriopoulos, N., Chen, S., Sägmüller, J. G., Hoehne, M., Burst, V., Liebau, M. C., Reinhardt, H. C., Benzing, T., and Schermer, B. 2011. NPHP4, a cilia-associated protein, negatively regulates the Hippo pathway. *The Journal of Cell Biology*. 193(4):633–42.

Han, Y.-G., Kim, H. J., Dlugosz, A. A., Ellison, D. W., Gilbertson, R. J., and Alvarez-Buylla, A. 2009. Dual and opposing roles of primary cilia in medulloblastoma development. *Nature Medicine*. 15(9):1062–5.

Han, Y.-G., Kwok, B. H., and Kernan, M. J. 2003. Intraflagellar transport is required in Drosophila to differentiate sensory cilia but not sperm. *Current Biology*. 13(19):1679–1686.

Hao, L., Thein, M., Brust-Mascher, I., Civelekoglu-Scholey, G., Lu, Y., Acar, S., Prevo, B., Shaham, S., and Scholey, J. M. 2011. Intraflagellar transport delivers tubulin isotypes to sensory cilium middle and distal segments. *Nature Cell Biology*. 13(7):790–8.

Hartenstein, V. and Posakony, J. W. 1989. Development of adult sensilla on the wing and notum of Drosophila melanogaster. *Development*. 107(2):389–405.

Hartenstein, V. 1988. Development of Drosophila larval sensory organs: spatiotemporal pattern of sensory neurones, peripheral axonal pathways and sensilla differentiation. *Development*. 102(4):869–886.

Harvey, K. and Tapon, N. 2007. The Salvador-Warts-Hippo pathway - an emerging tumour-suppressor network. *Nature Reviews Cancer*. 7(3):182–91.

Hassounah, N. B., Bunch, T. A., and McDermott, K. M. 2012. Molecular pathways: The role of primary cilia in cancer progression and therapeutics with a focus on hedgehog signaling. *Clinical Cancer Research*. 18(9):2429–2435. arXiv: NIHMS150003.

Haycraft, C. J., Banizs, B., Aydin-Son, Y., Zhang, Q., Michaud, E. J., and Yoder, B. K. 2005. Gli2 and Gli3 localize to cilia and require the intraflagellar transport protein polaris for processing and function. *PLOS Genetics*. 1(4):e53.

Hayward, D., Metz, J., Pellacani, C., and Wakefield, J. G. 2014. Synergy between multiple microtubule-generating pathways confers robustness to centrosome-driven mitotic spindle formation. *Developmental Cell*. 28(1):81–93.

Heiman, M. G. and Shaham, S. 2009. DEX-1 and DYF-7 establish sensory dendrite length by anchoring dendritic tips during cell migration. *Cell*. 137(2):344–55.

Hilgendorf, K. I., Johnson, C. T., and Jackson, P. K. 2016. The primary cilium as a cellular receiver: organizing ciliary GPCR signaling. *Current Opinion in Cell Biology*. 39:84–92.

Hirokawa, N. et al. 2006. Nodal Flow and the Generation of Left-Right Asymmetry. *Cell*. 125(1):33–45.

Hirsch, J. and Tryon, R. C. 1956. Mass screening and reliable individual measurement in the experimental behavior genetics of lower organisms. *Psychological Bulletin*. 53(5):402–10.

Honnappa, S., Gouveia, S. M., Weisbrich, A., Damberger, F. F., Bhavesh, N. S., Jawhari, H., Grigoriev, I., Rijssel, F. J. A. van, Buey, R. M., Lawera, A., Jelesarov, I., Winkler, F. K., Wüthrich, K., Akhmanova, A., and Steinmetz, M. O. 2009. An EB1-binding motif acts as a microtubule tip localization signal. *Cell*. 138(2):366–376.

Hopp, K., Heyer, C. M., Hommerding, C. J., Henke, S. A., Sundsbak, J. L., Patel, S., Patel, P., Consugar, M. B., Czarnecki, P. G., Gliem, T. J., Torres, V. E., Rossetti, S., and Harris, P. C. 2011. B9D1 is revealed as a novel Meckel syndrome (MKS) gene by targeted exon-enriched next-generation sequencing and deletion analysis. *Human Molecular Genetics*. 20(13):2524–34.

Hsiao, Y.-C., Tuz, K., and Ferland, R. J. 2012. Trafficking in and to the primary cilium. *Cilia*. 1(1):4.

Hu, Q. and Nelson, W. J. 2011. Ciliary diffusion barrier: the gatekeeper for the primary cilium compartment. *Cytoskeleton*. 68(6):313–24.

Huang, P. and Schier, A. F. 2009. Dampened Hedgehog signaling but normal Wnt signaling in zebrafish without cilia. *Development*. 136(18):3089–98.

Huangfu, D. and Anderson, K. V. 2005. Cilia and Hedgehog responsiveness in the mouse. *Proceedings of the National Academy of Sciences of the United States of America*. 102(32):11325–30.

Huangfu, D., Liu, A., Rakeman, A. S., Murcia, N. S., Niswander, L., and Anderson, K. V. 2003. Hedgehog signalling in the mouse requires intraflagellar transport proteins. *Nature*. 426(6962):83–7.

Hui, C.-C. and Angers, S. 2011. Gli proteins in development and disease. *Annual Review of Cell and Developmental Biology*. 27:513–37.

Huppke, P., Wegener, E., Böhrer-Rabel, H., Bolz, H. J., Zoll, B., Gärtner, J., and Bergmann, C. 2014. Tectonic gene mutations in patients with Joubert syndrome. *European Journal of Human Genetics*.

Ishikawa, H. and Marshall, W. F. 2011. Ciliogenesis: building the cell's antenna. *Nature Reviews Molecular Cell Biology*. 12(4):222–234.

Ishikawa, H., Kubo, A., Tsukita, S., and Tsukita, S. 2005. Odf2-deficient mother centrioles lack distal/subdistal appendages and the ability to generate primary cilia. *Nature Cell Biology*. 7(5):517–524.

Jakobsen, L., Vanselow, K., Skogs, M., Toyoda, Y., Lundberg, E., Poser, I., Falkenby, L. G., Bennetzen, M., Westendorf, J., Nigg, E. A., Uhlen, M., Hyman, A. A., and Andersen, J. S. 2011. Novel asymmetrically localizing components of human centrosomes identified by complementary proteomics methods. *The EMBO journal*. 30(8):1520–35.

Jarman, A. P. 2002. Studies of mechanosensation using the fly. *Human Molecular Genetics*. 11(10):1215–1218.

Jarman, A. P., Grau, Y., Jan, L. Y., and Jan, Y. N. 1993. atonal is a proneural gene that directs chordotonal organ formation in the Drosophila peripheral nervous system. *Cell*. 73(7):1307–1321.

Jarman, A. P., Sun, Y., Jan, L. Y., and Jan, Y. N. 1995. Role of the proneural gene, atonal, in formation of Drosophila chordotonal organs and photoreceptors. *Development*. 121(7):2019–2030.

Jenkins, P. M., McEwen, D. P., and Martens, J. R. 2009. Olfactory cilia: linking sensory cilia function and human disease. *Chemical Senses*. 34(5):451–64.

Jensen, V. L., Li, C., Bowie, R. V., Clarke, L., Mohan, S., Blacque, O. E., and Leroux, M. R. 2015. Formation of the transition zone by Mks5/Rpgrip1L establishes a ciliary zone of exclusion (CIZE) that compartmentalises ciliary signalling proteins and controls PIP2 ciliary abundance. *The EMBO Journal*:e201488044.

Jiang, K., Toedt, G., Montenegro Gouveia, S., Davey, N. E., Hua, S., Vaart, B. van der, Grigoriev, I., Larsen, J., Pedersen, L. B., Bezstarosti, K., Lince-Faria, M., Demmers, J., Steinmetz, M. O., Gibson, T. J., and Akhmanova, A. 2012. A Proteome-wide screen for mammalian SxIP motif-containing microtubule plus-end tracking proteins. *Current Biology*. 22(19):1800–7.

Jin, H., White, S. R., Shida, T., Schulz, S., Aguiar, M., Gygi, S. P., Bazan, J. F., and Nachury, M. V. 2010. The conserved Bardet-Biedl syndrome proteins assemble a coat that traffics membrane proteins to cilia. *Cell*. 141(7):1208–19.

Jinek, M., Chylinski, K., Fonfara, I., Hauer, M., Doudna, J. A., and Charpentier, E. 2012. A programmable dual-RNA-guided DNA endonuclease in adaptive bacterial immunity. *Science*. 337(6096):816–21.

Jones, D. T. 1999. Protein secondary structure prediction based on position-specific scoring matrices. *Journal of molecular biology*. 292(2):195–202.

Joseph, R. M. and Carlson, J. R. 2015. *Drosophila Chemoreceptors: A Molecular Interface Between the Chemical World and the Brain*. arXiv: NIHMS150003.

Katoh, M. 2005. WNT/PCP signaling pathway and human cancer (review). *Oncology reports*. 14(6):1583–8.

Keil, T. A. 1997. Functional morphology of insect mechanoreceptors. *Microscopy Research and Technique*. 39(6):506–531.

Keller, R., Shook, D., and Skoglund, P. 2008. The forces that shape embryos: physical aspects of convergent extension by cell intercalation. *Physical Biology*. 5(1):015007.

Kernan, M. J. 2007. Mechanotransduction and auditory transduction in Drosophila. *Pflügers Archiv : European Journal of Physiology*. 454(5):703–20.

Kernan, M., Cowan, D., and Zuker, C. 1994. Genetic dissection of mechanosensory transduction: Mechanoreception-defective mutations of Drosophila. *Neuron*. 12(6):1195–1206.

Kim, J., Chung, Y. D., Park, D.-Y., Choi, S., Shin, D. W., Soh, H., Lee, H. W., Son, W., Yim, J., Park, C.-S., Kernan, M. J., and Kim, C. 2003. A TRPV family ion channel required for hearing in Drosophila. *Nature*. 424(6944):81–84.

Kiselak, E. A., Shen, X., Song, J., Gude, D. R., Wang, J., Brody, S. L., Strauss, J. F., and Zhang, Z. 2010. Transcriptional regulation of an axonemal central apparatus gene, sperm-associated antigen 6, by a SRY-related high mobility group transcription factor, S-SOX5. *The Journal of Biological Chemistry*. 285(40):30496–505.

Kleylein-Sohn, J., Westendorf, J., Le Clech, M., Habedanck, R., Stierhof, Y. D., and Nigg, E. A. 2007. Plk4-Induced Centriole Biogenesis in Human Cells. *Developmental Cell*. 13(2):190–202.

Klos Dehring, D. A., Vladar, E. K., Werner, M. E., Mitchell, J. W., Hwang, P., and Mitchell, B. J. 2013. Deuterosome-Mediated Centriole Biogenesis. *Developmental Cell*. 27(1):103–112.

Kremer, J. R., Mastronarde, D. N., and McIntosh, J. R. 1996. Computer visualization of three-dimensional image data using IMOD. *Journal of structural biology*. 116(1):71–6.

Kyttälä, M., Tallila, J., Salonen, R., Kopra, O., Kohlschmidt, N., Paavola-Sakki, P., Peltonen, L., and Kestilä, M. 2006. MKS1, encoding a component of the flagellar apparatus basal body proteome, is mutated in Meckel syndrome. *Nature genetics*. 38(2):155–7.

Lai, E. C. and Orgogozo, V. 2004. A hidden program in Drosophila peripheral neurogenesis revealed: fundamental principles underlying sensory organ diversity. *Developmental Biology*. 269(1):1–17.

Lambacher, N. J., Bruel, A.-L., Dam, T. J. P. van, Szymańska, K., Slaats, G. G., Kuhns, S., McManus, G. J., Kennedy, J. E., Gaff, K., Wu, K. M., Lee, R. van der, Burglen, L., Doummar, D., Rivière, J.-B., Faivre, L., Attié-Bitach, T., Saunier, S., Curd, A., Peckham, M., Giles, R. H., Johnson, C. A., Huynen, M. A., Thauvin-Robinet, C., and Blacque, O. E. 2015. TMEM107 recruits ciliopathy proteins to subdomains of the ciliary transition zone and causes Joubert syndrome. *Nature Cell Biology*. 18(1):122–131.

Lambrus, B. G., Uetake, Y., Clutario, K. M., Daggubati, V., Snyder, M., Sluder, G., and Holland, A. J. 2015. P53 protects against genome instability following centriole duplication failure. *Journal of Cell Biology*. 210(1):63–77.

Laufer, E., Nelson, C. E., Johnson, R. L., Morgan, B. A., and Tabin, C. 1994. Sonic hedgehog and Fgf-4 act through a signaling cascade and feedback loop to integrate growth and patterning of the developing limb bud. *Cell*. 79(6):993–1003.

Lee, E., Sivan-Loukianova, E., Eberl, D. F., and Kernan, M. J. 2008. An IFT-A protein is required to delimit functionally distinct zones in mechanosensory cilia. *Current Biology*. 18(24):1899–906.

Lee, J., Moon, S., Cha, Y., and Chung, Y. D. 2010. Drosophila TRPN (=NOMPC) channel localizes to the distal end of mechanosensory cilia. *PLOS One*. 5(6):e11012.

Lee, Y. L., Sante, J., Comerci, C. J., Cyge, B., Menezes, L. F., Li, F.-Q., Germino, G. G., Moerner, W. E., Takemaru, K.-I., and Stearns, T. 2014. Cby1 promotes Ahi1 recruitment to a ring-shaped domain at the centriole-cilium interface and facilitates proper cilium formation and function. *Molecular Biology of the Cell*. 25(19):2919–2933.

Lemmon, M. A. and Schlessinger, J. 2010. Cell signaling by receptor tyrosine kinases. *Cell*. 141(7):1117–34.

Lerit, D. A. and Poulton, J. S. 2016. Centrosomes are multifunctional regulators of genome stability. *Chromosome Research*. 24(1):5–17.

Leroy, F., Lamotte d'Incamps, B., Imhoff-Manuel, R. D., and Zytnicki, D. 2014. Early intrinsic hyperexcitability does not contribute to motoneuron degeneration in amyotrophic lateral sclerosis. *eLife*. 3:1–24.

Li, C., Jensen, V. L., Park, K., Kennedy, J., Garcia-Gonzalo, F. R., Romani, M., De Mori, R., Bruel, A.-L., Gaillard, D., Doray, B., Lopez, E., Rivière, J.-B., Faivre, L., Thauvin-Robinet, C., Reiter, J. F., Blacque, O. E., Valente, E. M., and Leroux, M. R. 2016. MKS5 and CEP290 Dependent Assembly Pathway of the Ciliary Transition Zone. *PLOS Biology*. 14(3):e1002416.

Liang, X., Madrid, J., Gärtner, R., Verbavatz, J. M., Schiklenk, C., Wilsch-Bräuninger, M., Bogdanova, A., Stenger, F., Voigt, A., and Howard, J. 2013a. A NOMPC-dependent membrane-microtubule connector is a candidate for the gating spring in fly mechanoreceptors. *Current Biology*. 23(9):755–763.

Liang, X., Madrid, J., Gärtner, R., Verbavatz, J.-M., Schiklenk, C., Wilsch-Bräuninger, M., Bogdanova, A., Stenger, F., Voigt, A., and Howard, J. 2013b. A NOMPC-Dependent Membrane-Microtubule Connector Is a Candidate for the Gating Spring in Fly Mechanoreceptors. *Current Biology*. 23(9):755–763.

Liang, X., Madrid, J., Saleh, H. S., and Howard, J. 2011. NOMPC, a member of the TRP channel family, localizes to the tubular body and distal cilium of Drosophila campaniform and chordotonal receptor cells. *Cytoskeleton*. 68(1):1–7.

Linck, R. W. and Stephens, R. E. 2007. Functional protofilament numbering of ciliary, flagellar, and centriolar microtubules. *Cell Motility and the Cytoskeleton*. 64(7):489–495.

Lindsley, D. L. and Zimm, G. G. 1992. *The Genome of Drosophila melanogaster.*

Liu, A., Wang, B., and Niswander, L. A. 2005. Mouse intraflagellar transport proteins regulate both the activator and repressor functions of Gli transcription factors. *Development*. 132(13):3103–3111.

Lodh, S., O'Hare, E. A., and Zaghloul, N. A. 2014. Primary cilia in pancreatic development and disease. *Birth Defects Research Part C - Embryo Today: Reviews*. 102(2):139–158. arXiv: NIHMS150003.

Lupas, A., Van Dyke, M., and Stock, J. 1991. Predicting coiled coils from protein sequences. *Science*. 252(5009):1162–4.

Ma, L. and Jarman, A. P. 2011. Dilatory is a Drosophila protein related to AZI1 (CEP131) that is located at the ciliary base and required for cilium formation. *Journal of Cell Science*. 124(15):2622–30.

Marshall, W. F. and Rosenbaum, J. L. 2001. Intraflagellar transport balances continuous turnover of outer doublet microtubules: implications for flagellar length control. *The Journal of Cell Biology*. 155(3):405–14.

Marshall, W. F. 2009. Centriole evolution. *Current Opinion in Cell Biology*. 21(1):14–19.

Marshall, W. F. 2013. *Methods in Enzymology Cilia Part A*: pp. 243–261.

Martinez-Campos, M., Basto, R., Baker, J., Kernan, M., and Raff, J. W. 2004. The Drosophila pericentrin-like protein is essential for cilia/flagella function, but appears to be dispensable for mitosis. *The Journal of Cell Biology*. 165(5):673–83.

Matsui, T. and Bessho, Y. 2012. Left-right asymmetry in zebrafish. *Cellular and Molecular Life Sciences*. 69(18):3069–77.

Meunier, S. and Vernos, I. 2012. Microtubule assembly during mitosis - from distinct origins to distinct functions? *Journal of Cell Science*. 125(12):2805–2814.

Mitchell, D. R. 2016. Evolution of Cilia. *Cold Spring Harbor Perspectives in Biology*:a028290.

Monk, K. R., Feltri, M. L., and Taveggia, C. 2015. New insights on schwann cell development. *Glia*. 63(8):1–18.

Moritz, M., Braunfeld, M. B., Sedat, J. W., Alberts, B., and Agard, D. A. 1995. Microtubule nucleation by gamma-tubulin-containing rings in the centrosome. *Nature*. 378(6557):638–40.

Mottier-Pavie, V. and Megraw, T. L. 2009. Drosophila bld10 is a centriolar protein that regulates centriole, basal body, and motile cilium assembly. *Molecular Biology of the Cell*. 20(10):2605–2614.

Mougou-Zerelli, S., Thomas, S., Szenker, E., Audollent, S., Elkhartoufi, N., Babarit, C., Romano, S., Salomon, R., Amiel, J., Esculpavit, C., Gonzales, M., Escudier, E., Leheup, B., Loget, P., Odent, S., Roume, J., Gérard, M., Delezoide, A.-L., Khung, S., Patrier, S., Cordier, M.-P., Bouvier, R., Martinovic, J., Gubler, M.-C., Boddaert, N., Munnich, A., Encha-Razavi, F., Valente, E. M., Saad, A., Saunier, S., Vekemans, M., and Attié-Bitach, T. 2009. CC2D2A mutations in Meckel and Joubert syndromes indicate a genotype-phenotype correlation. *Human Mutation*. 30(11):1574–82.

Nachury, M. V. 2014. How do cilia organize signalling cascades? *Philosophical Transactions of the Royal Society of London. Series B, Biological sciences*. 369(1650):20130465–.

Nachury, M. V., Seeley, E. S., and Jin, H. 2010. Trafficking to the ciliary membrane: how to get across the periciliary diffusion barrier? *Annual Review of Cell and Developmental Biology*. 26:59–87.

Newton, F. G., Lage, P. I. zur, Karak, S., Moore, D. J., Göpfert, M. C., and Jarman, A. P. 2012. Forkhead transcription factor Fd3F cooperates with Rfx to regulate a gene expression program for mechanosensory cilia specialization. *Developmental Cell*. 22(6):1221–33.

Ng, J. M. Y. and Curran, T. 2011. The Hedgehog's tale: developing strategies for targeting cancer. *Nature Reviews Cancer*. 11(7):493–501.

Nicholson, L., Singh, G. K., Osterwalder, T., Roman, G. W., Davis, R. L., and Keshishian, H. 2008. Spatial and temporal control of gene expression in Drosophila using the inducible GeneSwitch GAL4 System. I. Screen for larval nervous system drivers. *Genetics*. 178(1).

Nigg, E. a. and Raff, J. W. 2009. Centrioles, centrosomes, and cilia in health and disease. *Cell*. 139(4):663–78.

Nonaka, S., Tanaka, Y., Okada, Y., Takeda, S., Harada, a., Kanai, Y., Kido, M., and Hirokawa, N. 1998. Randomization of left-right asymmetry due to loss of nodal cilia generating leftward flow of extraembryonic fluid in mice lacking KIF3B motor protein. *Cell*. 95(6):829–37.

Novak, Z. A., Wainman, A., Gartenmann, L., and Raff, J. J. W. 2016. Cdk1 phosphorylates Drosophila Sas-4 to recruit Polo to daughter centrioles and convert them to centrosomes. *Developmental Cell*. 37(6):545–557.

Novak, Z. A. et al. 2014. Asterless licenses daughter centrioles to duplicate for the first time in Drosophila embryos. *Current Biology*. 24(11):1276–82.

Nüsslein-Volhard, C. and Wieschaus, E. 1980. Mutations affecting segment number and polarity in Drosophila. *Nature*. 287(5785):795–801.

Ocbina, P. J. R. and Anderson, K. V. 2008. Intraflagellar transport, cilia, and mammalian hedgehog signaling: Analysis in mouse embryonic fibroblasts. *Developmental Dynamics*. 237(8):2030–2038.

Ocbina, P. J. R., Tuson, M., and Anderson, K. V. 2009. Primary cilia are not required for normal canonical Wnt signaling in the mouse embryo. *PLOS One*. 4(8):e6839.

O'Connell, C. B. and Khodjakov, A. L. 2007. Cooperative mechanisms of mitotic spindle formation. *Journal of Cell Science*. 120(10):1717–1722.

Odate, T., Takeda, S., Narita, K., and Kawahara, T. 2016. 9 + 0 and 9 + 2 cilia are randomly dispersed in the mouse node. *Microscopy*. 65(2):119–126.

Oh, E. C. and Katsanis, N. 2012. Cilia in vertebrate development and disease. *Development*. 139(3):443–448.

Oh, E. C., Vasanth, S., and Katsanis, N. 2015. Metabolic regulation and energy homeostasis through the primary cilium. *Cell Metabolism*. 21(1):21–31. arXiv: 15334406.

Ong, A. C. and Gubler, M.-C. 2011. What's new in... Ciliopathies. *Medicine*. 39(2):119–125.

Pal, K. and Mukhopadhyay, S. 2015. Primary cilium and sonic hedgehog signaling during neural tube patterning: Role of GPCRs and second messengers. *Developmental Neurobiology*. 75(4):337–348.

Palazzo, R. E., Vogel, J. M., Schnackenberg, B. J., Hull, D. R., and Wu, X. 2000. Centrosome maturation. *Current Topics in Developmental Biology*. 49:449–70.

Pasca di Magliano, M. and Hebrok, M. 2003. Hedgehog signalling in cancer formation and maintenance. *Nature Reviews Cancer*. 3(12):903–911.

Pazour, G. J., Dickert, B. L., and Witman, G. B. 1999. The DHC1b (DHC2) isoform of cytoplasmic dynein is required for flagellar assembly. *The Journal of Cell Biology*. 144(3):473–81.

Pazour, G. J., Wilkerson, C. G., and Witman, G. B. 1998. A dynein light chain is essential for the retrograde particle movement of intraflagellar transport (IFT). *The Journal of Cell Biology*. 141(4):979–92.

Pedersen, L. B. and Rosenbaum, J. L. 2008. Intraflagellar transport (IFT) role in ciliary assembly, resorption and signalling. *Current Topics in Developmental Biology*. 85:23–61.

Pellegrino, M. and Nakagawa, T. 2009. Smelling the difference: controversial ideas in insect olfaction. *The Journal of Experimental Biology*. 212(13):1973–1979.

Pelletier, L., O'Toole, E., Schwager, A., Hyman, A. A., and Muller-Reichert, T. 2006. Centriole assembly in Caenorhabditis elegans. *Nature*. 444(7119):619–623.

Phillips, D. M. 1970. Insect sperm: their structure and morphogenesis. *The Journal of Cell Biology*. 44(2):243–77.

Phillis, R. W., Bramlage, A. T., Wotus, C., Whittaker, A., Gramates, L. S., Seppala, D., Farahanchi, F., Caruccio, P., and Murphey, R. K. 1993. Isolation of mutations affecting neural circuitry required for grooming behavior in Drosophila melanogaster. *Genetics*. 133(3):581–92.

Pigino, G., Geimer, S., Lanzavecchia, S., Paccagnini, E., Cantele, F., Diener, D. R., Rosenbaum, J. L., and Lupetti, P. 2009. Electron-tomographic analysis of intraflagellar transport particle trains in situ. *The Journal of Cell Biology*. 187(1):135–48.

Piperno, G. and Fuller, M. T. 1985. Monoclonal antibodies specific for an acetylated form of alpha-tubulin recognize the antigen in cilia and flagella from a variety of organisms. *Journal of Cell Biology*. 101(6):2085–2094.

Port, F., Chen, H.-M. H.-M., Lee, T., and Bullock, S. L. 2014. An optimized CRISPR/Cas toolbox for efficient germline and somatic genome engineering in Drosophila. *Proceedings of the National Academy of Sciences of the United States of America*. 111(29):2967–2976.

Powles-Glover, N. 2014. Cilia and ciliopathies: Classic examples linking phenotype and genotype-An overview. *Reproductive Toxicology*.

Praveen, K., Davis, E. E., and Katsanis, N. 2015. Unique among ciliopathies: primary ciliary dyskinesia, a motile cilia disorder. *F1000prime reports*. 7(March):36.

Qin, H., Diener, D. R., Geimer, S., Cole, D. G., and Rosenbaum, J. L. 2004. Intraflagellar transport (IFT) cargo: IFT transports flagellar precursors to the tip and turnover products to the cell body. *The Journal of Cell Biology*. 164(2):255–66.

Reina, J. and Gonzalez, C. 2014. When fate follows age: unequal centrosomes in asymmetric cell division. *Philosophical Transactions of the Royal Society of London. Series B, Biological sciences*. 369(1650):25–28.

Reiter, J. F., Blacque, O. E., and Leroux, M. R. 2012. The base of the cilium: roles for transition fibres and the transition zone in ciliary formation, maintenance and compartmentalization. *EMBO Reports*. 13(7):608–18.

Rezabkova, L., Kraatz, S. H. W., Akhmanova, A., Steinmetz, M. O., and Kammerer, R. A. 2016. Biophysical and structural characterization of the centriolar protein CEP104 interaction network. *Journal of Biological Chemistry*. 291(35):18496–18504.

Riemensperger, T., Pech, U., Dipt, S., and Fiala, A. 2012. Optical calcium imaging in the nervous system of Drosophila melanogaster. *Biochimica et Biophysica Acta - General Subjects*. 1820(8):1169–1178.

Riparbelli, M. G., Cabrera, O. A., Callaini, G., and Megraw, T. L. 2013. Unique properties of Drosophila spermatocyte primary cilia. *Biology Open*. 2(11):1137–47.

Riparbelli, M. G., Callaini, G., and Megraw, T. L. 2012. Assembly and persistence of primary cilia in dividing Drosophila spermatocytes. *Developmental cell*. 23(2):425–32.

Roberts, D. B. 1986. *Drosophila: a practical approach*.

Robertson, H. M., Preston, C. R., Phillis, R. W., Johnson-Schlitz, D. M., Benz, W. K., and Engels, W. R. 1988. A stable genomic source of P-element transposase in Drosophila melanogaster. *Genetics*. 118(3):461–70.

Rogowski, M., Scholz, D., and Geimer, S. 2013. Electron microscopy of flagella, primary cilia, and intraflagellar transport in flat-embedded cells. *Methods in Enzymology*. 524:243–63.

Rohatgi, R., Milenkovic, L., and Scott, M. P. 2007. Patched1 regulates hedgehog signaling at the primary cilium. *Science*. 317(5836):372–6.

Romani, M., Micalizzi, A., Kraoua, I., Dotti, M. T., Cavallin, M., Sztriha, L., Ruta, R., Mancini, F., Mazza, T., Castellana, S., Hanene, B., Carluccio, M. A., Darra, F., Máté, A., Zimmermann, A., Gouider-Khouja, N., and Valente, E. M. 2014. Mutations in B9D1

and MKS1 cause mild Joubert syndrome: expanding the genetic overlap with the lethal ciliopathy Meckel syndrome. *Orphanet Journal of Rare Diseases*. 9(1):72.

Roque, H., Wainman, A., Richens, J., Kozyrska, K., Franz, A., and Raff, J. W. 2012. Drosophila Cep135/Bld10 maintains proper centriole structure but is dispensable for cartwheel formation. *Journal of Cell Science*. 125(Pt 23):5881–6.

Rosenbaum, J. L. and Witman, G. B. 2002. Intraflagellar transport. *Nature Reviews Molecular Cell Biology*. 3(11):813–25.

Roy, S. 2012. Cilia and Hedgehog: when and how was their marriage solemnized? *Differentiation*. 83(2):S43–8.

Sang, L., Miller, J. J., Corbit, K. C., Giles, R. H., Brauer, M. J., Otto, E. A., Baye, L. M., Wen, X., Scales, S. J., Kwong, M., Erik, G., Sfakianos, M. K., Sandoval, W., Bazan, J. F., Garcia-gonzalo, F. R., Seol, A. D., Toole, J. F. O., Held, S., Reutter, H. M., Lane, W. S., Rafiq, M. A., Noor, A., Radha, A., Devi, R., Sheffield, V. C., Slusarski, D. C., Vincent, J. B., Doherty, D. A., Hildebrandt, F., Reiter, J. F., and Jackson, P. K. 2012. Mapping the Nephronophtisis-Jouber-Meckel-Gruber Protein Network reveals Ciliopathy DIsease Genes and Pathways. *Cell*. 145(4):513–528.

Sasai, N. and Briscoe, J. 2012. Primary cilia and graded Sonic Hedgehog signaling. *Wiley Interdisciplinary Reviews: Developmental Biology*. 1(5):753–772.

Satir, P., Mitchell, D. R., and Jékely, G. 2008. *Chapter 3 How Did the Cilium Evolve?*

Satish Tammana, T. V., Tammana, D., Diener, D. R., Rosenbaum, J., Tammana, T. V. S., Tammana, D., Diener, D. R., and Rosenbaum, J. 2013. Centrosomal protein CEP104 (Chlamydomonas FAP256) moves to the ciliary tip during ciliary assembly. *Journal of Cell Science*. 126(Pt 21):5018–5029.

Schindelin, J., Arganda-Carreras, I., Frise, E., Kaynig, V., Longair, M., Pietzsch, T., Preibisch, S., Rueden, C., Saalfeld, S., Schmid, B., Tinevez, J.-Y., White, D. J., Hartenstein, V., Eliceiri, K., Tomancak, P., and Cardona, A. 2012. Fiji: an open-source platform for biological-image analysis. *Nature Methods*. 9(7):676–82.

Schmidt, T. I., Kleylein-Sohn, J., Westendorf, J., Le Clech, M., Lavoie, S. B., Stierhof, Y. D., and Nigg, E. A. 2009. Control of Centriole Length by CPAP and CP110. *Current Biology*. 19(12):1005–1011.

Schneider, L., Clement, C. A., Teilmann, S. C., Pazour, G. J., Hoffmann, E. K., Satir, P., and Christensen, S. T. 2005. PDGFRalphaalpha signaling is regulated through the primary cilium in fibroblasts. *Current Biology*. 15(20):1861–6.

Schouteden, C., Serwas, D., Palfy, M., and Dammermann, A. 2015. The ciliary transition zone functions in cell adhesion but is dispensable for axoneme assembly in C. elegans. *The Journal of Cell Biology*. 210(1):35–44.

Schwander, M., Kachar, B., and Müller, U. 2010. The cell biology of hearing. *The Journal of Cell Biology*. 190(1):9–20.

Schweickert, A., Weber, T., Beyer, T., Vick, P., Bogusch, S., Feistel, K., and Blum, M. 2007. Cilia-Driven Leftward Flow Determines Laterality in Xenopus.

Seeds, A. M., Ravbar, P., Chung, P., Hampel, S., Midgley, F. M., Mensh, B. D., and Simpson, J. H. 2014. A suppression hierarchy among competing motor programs drives sequential grooming in Drosophila. *eLife*. 3:e02951.

Seeley, E. S. and Nachury, M. V. 2010. The perennial organelle: assembly and disassembly of the primary cilium. *Journal of Cell Science*. 123(Pt 4):511–8.

Shapiro, A. J., Davis, S. D., Ferkol, T., Dell, S. D., Rosenfeld, M., Olivier, K. N., Sagel, S. D., Milla, C., Zariwala, M. A., Wolf, W., Carson, J. L., Hazucha, M. J., Burns, K., Robinson, B., Knowles, M. R., and Leigh, M. W. 2014. Laterality defects other than situs inversus totalis in primary ciliary dyskinesia: Insights into situs ambiguus and heterotaxy. *Chest*. 146(5):1176–1186.

Silverman, M. A. and Leroux, M. R. 2009. *Intraflagellar transport and the generation of dynamic, structurally and functionally diverse cilia*.

Simons, M., Gloy, J., Ganner, A., Bullerkotte, A., Bashkurov, M., Krönig, C., Schermer, B., Benzing, T., Cabello, O. A., Jenny, A., Mlodzik, M., Polok, B., Driever, W., Obara, T., and Walz, G. 2005. Inversin, the gene product mutated in nephronophthisis type II, functions as a molecular switch between Wnt signaling pathways. *Nature Genetics*. 37(5):537–543.

Singla, V. and Reiter, J. F. 2006. The primary cilium as the cell's antenna: signaling at a sensory organelle. *Science*. 313(5787):629–33.

Siskova, Z., Justus, D., Kaneko, H., Friedrichs, D., Henneberg, N., Beutel, T., Pitsch, J., Schoch, S., Becker, A., VonderKammer, H., and Remy, S. 2014. Dendritic structural degeneration is functionally linked to cellular hyperexcitability in a mouse model of alzheimer's disease. *Neuron*. 84(5):1023–1033.

Slaats, G. G., Isabella, C. R., Kroes, H. Y., Dempsey, J. C., Gremmels, H., Monroe, G. R., Phelps, I. G., Duran, K. J., Adkins, J., Kumar, S. A., Knutzen, D. M., Knoers, N. V., Mendelsohn, N. J., Neubauer, D., Mastroyianni, S. D., Vogt, J., Worgan, L., Karp, N., Bowdin, S., Glass, I. A., Parisi, M. A., Otto, E. A., Johnson, C. A., Hildebrandt, F., Haaften, G. van, Giles, R. H., and Doherty, D. 2015. MKS1 regulates ciliary INPP5E levels in Joubert syndrome. *Journal of Medical Genetics*. 53(1):pages.

Slep, K. C. and Vale, R. D. 2007. Structural Basis of Microtubule Plus End Tracking by XMAP215, CLIP-170, and EB1. *Molecular Cell*. 27(6):976–991.

Smith, M. B., Li, H., Shen, T., Huang, X., Yusuf, E., and Vavylonis, D. 2010. Segmentation and tracking of cytoskeletal filaments using open active contours. *Cytoskeleton*. 67(11):693–705.

Sorokin, S. P. 1968. Reconstructions of centriole formation and ciliogenesis in mammalian lungs. *Journal of Cell Science*. 3(2):207–30.

Spektor, A. et al. 2007. Cep97 and CP110 Suppress a Cilia Assembly Program. *Cell*. 130(4):678–690.

Srour, M., Hamdan, F. F., McKnight, D., Davis, E., Mandel, H., Schwartzentruber, J., Martin, B., Patry, L., Nassif, C., Dionne-Laporte, A., Ospina, L. H., Lemyre, E., Massicotte, C., Laframboise, R., Maranda, B., Labuda, D., Décarie, J.-C., Rypens, F., Goldsher, D., Fallet-Bianco, C., Soucy, J.-F., Laberge, A.-M., Maftei, C., Boycott, K., Brais, B., Boucher, R.-M., Rouleau, G. A., Katsanis, N., Majewski, J., Elpeleg, O., Kukolich, M. K., Shalev, S., and Michaud, J. L. 2015. Joubert Syndrome in French Canadians and Identification of Mutations in CEP104. *The American Journal of Human Genetics*. 97(5):744–753.

Stanley, H. P., Bowman, J. T., Romrell, L. J., Reed, S. C., and Wilkinson, R. F. 1972. Fine structure of normal spermatid differentiation in Drosophila melanogaster. *Journal of Ultrastructure Research*. 41(5-6):433–466.

Stepanek, L. and Pigino, G. 2016. Microtubule doublets are double-track railways for intraflagellar transport trains. *Science*. 352(6286):721–4.

Styczynska-Soczka, K. and Jarman, A. P. 2015. The Drosophila homologue of Rootletin is required for mechanosensory function and ciliary rootlet formation in chordotonal sensory neurons. *Cilia*. 4(1):9.

Sung, C.-H. and Leroux, M. R. 2013. The roles of evolutionarily conserved functional modules in cilia-related trafficking. *Nature Cell Biology*. 15(12):1387–97.

Szymanska, K., Berry, I., Logan, C. V., Cousins, S. R., Lindsay, H., Jafri, H., Raashid, Y., Malik-Sharif, S., Castle, B., Ahmed, M., Bennett, C., Carlton, R., and Johnson, C. A. 2012. Founder mutations and genotype-phenotype correlations in Meckel-Gruber syndrome and associated ciliopathies. *Cilia*. 1(1):18.

Szymanska, K., Hartill, V. L., and Johnson, C. A. 2014. Unraveling the genetics of Joubert and Meckel-Gruber syndromes. *Journal of Pediatric Genetics*. 3(2):65–78.

Takao, D. and Verhey, K. J. 2015. Gated entry into the ciliary compartment. *Cellular and Molecular Life Sciences*.

Takeda, S., Yonekawa, Y., Tanaka, Y., Okada, Y., Nonaka, S., and Hirokawa, N. 1999. Left-right asymmetry and kinesin superfamily protein KIF3A: new insights in determination of laterality and mesoderm induction by kif3A-/- mice analysis. *The Journal of Cell Biology*. 145(4):825–36.

Tallila, J., Jakkula, E., Peltonen, L., Salonen, R., and Kestilä, M. 2008. Identification of CC2D2A as a Meckel syndrome gene adds an important piece to the ciliopathy puzzle. *The American Journal of Human Genetics*. 82(6):1361–7.

Tammachote, R., Hommerding, C. J., Sinders, R. M., Miller, C. A., Czarnecki, P. G., Leightner, A. C., Salisbury, J. L., Ward, C. J., Torres, V. E., Gattone, V. H., and Harris, P. C. 2009. Ciliary and centrosomal defects associated with mutation and depletion of the Meckel syndrome genes MKS1 and MKS3. *Human Molecular Genetics*. 18(17):3311–3323.

Tanos, B. E., Yang, H. J., Soni, R., Wang, W. J., Macaluso, F. P., Asara, J. M., and Tsou, M. F. B. 2013. Centriole distal appendages promote membrane docking, leading to cilia initiation. *Genes and Development*. 27(2):163–168.

Tates, D. 1971. Cytodifferentiation during spermatogenesis in Drosophila melanogaster. PhD thesis. Rijksuniversiteit Leiden.

Teglund, S. and Toftgard, R. 2010. Hedgehog beyond medulloblastoma and basal cell carcinoma. *Biochimica et Biophysica Acta - Reviews on Cancer*. 1805(2):181–208.

Tokuyasu, K. T. 1974. Dynamics of spermiogenesis in Drosophila melanogaster. IV. Nuclear transformation. *Journal of Ultrastructure Research*. 48(2):284–303.

Tokuyasu, K. T., Peacock, W. J., and Hardy, R. W. 1972a. Dynamics of spermiogenesis in Drosophila melanogaster. I. Individualization process. *Zeitschrift für Zellforschung und Mikroskopische Anatomie*. 124(4):479–506.

Tokuyasu, K. T., Peacock, W. J., and Hardy, R. W. 1972b. Dynamics of spermiogenesis in Drosophila melanogaster. II. Coiling process. *Zeitschrift für Zellforschung und Mikroskopische Anatomie*. 127(4):492–525.

Tokuyasu, K. 1975. Dynamics of spermiogenesis in Drosophila melanogaster. VI. Significance of "onion" nebenkern formation. *Journal of Ultrastructure Research*. 53(1):93–112.

Tsang, W. Y., Spektor, A., Luciano, D. J., Indjeian, V. B., Chen, Z., Salisbury, J. L., Sánchez, I., and Dynlacht, B. D. 2006. CP110 cooperates with two calcium-binding proteins to

regulate cytokinesis and genome stability. *Molecular Biology of the Cell*. 17(8):3423–34.

Uga, S. and Kuwabara, M. 1965. On the Fine Structure of the Chordotonal Sensillum in Antenna of Drosophila melanogaster. *Microscopy*. 14(3):173–181.

Vannuccini, E., Paccagnini, E., Cantele, F., Gentile, M., Dini, D., Fino, F., Diener, D., Mencarelli, C., and Lupetti, P. 2016. Two classes of short intraflagellar transport train with different 3D structures are present in Chlamydomonas flagella. *Journal of Cell Science*. 129(10):2064–74.

Varjosalo, M., Li, S.-P., and Taipale, J. 2006. Divergence of hedgehog signal transduction mechanism between Drosophila and mammals. *Developmental cell*. 10(2):177–86.

Veleri, S., Manjunath, S. H., Fariss, R. N., May-Simera, H., Brooks, M., Foskett, T. A., Gao, C., Longo, T. A., Liu, P., Nagashima, K., Rachel, R. A., Li, T., Dong, L., and Swaroop, A. 2014. Ciliopathy-associated gene Cc2d2a promotes assembly of subdistal appendages on the mother centriole during cilia biogenesis. *Nature Communications*. 5:4207.

Vogel, T. W., Carter, C. S., Abode-Iyamah, K., Zhang, Q., and Robinson, S. 2012. The role of primary cilia in the pathophysiology of neural tube defects. *Neurosurgical Focus*. 33(4):E2.

Vorobjev, I. A. and Chentsov, Y. S. 1982. Centrioles in the cell cycle of L cells. *The Journal of Cell Biology*. 18(5):478–483.

Voronina, V. A., Takemaru, K.-I., Treuting, P., Love, D., Grubb, B. R., Hajjar, A. M., Adams, A., Li, F.-Q., and Moon, R. T. 2009. Inactivation of Chibby affects function of motile airway cilia. *The Journal of Cell Biology*. 185(2):225–33.

Walker, R. G., Willingham, A. T., and Zuker, C. S. 2000. A Drosophila Mechanosensory Transduction Channel. *Science*. 287(5461).

Wallingford, J. B. and Mitchell, B. 2011. Strange as it may seem: The many links between Wnt signaling, planar cell polarity, and cilia. *Genes and Development*. 25(3):201–213.

Wang, B., Fallon, J. F., and Beachy, P. A. 2000. Hedgehog-Regulated Processing of Gli3 Produces an Anterior/Posterior Repressor Gradient in the Developing Vertebrate Limb. *Cell*. 100(4):423–434.

Wang, W. J., Soni, R. K., Uryu, K., and Tsou, M. F. B. 2011. The conversion of centrioles to centrosomes: Essential coupling of duplication with segregation. *Journal of Cell Biology*. 193(4):727–739.

Weatherbee, S. D., Niswander, L. A., and Anderson, K. V. 2009. A mouse model for Meckel syndrome reveals Mks1 is required for ciliogenesis and Hedgehog signaling. *Human Molecular Genetics*. 18(23):4565–75.

Wheatley, D. 1995. Primary cilia in normal and pathological tissues. *Pathobiology*. 63(4):222–238.

Williams, C. L., Li, C., Kida, K., Inglis, P. N., Mohan, S., Semenec, L., Bialas, N. J., Stupay, R. M., Chen, N., Blacque, O. E., Yoder, B. K., and Leroux, M. R. 2011. MKS and NPHP modules cooperate to establish basal body/transition zone membrane associations and ciliary gate function during ciliogenesis. *The Journal of Cell Biology*. 192(6):1023–41.

Williams, C. L., Winkelbauer, M. E., Schafer, J. C., Michaud, E. J., and Yoder, B. K. 2008. Functional redundancy of the B9 proteins and nephrocystins in Caenorhabditis elegans ciliogenesis. *Molecular Biology of the Cell*. 19(5):2154–68.

Willingham, A. T. and Keil, T. 2004. A tissue specific cytochrome P450 required for the structure and function of Drosophila sensory organs. *Mechanisms of Development*. 121(10):1289–1297.

Wong, S. Y., Seol, A. D., So, P.-L., Ermilov, A. N., Bichakjian, C. K., Epstein, E. H., Dlugosz, A. A., and Reiter, J. F. 2009. Primary cilia can both mediate and suppress Hedgehog pathway-dependent tumorigenesis. *Nature Medicine*. 15(9):1055–61.

Wu, Z. et al. 2011. A combinatorial semaphorin code instructs the initial steps of sensory circuit assembly in the Drosophila CNS. *Neuron*. 70(2):281–98.

Yamashita, Y. M., Jones, D. L., and Fuller, M. T. 2003. Orientation of asymmetric stem cell division by the APC tumor suppressor and centrosome. *Science*. 301(5639):1547–50.

Yan, X., Zhao, H., and Zhu, X. 2016. Production of Basal Bodies in bulk for dense multicilia formation. *F1000Research*. 5:1533.

Yang, T. T., Su, J., Wang, W.-J., Craige, B., Witman, G. B., Bryan Tsou, M.-F., and Liao, J.-C. 2015. Superresolution Pattern Recognition Reveals the Architectural Map of the Ciliary Transition Zone. *Scientific Reports*. 5:14096.

Yee, L. E., Garcia-Gonzalo, F. R., Bowie, R. V., Li, C., Kennedy, J. K., Ashrafi, K., Blacque, O. E., Leroux, M. R., and Reiter, J. F. 2015. Conserved Genetic Interactions between Ciliopathy Complexes Cooperatively Support Ciliogenesis and Ciliary Signaling. *PLOS Genetics*. 11(11).

Yoshiba, S., Shiratori, H., Kuo, I. Y., Kawasumi, A., Shinohara, K., Nonaka, S., Asai, Y., Sasaki, G., Belo, J. A., Sasaki, H., Nakai, J., Dworniczak, B., Ehrlich, B. E., Pennekamp, P., and Hamada, H. 2012. Cilia at the node of mouse embryos sense fluid flow for left-right determination via Pkd2. *Science*. 338(6104):226–31.

Zhang, W., Cheng, L. E., Kittelmann, M., Li, J., Petkovic, M., Cheng, T., Jin, P., Guo, Z., Göpfert, M. C., Jan, L. Y., and Jan, Y. N. 2015a. Ankyrin Repeats Convey Force to Gate the NOMPC Mechanotransduction Channel. *Cell*. 162(6):1391–1403.

Zhang, W., Yan, Z., Jan, L. Y., and Jan, Y. N. 2013. Sound response mediated by the TRP channels NompC, Nanchung, and Inactive in chordotonal organs of Drosophila larvae. *Proceedings of the National Academy of Sciences of the United States of America*. 110(33):13612–7.

Zhang, X.-H., Tee, L. Y., Wang, X.-G., Huang, Q.-S., and Yang, S.-H. 2015b. Off-target Effects in CRISPR/Cas9-mediated Genome Engineering. *Molecular Therapy. Nucleic Acids*. 4(11):e264.

Zhang, Y., Seo, S., Bhattarai, S., Bugge, K., Searby, C. C., Zhang, Q., Drack, A. V., Stone, E. M., and Sheffield, V. C. 2014. BBS mutations modify phenotypic expression of CEP290-related ciliopathies. *Human Molecular Genetics*. 23(1):40–51.

Zitserman, D. and Roegiers, F. 2011. Live-cell imaging of sensory organ precursor cells in intact Drosophila pupae. *Journal of Visualized Experiments*. (Figure 1):1–4.